Volume III, 1959

TRANSACTIONS of the SOCIETY OF RHEOLOGY

Editor: R. D. ANDREWS
Massachusetts Institute of Technology

Preface 1

E. H. Lee: Presentation of the Bingham Medal to Ronald S. Rivlin 3

J. J. Bikerman and Ching-Rong Huang: Polyethylene Adhesive Joints .. 5

Aris Phillips: The Theory of Locking Materials 13

R. H. Shoulberg, F. H. Zimmerli, and O. C. Kohler: An Apparatus for Measuring the Dynamic Mechanical Properties of High Polymers at Low Frequencies 27

E. H. Lee, J. R. M. Radok, and W. B. Woodward: Stress Analysis for Linear Viscoelastic Materials 41

John G. Brodnyan: The Concentration Dependence of the Newtonian Viscosity of Prolate Ellipsoids 61

Elliot A. Kearsley: An Analysis of an Absolute Torsional Pendulum Viscometer 69

Joseph A. Faucher: Viscoelastic Behavior of Polyethylene and Polypropylene 81

R. E. Nettleton: Thermodynamics of Transport Processes in Liquids .. 95

Charles Mack: Secondary Stresses in Anisotropic Amorphous Media ... 101

Thor L. Smith: Volume Changes and Dewetting in Glass Beads—Polyvinyl Chloride Elastomeric Composites Under Large Deformations 113

Irvin M. Krieger and Thomas J. Dougherty: A Mechanism for Non-Newtonian Flow in Suspensions of Rigid Spheres 137

Wladimir Philippoff: The Temperature Dependence of Flow Birefringence Parameters 153

D. H. Kaelble: Theory and Analysis of Peel Adhesion: Mechanisms and Mechanics 161

Frederick H. Gaskins and Wladimir Philippoff: The Behavior of Jets of Viscoelastic Fluids 181

Communication Problems in Industrial Rheology 205

Abstracts of Additional Papers Presented at the Society of Rheology Meeting, November 5–7, 1958 207

INTERSCIENCE PUBLISHERS NEW YORK • LONDON

PROPERTY OF
Standard Oil Co[illegible] Ind.)
RESEARCH
LIBRARY

Copyright © 1960 by
INTERSCIENCE PUBLISHERS, INC.

Library of Congress Catalog
Card Number 57-11926

INTERSCIENCE PUBLISHERS, INC.
250 Fifth Avenue, New York 1, N. Y.

For Great Britain and Northern Ireland:
INTERSCIENCE PUBLISHERS LTD.
88/90 Chancery Lane, London, W. C. 2

PRINTED IN THE UNITED STATES OF AMERICA BY MACK PRINTING CO., EASTON, PA.

Preface

This volume of the Transactions of the Society of Rheology contains papers which were presented at the Annual Meeting of the Society which was held at the Franklin Institute in Philadelphia, Pennsylvania, on November 5–7, 1958. For those papers which are not presented in full, abstracts are given, and in some cases an indication is included of where the complete paper has been, or is to be, published.

The Bingham Medal, which is presented annually in recognition of the accomplishments of an outstanding scientist in the field of rheology, was presented at the 1958 Meeting to Ronald S. Rivlin. The Bingham Medal Presentation Address, by E. H. Lee, is given at the beginning of this volume. Professor Rivlin's Medalist Address, "Mathematics and Rheology," has been published in the May 1959 issue of *Physics Today*. Former recipients of the Bingham Medal, since the inception of the award, are as follows:

Melvin Mooney	1948	John D. Ferry	1953
Henry Eyring	1949	Turner Alfrey, Jr.	1954
W. F. Fair, Jr.	1950	Herbert Leaderman	1955
Percy W. Bridgman	1951	Arthur V. Tobolsky	1956
A. Nadai	1952	Clarence M. Zener	1957

The appearance of the present volume has been delayed to a greater than usual extent by an unusually protracted reviewing period for the manuscripts. It is planned to decrease this time lag considerably in the future volumes, and Volume IV, containing papers for the 1959 Thirtieth Anniversary Meeting, under the editorship of E. H. Lee of Brown University, will appear soon after the present volume is issued.

Officers of the Society, who are elected for a two-year term, are for the years 1957–59 as follows:

President:

J. H. Dillon
Textile Research Institute
Princeton, N. J.

Vice-President:

J. H. Elliott
Research Center
Hercules Powder Co.
Wilmington, Del.

Secretary-Treasurer:

W. R. Willets
Titanium Pigment Corp.
99 Hudson Street
New York 13, N. Y.

Editor:

R. D. Andrews, Jr.
Plastics Research Laboratory
Room 7-006, M. I. T.
Cambridge 39, Mass.

The Executive Committee of the Society consists of the officers listed above, together with the most recent Past President (F. D. Dexter), the Assistant Editor (E. H. Lee), and two elected members (R. S. Rivlin and R. S. Marvin).

R. D. Andrews, Jr.

Cambridge, Massachusetts
April, 1960

TRANSACTIONS OF THE SOCIETY OF RHEOLOGY III, 3–4 (1959)

Presentation of the Bingham Medal to Ronald S. Rivlin

E. H. LEE, *Brown University, Providence, Rhode Island*

I would first like to congratulate the Committee of Award on a most appropriate choice for the Bingham Medalist for 1958. I know that you will all agree that Professor Ronald S. Rivlin's outstanding contributions to the field of rheology have had a

ctivities up to that time.
y is well known to you,
his scientific activities.
I an undergraduate, fol-
oratories of the General
ffect of hydrogen on the
le joined this Company
re made valuable con-
ntal aspects of such
ca.
munications Research
lectromagnetic wave
contact with Dr. L.

1, 5–12 (1959)

rtment of
chnology,

des this
(metal,
intains
tween
cently
ist is
in a
leter-
se of
two
lds.
ins
ace
the
lly
e-
i-
d

was accomplished by [illegible]
and precipitating it [illegible]
the resulting mater[illegible]
described below ha[illegible]
purified by fractional precipitation.

II. Experimental Procedure

Butt joints of two types were used; they were designed to avoid, as far as possible, the complications caused by stress concentration at the 3-phase boundary line. In the type shown at the left of Figure 1, the adherends were steel or glass cylinders, 5 cm. long and 1.9 cm. in diameter. Calculated amounts of polyethylene powder were placed on the basis face of one cylinder, three spacers (small pieces of metal foil) were put on this face at equal distances from each other, and the other cylinder was placed on them, with one of its bases facing down. The clearance between the two cylinders is greatly exaggerated in the figure. The amount of polyethylene was calculated so as to form, on melting, a small drop in the middle of the basis faces. As molten polyethylene wetted the solids, the drop acquired the shape indicated in the figure. After cooling below the freezing range, the adhesive still retained a similar shape. Because its cross section was smaller at the "waistline" than at the adherend-adhesive interfaces, stress concentrations obtaining in these interfaces were believed to be irrelevant; and indeed the rupture usually occurred so far from the interfaces that, after rupture, polyethylene was visible with the naked eye on both cylinders.

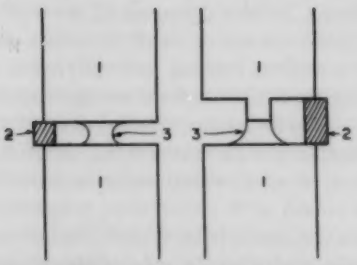

Fig. 1. Vertical cross section of the adherends used, the clearance between them being exaggerated. (1) Adherends. (2) Spacers. (3) The adhesive film.

0.3175 cm. tall. [illegible] brass, bronze or steel p[illegible] of [illegible], 0.3200 and 0.3225 cm. thickness were used. Stress concentrations at the 3-phase boundary were believed to be unimportant because of the shape of the adhesive layer indicated in the figure; here again the thickness of this layer is greatly exaggerated (for instance, a hundredfold).

The working surfaces of the metal cylinders were ground on Carborundum paper and polished with an aqueous suspension of alumina until flat within one or a few interference fringes, washed with distilled water, and degreased in toluene vapor. The degreasing was repeated before every application of the adhesive, but grinding and polishing a given cylinder were done again only if the surface ceased to be (nearly) optically flat. The glass cylinders were ground by the manufacturer.

The joints were heated in an oven or with a heating tape above the melting range of the polyethylene used. They were cooled slowly (together with the oven), or at a fair rate (in air) or rapidly (in cold water), but apparently the number of experiments was insufficient to detect any difference between the results of these 3 treatments.

The joints were broken either in a Suter tensile tester in which the load increased approximately 7×10^6 dynes in a second, or in an Instron-type machine in which the cross-head advanced either 0.001 or 0.002 cm. in a second. The breaking stresses at the higher speed in this machine were about 5% greater than at the lower speed. The data represented in Figure 2 were obtained with the Suter tester, and those of Figures 3 and 4 with the Instron-type instrument at 0.001 cm./sec.

The specimens serving for the determination of the tensile strength of the polyethylenes were either cylindrical rods (for instance, 7 cm. long and 0.7 cm. in diameter) with thick ends, or "double spades" whose straight part had the dimensions of, e.g., $5.3 \times 1.3 \times 0.3$ cm.

III. Experimental Results

No values can be listed for the strength of adhesive joints made with commercial polyethylene wax either as received or mixed with chlorinated paraffin wax or modified rosin, or vulcanized with sulfur;

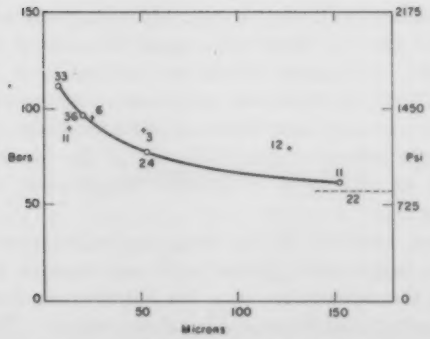

Fig. 2. Breaking stress of polyethylene joints. Ordinate: Breaking stress. Abscissa: Thickness of the adhesive film. The figures at the experimental points indicate the number of repeat experiments. The dashed line indicates the tensile strength of the material in bulk. Purified Epolene N. Heated to 130–140°C. Circles: Steel-to-steel joints. Crosses: Glass-to-glass joints.

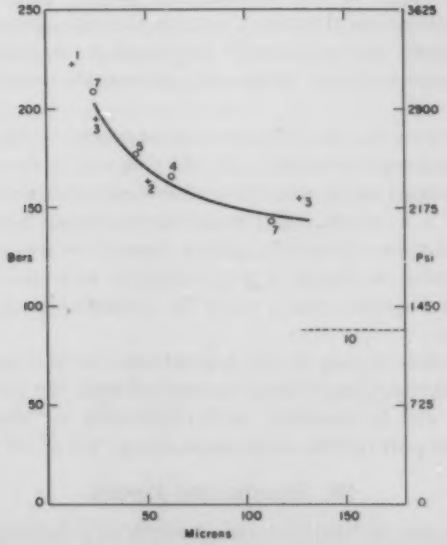

Fig. 3. See legend to Fig. 2. Purified Dylan 3700. Heated to 150–185°C. Circles: Steel-to-steel joints. Crosses: Steel-to-glass joints.

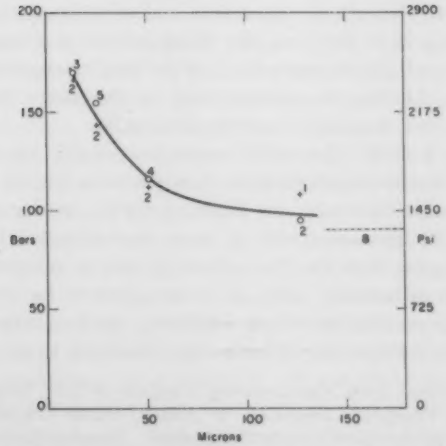

Fig. 4. See legend to Fig. 2. Purified Marlex 50. Heated to 150–160°C. Circles: Steel-to-glass joints. Crosses: Glass-to-glass joints.

so many of these joints broke in handling that no average strength could be computed. The main data obtained for "adhesionable" polyethylenes are represented in Figures 2, 3, and 4. Their abscissa indicates the thickness of the adhesive film, and the breaking stress is plotted along the ordinate. The numbers at the experimental points denote the number of repeat experiments on which the value given is based. The dashed line near the right-hand edge of each graph shows the tensile strength of the material, determined on relatively large samples.

It is seen that the breaking stress of the joints in all instances is greater than the tensile strength of the material in bulk, and that at great thicknesses of the "glue line" the former value approaches the latter. Thus, as soon as the weak boundary layers are removed, the strength of an adhesive joint is determined above all by the strength of the adhesive in it. The increase of strength in thin layers presumably is due chiefly to the smaller probability of bad flaws in thinner specimens[4] in the instance of polyethylene wax, Figure 2, because this wax is almost a Hookean solid. In the other two instances that effect presumably is intensified by the greater difficulty of plastic flow in narrower clearances. The two other possible effects,

namely, (*a*) the dependence of texture and of residual stresses on the rate of cooling and, thus, on the thickness of the heat-insulating adhesive film, and (*b*) the dependence of the local stresses caused by the external force (during the rupture test) on the above thickness, are believed to be less important in our experiments.

In Figures 2 and 3 the circles represent results for steel-to-steel joints, while crosses mean glass-to-glass joints in Figure 2 and steel-to-glass joints in Figure 3. In Figure 4 circles are for steel-to-glass and crosses for glass-to-glass. It may be concluded from inspection of the figures that the strength of a joint is independent of the nature of the adherend; thus, it is not affected by the molecular adhesion between adherend and adhesive; such adhesion obviously would depend on the nature of both of the materials in contact.

The authors thank Lord Manufacturing Company of Erie, Pennsylvania, and Owens-Corning Fiberglas Corporation of Ashton, Rhode Island, for research grants which made the above investigation possible. Eastman Chemical Products, Inc., Koppers Company, and Shell Chemical Corporation kindly supplied the polyethylenes used in this work.

References

1. Bikerman, J. J., *J. Colloid Sci.*, **2,** 163 (1947).
2. Bikerman, J. J., *Proc. Intern. Congr. Surface Activity, 2nd Congr., London,* **1957, 3,** 427.
2a. Bikerman, J. J., *Adhesives Age,* **2,** No. 2, 23 (1959).
3. Bikerman, J. J., Division of Paint, Plastics, and Printing Ink Chemistry, Am. Chem. Soc., Papers presented at the San Francisco Meeting, April 1958, p. 141.
4. Bikerman, J. J., *J. Soc. Chem. Ind.* (*London*), **40,** 23 (1941).

Synopsis

Polyethylenes, from which substances capable of producing weak boundary layers were removed, adhered to metals and glasses, and the breaking stress of the joints was closely related to the tensile strength of the polyethylenes in bulk, independent of the nature of the adherends. Thus, the "rheological" theory of adhesive joints was sustained.

ADDENDUM

Gladly complying with the suggestion of a referee, we expand in the following some of the statements made in the body of the paper.

1. Experimentally, no significant difference between breaking stresses in the arrangement of Figure 1 left and Figure 1 right was

observed. This can be seen, for instance, in Figure 4 in which circles represent results on systems of "Figure 1 right," and crosses, on systems of "Figure 1 left" type. The agreement between the two sets of values indicates that the stress concentrations were similar in the two instances. The polyethylene "pancake" almost always broke relatively far from the two adherends, so that adhesive was visible on both rupture surfaces with the unaided eye. It may be asked why rupture did not start at the edge of the pin in Figure 1 right, as there should be a considerable stress concentration at the 3-phase boundary along this edge. The explanation, in all probability, is given by the observation that molten polyethylene rose around the pin and, on solidification, formed a thin sleeve covering the latter. Thus, the joint was a butt joint below the basis of the pin and a tubular lap joint above it. If r is the radius of the pin, then as a first approximation the strength of the former would be $\pi r^2 \sigma_t$, and of the latter, $2\pi r l \sigma_s$, l being the height of the pin, σ_t the tensile strength of the adhesive, and σ_s its shearing strength. As $2l$ was twice as great as r, the butt joint would be the weaker of the two as long as $\sigma_s > \sigma_t/2$. In reality the situation is much more complex because the polyethylene sleeve around a steel pin must be in a state of considerable radial and circumferential strain; polyethylenes contract about 12–15 volume-% during freezing while the contraction of steel in the same temperature interval is less than 1%. The theory of a sleeve shrunk on a rigid cylinder has been worked out,*† but its equations cannot be applied in the present instance because the mobility of polyethylene in the intermediate stages between definitely liquid and definitely solid is not well known.

2. We attribute the decrease in the strength of polyethylene wax joints on increasing the "glue line" thickness to the greater probability of a bad flaw in a thicker specimen. The number of our experiments was not sufficient to test this contention by statistical analysis, but at least in one instance the prediction of the theory seems to be confirmed. The 11 measurements on polyethylene wax films between glass cylinders with a film thickness of 13 μ, see Figure 2, covered the range of 77.6 to 105.9 bars. If the adhesive film had a truly cylindrical shape, then 77.6 bars should be the mean breaking stress of joints $13 \times 11 = 143$ μ thick (see ref. 4 in the main

* H. Poritsky, *Physics*, **5**, 406 (1934).

† G. D. Redston and J. E. Stanworth, *J. Soc. Glass Technol.*, **29**, 48 (1945).

body of the paper). The main breaking stress of the 12 joints of 127 μ was 79.3 bars; that is, in accord with the expectation. The results on cylinder-pin systems (circles in Fig. 2) are less favorable but may be accounted for by the greater divergence of the shape of the adhesive film from the theoretical shape. In these systems the ranges of the breaking stresses were, e.g., 93.8–129.2 bars for the 33 tests at a film thickness of 8 μ, and 41.64–102.0 bars for the 11 tests at the thickness of 155 μ.

The main argument for the probability theory of the curve of Figure 2 is, however, that the alternative explanations seem to be unacceptable. Plastic flow in polyethylene wax may be ruled out; the stress-strain curves of this material are almost straight lines, and the distance between two marks on a wax rod is practically identical before and after extension to rupture. The effect of the film thickness on rate of cooling and, consequently, on the tensile strength of the adhesive cannot be considerable as was demonstrated by the experiments mentioned in Section II of the paper.

On the contrary, the behavior of high-melting polyethylenes (Figs. 3 and 4) would be expected to be influenced by their plasticity because the bars increase in length 2 to 5 times before breaking, and only a part of this elongation was reversible. Unfortunately, this reversible part has not been measured on the samples referred to in the paper, but it was about 75% for thin polyethylene films (about 0.01–0.03 cm. thick); in these films, 100 units of length were extended to 120 in the moment of rupture and became 105 after the rupture. Presumably, this elasticity during flow is responsible for the fact that the curves of Figures 3 and 4 are so different from those predicted by the theory of squeezing a perfectly plastic drop between two rigid plates. This theory, usually attributed to Prandtl (1923) and reproduced in textbooks,* predicts the breaking stress (as long as the radius of the joint is constant and much greater than the thickness of the adhesive film) to be inversely proportional to this thickness. The actual effect is definitely smaller. For instance, in Figure 3, the 7 experiments at 23 μ gave rupture stresses of 197.2 to 222.0 bars, and the 7 experiments at 114 μ, 130.3 to 151.7 bars. Prandtl's equations would give 39 to 44 bars for the strength of the thicker joints.

* F. K. Th. van Iterson, *Plasticity in Engineering*. Blackie, London, Glasgow, 1947, p. 88.

TRANSACTIONS OF THE SOCIETY OF RHEOLOGY III, 13–26 (1959)

The Theory of Locking Materials*

ARIS PHILLIPS, *Department of Civil Engineering, Yale University, New Haven, Connecticut*

I. Introduction

According to the nomenclature introduced by Prager,[1] materials may be classified into soft and hard. For a soft material the stress increment required to produce a specified strain increment diminishes with increasing deformation. For a hard material this stress increment grows as the deformation proceeds. Examples of the two types of materials are aluminum, which is a soft material, and cellular rubber, which is a hard material.

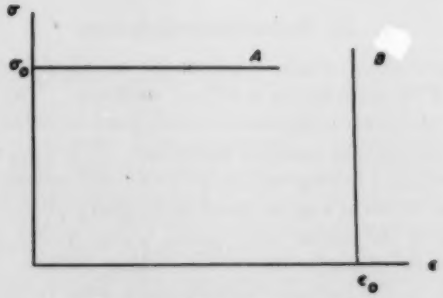

Figure 1.

An extreme case of a soft material is the rigid-plastic one, Figure 1 (line A). For such a material the stress increases up to the yield stress σ_0 without any strain, and then the stress stays at σ_0 while the strain can increase to any value. An extreme case of a hard material

* The results presented in this paper were obtained in the course of research sponsored by the Office of Naval Research.

is the ideal locking one, Figure 1 (line B). For such a material the strain increases without any stress up to the locking strain ϵ_0, and then the strain locks at ϵ_0 and cannot be increased while the stress can be increased to any value.

In this paper we shall consider possible stress-strain laws of ideal locking materials, and with the help of an example discuss a peculiarity of the concept of locking. The lack of experimental results for combined stresses concerning the deformational response of materials which in a simple tension or simple compression test exhibit the stress-strain curve of a hard material, obliges us to be guided in this investigation by theoretical considerations only.

Prager,[1] in his discussion of the ideal locking materials, points out that theoretical speculations in plasticity about the structure of the yield condition or stress-strain law repeatedly guided investigators to unexpected experimental results and that the same may be expected to happen in the field of locking materials. The present writer concurs with the ideas expressed above, and he also believes that an investigation of the peculiarities of the locking concept will help in improving our understanding of the structure of the stress-strain laws of real materials.

II. Stress-Strain Relations

Very general stress-strain relations for an ideal locking material can be found by introducing a *locking condition*. This is a relation between the six strain components which must be satisfied at a point of a body when locking exists at this point. A locking condition can be represented by a *locking surface* in the six-dimensional strain space. Then locking occurs at a given point of the body when and only when the endpoint of the vector $\bar{\epsilon}(\epsilon_{11}, \epsilon_{22}, \epsilon_{33}, \sqrt{2}\epsilon_{12}, \sqrt{2}\epsilon_{23}, \sqrt{2}\epsilon_{31})$, representing the state of strain, lies on the locking surface.

In addition to the locking condition there must be available a *locking rule*. Consider the six-dimensional stress space in which the stress at a given point of a body is represented by the vector $\bar{\sigma}(\sigma_{11}, \sigma_{22}, \sigma_{33}, \sqrt{2}\sigma_{12}, \sqrt{2}\sigma_{23}, \sqrt{2}\sigma_{31})$. By superimposing the stress space on the strain space we can express the locking rule as a relation between the directions of the two vectors $\bar{\epsilon}$ and $\bar{\sigma}$. In Prager's formulation of the theory of locking materials it is assumed that the vector $\bar{\sigma}$ is normal to the plane which is tangent to the locking surface at the endpoint of $\bar{\epsilon}$, Figure 2. Such a locking rule can be expressed analytically by

$$\sigma_{ij} = \lambda(\partial g/\partial \epsilon_{ij}) \tag{1}$$

where

$$g(\epsilon_{11}, \epsilon_{22}, \epsilon_{33}, \epsilon_{12}, \epsilon_{23}, \epsilon_{31}) = k \tag{2}$$

is the locking condition. In eq. (1) the factor λ is a proportionality factor. Equations (1) and (2) together with the relation $\sigma_{ij} = 0$ for $g < k$ are a complete system of stress-strain relations for the ideal locking material.

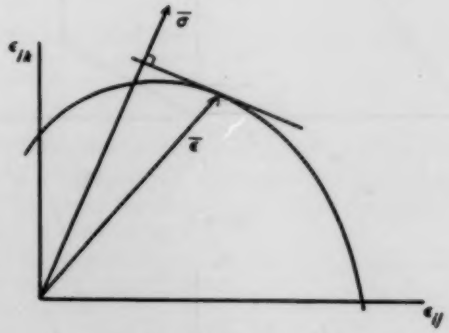

Figure 2.

In this paper we shall assume that there are two independent rheological equations of state, one for the change in volume and the other for the change in shape. This assumption is introduced because it is generally accepted that materials behave differently when changing shape than when changing volume.[2] Of course the assumption of the independence of the two rheological equations of state is strictly valid only for small strains.[3] This assumption of two independent rheological equations of state has been used by Prager in a recent paper.[4] He introduced a material which follows Hooke's law for changes in shape while it has a volumetric equation of state of the elastic-locking type, Figure 3. In the present paper we shall assume that both equations of state are of the ideal locking type, Figure 4, and we wish to explore the behavior resulting from such a choice.

The volumetric equation of state for our material is

$$\begin{aligned} \sigma_m &= 0 \quad \text{for} \quad |\epsilon_m| < |k_m| \\ \sigma_m &= \text{indefinite for } \epsilon_m = k_m \end{aligned} \tag{3}$$

where σ_m and ϵ_m are the mean stress and mean strain, respectively, and k_m is the value which ϵ_m must reach in order for the volumetric locking to occur. Obviously $|\epsilon_m|$ is always smaller or equal to $|k_m|$.

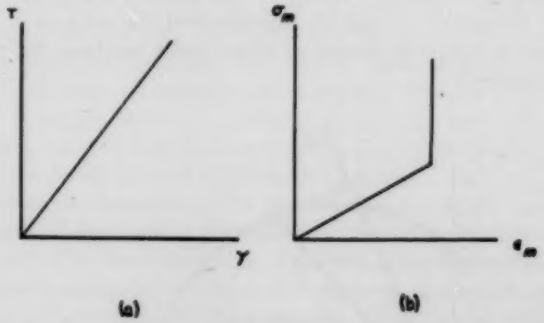

Figure 3.

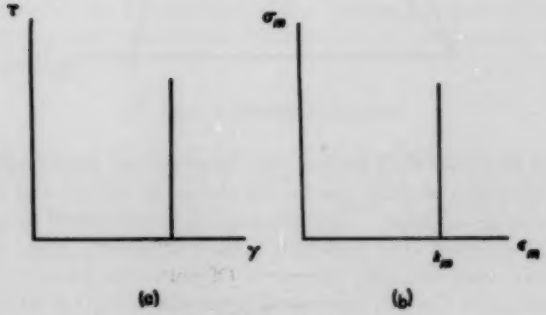

Figure 4.

To write the distortional equation of state we must introduce the distortional locking condition

$$g(e_{11}, e_{22}, e_{33}, e_{12}, e_{23}, e_{31}) = k \tag{4}$$

where e_{ij} are the six components of the strain deviation, g is a function of these components, and k is the value which this function g must take for distortional locking to occur. When $g < k$ no deviatoric stresses are possible; for $g = k$ deviatoric stresses are possible; and finally g can never take values greater than k. From the locking con-

dition it is apparent that at locking the six components of strain deviation do not need to remain constant; it is only required that any change in the values of these components will be such that the function g will retain the value k.

To introduce the locking rule we proceed as follows:

From the stress-strain diagram B in Figure 1 it follows that at the locking stage,

$$\sigma d\epsilon = 0$$

Generalizing for combined stresses we can write, using the summation convention,

$$s_{ij}de_{ij} = 0 \tag{5}$$

where de_{ij} is the increment of the component e_{ij} of the strain deviation and s_{ij} is the corresponding component of the stress deviation. Equation (5) says that the distortional strain energy per unit volume cannot change at the locking stage.

Because at locking the function g has a constant value, it follows that

$$dg = (\partial g/\partial e_{ij})de_{ij} = 0 \tag{6}$$

Hence, from eqs. (5) and (6) it follows that the vector with the components s_{ij} is parallel to the vector with the components $\partial g/\partial e_{ij}$. Therefore we can write

$$s_{ij} = \lambda(\partial g/\partial e_{ij}) \tag{7}$$

where λ is a positive factor of proportionality which as a rule depends on the coordinates x,y,z. We conclude that eqs. (4) and (7) represent the equation of state for change in shape.

The argument could be advanced that in analogy with the theory of rigid plastic bodies we should use the incremental stress-strain relations

$$ds_{ij} = \lambda(\partial g/\partial e_{ij}) \tag{8}$$

instead of the relations (7). That such stress-strain relations as given by eq. (8) are not acceptable follows from the following discussion. Let us consider eq. (7) first. In Figure 5 we give a schematic two-dimensional representation of the locking condition $g = k$. When distortional locking occurs, the endpoint A of the vector $\bar{e}$ with the

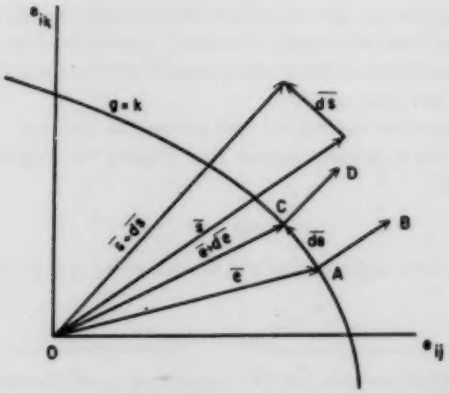

Figure 5.

components e_{ij} is on the surface g. At the same time the vector AB with the components $\partial g/\partial e_{ij}$ is normal to the surface at A, and the vector $\overline{s}$ with the components s_{ij} is parallel to AB. A change $\overline{ds}$ in the stress will produce a new stress vector $\overline{s} + \overline{ds}$, and the corresponding change in the strain will be found by obtaining a new normal CD to the surface $g = k$. This normal CD is parallel to the vector $\overline{s} + \overline{ds}$. Then the change $\overline{de}$ in the strain due to the change $\overline{ds}$ in stress will be given by the vector AC. Any arbitrary infinitesimal change $\overline{ds}$ in the stress is generally permitted because, in general, we should always be able to find a normal CD to the surface parallel to the stress vector.

Consider now the incremental stress-strain relations (8). In this case $\overline{ds}$, and not $\overline{s}$, is parallel to the normal AB. Therefore, the stress increment is fixed in direction, independently of the direction of strain increment $\overline{de}$. It follows that there is an infinite number of strain increments corresponding to the same stress increment; that is, we have a condition of instability. If such an instability should be avoided stress-strain relations of the type (8) cannot be used.

Another remark which should be made is that the locking surface should have no portion which is plane. Indeed, if a finite portion of the locking surface is plane, then it is easy to see that an infinitesimal increment in the stress deviator may produce finite increments in the strain deviator, a situation which is not permissible in stress-strain

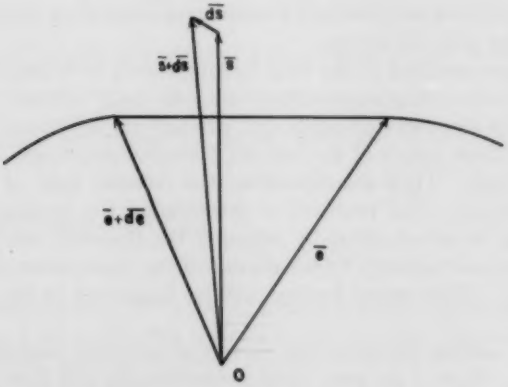

Figure 6.

relations. From Figure 6 it is seen that to the strain deviator vector $\bar{e}$ there corresponds the stress deviator vector $\bar{s}$ normal to the plane portion of the locking surface. A small change $\overline{ds}$ of $\bar{s}$ will change the direction of the stress deviator vector from that of $\bar{s}$ to that of $\bar{s} + \overline{ds}$, so that the endpoint of $\bar{e}$ cannot any longer be on the same plane portion of the locking surface. Hence $\overline{de}$ must be of finite length whereas $\overline{ds}$ is infinitesimal.

III. The Basic Problem of Locking

Comparing the stress-strain relations of the ideal locking material with those of the rigid plastic one of the total strain theory, it is concluded that the ideal locking material does not follow from the rigid plastic one by a simple interchange of the stresses and strains. Of course, the distortional equation of state of the ideal locking material follows from that of the rigid plastic one by the simple interchange of stresses and strains. The same procedure, however, is not valid for the volumetric equation of state because $\epsilon_m = 0$ for $|\sigma_m| < |k_m|$ and $\epsilon_m =$ indefinite for $\sigma_m = k_m$ is *not* the volumetric equation of state of the rigid plastic material (unless, of course, we assume $|k_m| = \infty$). This observation and the remark that the differential equations of equilibrium for the stresses and the compatibility equations for the strains do not have the same form, show that the solution of problems with ideal locking materials cannot be achieved by a formal repetition

of the procedure used for rigid plastic materials and an interchange of the stresses with the strains.

The basic problem of the ideal locking theory is to find the values of the boundary displacements for which the body will lock so that an increase in the external loads will produce no additional displacements. These values of the boundary displacements are the *locking displacements*. They correspond to the collapse load of the rigid plastic theory. The problem of determining the locking displacements can be solved either by means of the theorems introduced by Prager[1] or more directly by integration of the appropriate differential equations. This second method will be illustrated in the next section.

To the locking displacements there corresponds a locking mode in the body. Part of the body locks volumetrically and part of it locks distortionally. In general, volumetric and distortional locking may coexist over the same region of the body. In some cases, however, the two types of locking cannot coexist in the same region. Indeed, suppose that we have a problem of spherical or axial symmetry in which $v = w = 0$ so that the only nonvanishing displacement component is u and this component depends on the coordinate r only. This is, for example, the case in the problems of the hollow sphere, and of the long hollow cylinder. In such a case the two equations $\epsilon_m = k_m$ and $g = k$ give two differential equations for $u(r)$ which have different solutions. It follows that it is impossible for both solutions to be valid over the same region of the body and therefore in this case of locking the body will be divided into two parts, one of which locks volumetrically while the other locks distortionally. The calculation of the locking displacements and of the locking mode will be given in the next section for the problem of the hollow sphere.

IV. The Hollow Sphere

(a) *Strains and Displacements*

We consider a hollow sphere of inner radius a and outer radius b. The displacements of the inner and outer surface are denoted by u_a and u_b, respectively. We shall assume that the ratio $u_a/u_b = s$ is fixed. We want to find the value of u_a for which locking occurs.

Because of spherical symmetry we have $\epsilon_\varphi = \epsilon_\vartheta$ and the strain-displacement relations are

$$\epsilon_\theta = u/r, \qquad \epsilon_r = du/dr \tag{9}$$

Volumetric locking will occur at a point when at this point

$$\epsilon_r + 2\epsilon_\theta = 3k_m \tag{10}$$

which, with the help of eqs. (9), gives the differential equation

$$(du/dr) + 2(u/r) - 3k_m = 0 \tag{11}$$

The solution of this equation is

$$u = (C/r^2) + k_m r \tag{12}$$

Distortional locking will occur at a point when at this point $g = k$. As function g we shall select the octahedral shearing strain γ_0 so that the distortional locking condition has the form

$$g = \gamma_0 = \frac{2}{3}\left[(\epsilon_r - \epsilon_\theta)^2 + (\epsilon_\theta - \epsilon_\varphi)^2 + (\epsilon_\varphi - \theta_r)^2\right]^{1/2} = k \tag{13}$$

Because of the existing spherical symmetry this condition becomes

$$\epsilon_\theta - \epsilon_r = 3k/2\sqrt{2} = k_1 \tag{14}$$

where k_1 is a new material constant. With the help of eqs. (9), eq. (14) becomes

$$(du/dr) - (u/r) + k_1 = 0 \tag{15}$$

the solution of which is

$$u = C_1 r - k_1 r \ln r \tag{16}$$

Obviously, expressions (12) and (16) cannot both be valid over the same region simultaneously. It is, however, possible that one expression is valid over part of the hollow sphere, while the other is valid over the rest of the sphere. Let us assume that expression (16) is valid between $r = a$ and $r = t$, and that expression (12) is valid between $r = t$ and $r = b$. Then we have

$$u_a = C_1 a - k_1 a \ln a$$

from which C_1 can be calculated, so that finally we find

$$u = (u_a/a)r + k_1 r \ln (a/r) \tag{17}$$

for $a \leqq r \leqq t$. Similarly we find

$$u_b = (C/b^2) + k_m b$$

from which C can be calculated, and thus we find

$$u = u_b(b^2/r^2) - k_m\, b^3/r^2 + k_m r \tag{18}$$

for $t \leqq r \leqq b$.

The strain components are as follows:

$$\epsilon_\vartheta = (u_a/a) + k_1 \ln (a/r), \qquad \epsilon_r = (u_a/a) + k_1 \ln (a/r) - k_1 \tag{19}$$

for $a \leqq r \leqq t$,

$$\begin{aligned} \epsilon_\vartheta &= u_b(b^2/r^2) - k_m(b^3/r^3) + k_m \\ \epsilon_r &= -2u_b(b^2/r^3) + 2k_m(b^3/r^3) + k_m \end{aligned} \tag{20}$$

for $t \leqq r \leqq b$.

The following boundary conditions are now available for the determination of the quantities u_a, u_b, and t. At $r = t$ we must have:

$$\epsilon_r + 2\epsilon_\vartheta = 3k_m \tag{i}$$

when using expressions (19);

$$\epsilon_\vartheta - \epsilon_r = k_1 \tag{ii}$$

when using expressions (20); and (iii) the same values for u when using eqs. (17) and (18). The first condition gives

$$u_a = -k_1 a \ln (a/t) + k_1(a/3) + ak_m \tag{21}$$

the second condition gives

$$u_b = k_1(t^3/3b^2) + k_m b \tag{22}$$

and finally the third condition is identically satisfied. Equations (21), (22), and relation $u_a/u_b = s$ determine the locking displacements u_{a1}, u_{b1}, and the corresponding value of t (radius of the boundary separating the two locking regions).

It can be shown quite easily that the assumption $a \leqq r \leqq t$ for distortional locking and $t \leqq r \leqq b$ for volumetric locking is the only possible one. We have to show that the region of distortional locking, if existing, must be bounded by the inner boundary; and that the region of volumetric locking, if existing, must be bounded by the outer boundary. Indeed, let us consider the elastic-locking material remembering that the ideal locking material is an idealization of the elastic-locking material; that is, of a material which is first elastic and then it locks.

If we consider the solution of the elastic hollow sphere under internal and external pressure we find (see ref. 5);

$$\epsilon_\varphi - \epsilon_r = 3B/r^3 \tag{23}$$

$$3\epsilon_m = \epsilon_r + 2\epsilon_\varphi = 3A \tag{24}$$

where B and A are constants independent of r but dependent on the boundary conditions. From eq. (24) we see that volumetric locking must occur over the entire portion of the sphere which has not already locked distortionally as soon as $3\epsilon_m$ becomes equal to $3k_m$. Similarly, eq. (23) shows that distortional locking must start at the inner boundary because there, for $r = a$, $\epsilon_\varphi - \epsilon_r$ is a maximum. Hence, as the loading proceeds, either (i) $\epsilon_\varphi - \epsilon_r$ becomes equal to k_1 at $r = a$ first, or (ii) ϵ_m becomes equal to k_m over the entire hollow sphere first.

In case (ii), volumetric locking occurs over the entire sphere and no distortional locking is possible. In case (i), distortional locking will occur at the inner boundary, and as the loading proceeds, the region of distortional locking will extend in size until either the entire sphere will become distortionally locked, or until for some value of t the portion of the sphere which has not locked distortionally will lock volumetrically (because ϵ_m finally becomes equal to k_m at this region).

Therefore, reverting again to the ideal-locking material, we conclude that distortional locking, if it will appear at all, will appear at the inner boundary, whereas volumetric locking, if it will appear at all, will appear at the outer boundary.

(*b*) *Stresses*

In the region of distortional locking, $a \leqq r \leqq t$, the following relations are valid:

$$\sigma_m = 0 \tag{25}$$

because of *no* volumetric locking, and

$$s_{ij} = \lambda(\partial g/\partial e_{ij}) \tag{26}$$

because of distortional locking. The octahedral shearing strain can be written also in the form

$$g = \gamma_0 = \frac{2}{\sqrt{3}} \sqrt{e_{rr}^2 + e_{\theta\theta}^2 + e_{\varphi\varphi}^2} = k \tag{27}$$

Hence

$$\frac{\partial g}{\partial e_{ij}} = \frac{2}{\sqrt{3}} \frac{e_{ij}}{\sqrt{e_{rr}^2 + e_{\vartheta\vartheta}^2 + e_{\varphi\varphi}^2}} \tag{28}$$

from which it follows that

$$\sigma_{ij} = (\sqrt{2}\lambda/k_1)e_{ij} \tag{29}$$

From eq. (25) it follows that eq. (29) can be written in the form

$$\sigma_r = (\sqrt{2}\lambda/k_1)(\epsilon_r - \epsilon_m), \qquad \sigma_\vartheta = \sigma_\varphi = (\sqrt{2}\lambda/k_1)(\epsilon_\vartheta - \epsilon_m) \tag{30}$$

from which we find

$$\sigma_r - \sigma_\vartheta = (\sqrt{2}\lambda/k_1)(\epsilon_r - \epsilon_\vartheta) \tag{31}$$

On the other hand

$$3\sigma_m = \sigma_r + 2\sigma_\vartheta = 0 \tag{32}$$

Hence, eqs. (31) and (32) give

$$\sigma_r = (2\sqrt{2}/3)(\lambda/k_1)(\epsilon_r - \epsilon_\vartheta) \tag{33}$$

which with the help of eq. (14) becomes

$$\sigma_r = -(2\sqrt{2}/3)\lambda \tag{34}$$

Then eq. (32) gives

$$\sigma_\vartheta = (\sqrt{2}/3)\lambda \tag{35}$$

The equation of equilibrium is

$$(d\sigma_r/dr) + 2(\sigma_r - \sigma_\vartheta)/r = 0 \tag{36}$$

which, because of eqs. (34) and (35) becomes

$$(d\lambda/dr) + (3\lambda/r) = 0 \tag{37}$$

Integrating we find

$$\lambda = C/r^3 \tag{38}$$

from which it follows that

$$\sigma_r = -(2\sqrt{2}/3)(C/r^3), \qquad \sigma_\vartheta = (\sqrt{2}/3)(C/r^3) \tag{39}$$

for the region $a \leqq r \leqq t$.

In the region of volumetric locking, $t \leqq r \leqq b$, we have the following relations:

$$\varepsilon_{ij} = 0 \tag{40}$$

because of *no* distortional locking, and

$$\sigma_m = \text{indefinite} \tag{41}$$

because of volumetric locking. Equation (40) gives

$$\sigma_r = \sigma_\vartheta = \sigma_\varphi = \sigma_m \tag{42}$$

and equation of equilibrium (36) becomes

$$d\sigma_r/dr = 0 \tag{43}$$

from which we find

$$\sigma_r = C_1 \tag{44}$$

At $r = t$ the value of σ_r from eq. (44) must be the same as the value of σ_r from eq. (39). Hence

$$-(2\sqrt{2}/3)(C/t^3) = C_1 \tag{45}$$

Recapitulating we write

$$a \leqq r \leqq t\text{: } \sigma_r = -(2\sqrt{2}/3)(C/r^3), \qquad \sigma_\theta = (\sqrt{2}/3)(C/r^3) \tag{46}$$

$$b \leqq r = b\text{: } \sigma_r = -(2\sqrt{2}/3)(C/t^3), \qquad \sigma_\theta = -(2\sqrt{2}/3)(C/t^3)$$

It is seen that there is always a stress discontinuity for σ_θ at $r = t$.

(c) *Discussion*

If σ_{ra} is the radial stress at $r = a$ and σ_{rb} is the radial stress at $r = b$, then from eqs. (46) we find

$$\sigma_{ra}/\sigma_{rb} = t^3/a^3 \tag{47}$$

As t has already been determined from the displacements, eq. (47) determines the ratio of the inner to outer pressure corresponding to the locking displacements. We observe that the values of σ_{ra} and σ_{rb} are not determined; only their ratio is fixed. We remark also that σ_{ra} and σ_{rb} must always have the same sign because t^3/a^3 is always positive.

From eq. (47) we also see that if the ratio σ_{ra}/σ_{rb} is known, then t is also known. The value of t together with the value of u_a/u_b and eqs. (21) and (22) gives the values of the locking displacements.

From eqs. (21), (22), and (47) it is seen that the radius t of the surface separating the two locking regions is a function of the ratios u_{al}/u_{bl} or σ_{ra}/σ_{rb}. By changing either of these two ratios we can move the surface separating the two locking regions, so that an element of the hollow sphere may change from a condition of distortional locking to a condition of volumetric locking and vice versa. Such a change will be followed, of course, by a change in the stress and strain distribution.

Thus, it is seen that at locking there exist no corresponding single set of values (u_{al}, u_{bl}) but rather a continuous range of sets of values (u_{al}, u_{bl}), with each value of the ratio u_{al}/u_{bl} corresponding to a definite value of the radius t. Once the hollow sphere has locked for a given value of t and for the corresponding values of u_{al} and u_{bl}, we can change the set (u_{al}, u_{bl}, t) to a new set (u'_{al}, u'_{bl}, t') satisfying eqs. (21) and (22), and the hollow sphere will still remain locked. As t cannot become smaller than a or larger than b, it follows that there are limits imposed on the selection of the locking displacements.

References

1. Prager, W., *Trans. Soc. Rheol.*, **1**, 169 (1957).

2. Reiner, M., in *Rheology, Theory and Applications*, F. R. Eirich, ed., Vol. I, Academic Press, New York, 1956, Chap. 2.

3. Freudenthal, A., *The Inelastic Behavior of Engineering Materials and Structures*, Wiley, New York, 1950, p. 220.

4. Prager, W., *Proc. of the IX Intern. Congr. Appl. Mechanics, 9th Congr., Brussels, 1957*, **5**, 205.

5. Phillips, A., *Introduction to Plasticity*, Ronald, New York, 1956, p. 170.

Synopsis

The concept of the ideal locking material, which has been introduced by Prager, is considered for the case of materials which have two equations of state, one for the change in volume and the other for the change in shape. Possible stress-strain relations are discussed. The concepts of volumetric locking and of distortional locking are introduced, and it is shown by means of an example that there are cases in which these two modes of locking are incompatible over the same region of the body. The fundamental differences between locking materials and ideal plastic materials are pointed out. The problem of locking of a hollow sphere is discussed in detail.

TRANSACTIONS OF THE SOCIETY OF RHEOLOGY III, 27–40 (1959)

An Apparatus for Measuring the Dynamic Mechanical Properties of High Polymers at Low Frequencies

R. H. SHOULBERG, F. H. ZIMMERLI, and O. C. KOHLER,
Rohm and Haas Co., Philadelphia, Pennsylvania

I. Introduction

The wide interest currently shown in the dynamic mechanical properties of polymers, both in bulk and in solution, obviates the need for any lengthy introduction to measurements of this type. Several authors have treated the theory and methods for determining these properties; excellent reviews and extensive bibliographies can be found in the recently published *Rheology*.[1]

Morrisson, Zapas, and De Witt[2] have described a torsional pendulum apparatus for measuring the response of a sample to the application of a stress whose magnitude varies sinusoidally with time. This apparatus has virtues in simplicity of construction and operation, in its capability for handling both solid and liquid samples, and in its capabilities for scanning intensively the range of frequency between 10^{-4} and 10 cycles/sec.

The apparatus described in this report was patterned after that of Morrisson, Zapas, and De Witt, but has extensive modifications. In the development of the apparatus, certain difficulties were encountered which should be of interest to other investigators of dynamic mechanical properties.

The two principal objectives achieved by the modifications have been the introduction of continuous automatic recording, on a single chart, of the applied stress and the sample strain; and the introduction of a constant impedance network which, in effect, allows accurate measurements of stress and strain over a large range of specimen rigidity without the need to alter the specimen geometry. In addi-

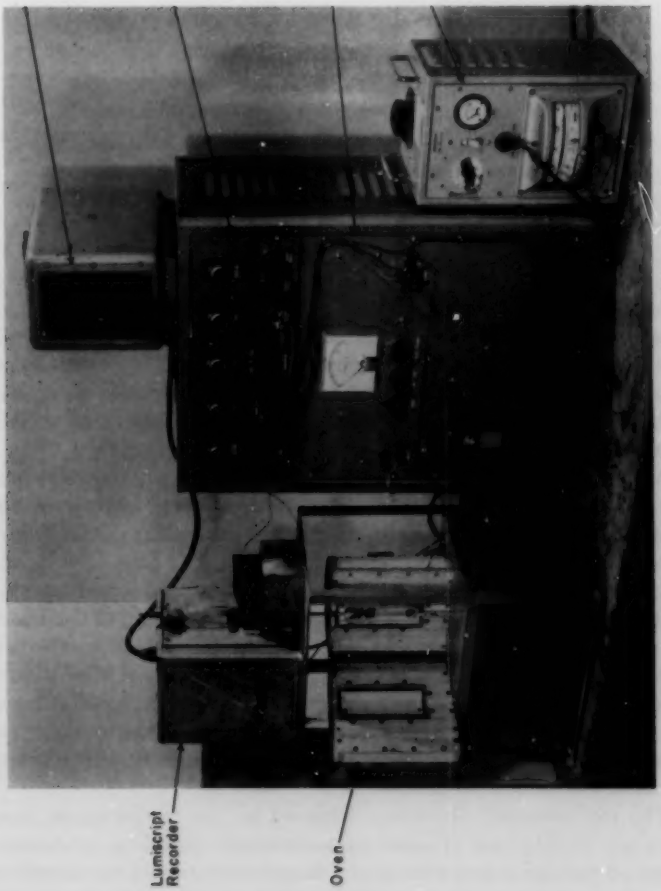

Fig. 1. Overall view of dynamic modulus apparatus.

tion to these features, the apparatus has been made quite compact, rapid changes in the temperature of the sample and its surroundings can be effected, and the stress can be easily changed both in amplitude and frequency.

The apparatus has been used to obtain data on a variety of solid samples; its use with liquid samples is just beginning. Some detailed results on a sample of poly(isopropyl methacrylate), in bulk, will be presented.

II. Description of Apparatus

The apparatus, shown in Figure 1, combines the basic design of Morrisson, Zapas, and De Witt[2] with the unique recording ability of a German Lumiscript RLt4 recorder manufactured by Hartmann and Braun. The torsion pendulum system is basically the same as previously described.[2] The recorder was nicely adaptable for the measurement of the sample strain because visible reflections from a high pressure mercury arc lamp provide an immediately available, yet permanent, record on sensitized chart paper. Normally the image is positioned by a system of mirrors mounted on galvanometers within the recorder. Since it is the oscillation of one of these mirrors which causes the image to sweep back and forth, the oscillation of the strained sample can be recorded if the sample is fitted with a properly designed mirror. Figure 2, a photograph of the sample suspension, shows the result of combining these features. The mirror for recording the strain is mounted on the upper edge of the torque producing coil, which is rigidly attached to the upper edge of the sample.

Calculations of dynamic properties are made from the trace of the torsion pendulum and from the trace of a recorder-mounted galvanometer which measures the torque-producing current passing through the coil. These traces are recorded simultaneously on a common time base on a single chart since the light beams can overlap without interference. The two traces need not have the same axis of symmetry, although by rotation of either the equilibrium position of the sample or of one or more of the mirrors, they can be made to have coincident axes. The traces should, of course, be coincident on the time axis, which means they should lie on the same horizontal line. This can easily be done by raising or lowering the entire sample suspension. Differences in phase and amplitude as frequency and/or

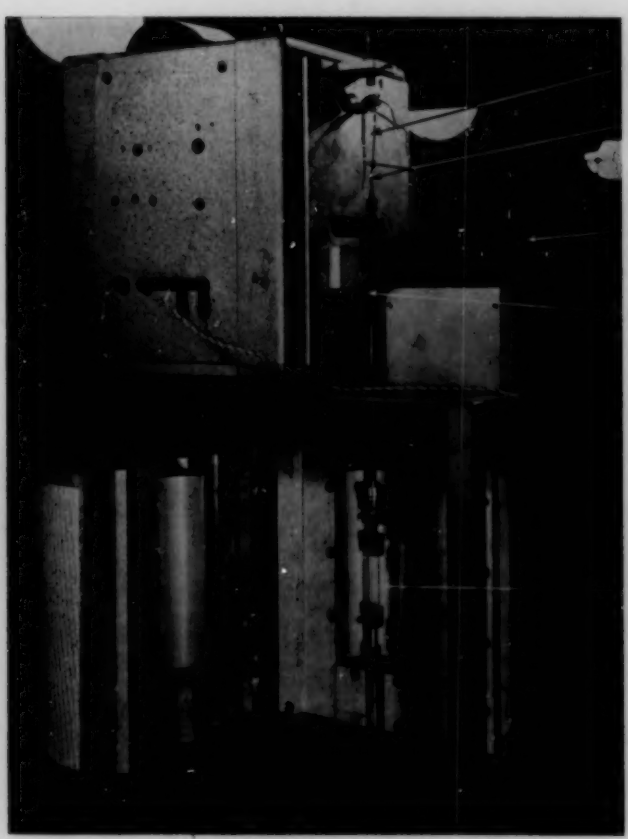

Fig. 2. Enlarged view of specimen suspension.

temperature are changed can thus be easily measured. Recently, the authors found that Lethersich[3] used a similar scheme. He employed a drum camera for recording, whereas in the present apparatus the lack of a need for film development has simplified the collection of data.

The sample suspension is comprised of a rectangular self-supporting coil of 120 turns of 32 gage copper wire hung in the field of a permanent magnetron magnet. A nonlinear magnetic field obtained

by making the pole pieces flat and the inner core round exactly compensates for the nonlinearity obtained in recording a rotating beam on a flat chart. The coil is suspended from a 37 gage copper wire about $3^1/_4$ in. long; electrical lead-in ribbons to the coil are pieces of 0.0007 in. gold foil about $^1/_{16}$ in. wide.

As noted, the mirror is attached to the upper end of the coil; the lower end of the coil supports a stainless steel tube which in turn holds the upper sample clamp. The lower sample clamp is guided in a support which allows vertical freedom of motion but restricts rotation. This support, which weighs about 20 g., can be buoyed up in a pool of mercury if necessary, so that tensile stresses in the specimen will have a negligible effect on measured values of the shear modulus. (A treatment of this effect is given in detail by Timoshenko.[4])

The sinusoidal driving torque is generated in a sine-wave potentiometer (Precision Potentiometer RVP3, Technology Instrument Co., Acton, Mass.) which is driven at 16 different speeds between 0.0004 and 1 cycles/sec. by means of either a 3 r.p.m. or a 60 r.p.m. Barcol synchronous motor driving an Insco geared speed reducer. The output shaft of the reducer also drives the recording film in the recorder via a flexible shaft; therefore, all records have the same cycle length—about 3 in.

Current applied to the torque-producing coil is supplied to the drive coil via an intermediate amplifier. Currents as high as 12 ma. can be applied to the coil. The amplifier is designed to load the 20,000

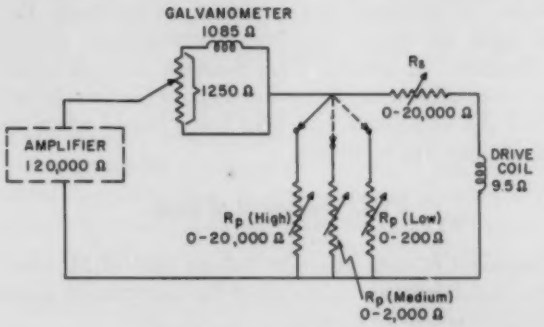

Fig. 3. Resistance network for apparatus.

ohm sine wave potentiometer negligibly and to provide the output current from a high impedance source. The amplifier feeds a resistance network which is shown in Figure 3. By suitable adjustments of R_s and R_p, according to a schedule, the drive coil is made to "see" an almost exactly constant resistance. (As a first approximation it is clear that if the sum of $R_p + R_s$ is made constant in all measurements, the drive coil will be in series with an effectively constant resistance because of the high resistance of the amplifier.) The current galvanometer coil, again because of the high resistance of the amplifier, always sees an external resistance of about 1250 Ω. Electromagnetic damping in the circuit is thus held constant. With this design each signal can be adjusted to produce oscillating amplitudes approximately equal to the recording film half-width, although the specimen rigidity may vary by a factor of a thousand.

The sample is surrounded by an oven which has been designed to combine adequate control of the sample temperature, rapid change of temperature when desired, and modest space requirements. It is constructed of two sections of Transite pipe arranged concentrically, with the space between them filled with glass wool. The sample chamber is heated by an auxiliary heater (25 Ω) and a control heater (125 Ω), each of which is composed of four sections distributed symmetrically about the axis of the oven and shielded from the sample and thermocouple by anodized aluminum semicylinders. The auxiliary heater is controlled by a thermostat (300°C. maximum) which is set slightly below the desired temperature. The control heater is operated from a Duenna controller (manufactured by Instruments for Research and Industry, Cheltenham, Pa.). It is actuated from an iron–Constantan thermocouple placed in the sample chamber. A circular brass chamber through which cooling water can be circulated can be mounted above the oven to prevent the driving coil and suspension wire from being heated when the oven is operated at high temperatures.

III. Treatment of Data

The treatment of data generally follows that of Morrisson et al., with some modifications; repetition of the information given therein will be avoided, wherever possible.

The basic equation of motion for the torsional pendulum is

$$I\left(\frac{d^2\theta}{dt^2}\right) + \left(\frac{\eta'}{A} + B\right)\frac{d\theta}{dt} + \left(\frac{G'}{A} + k_0\right)\theta = k_i i_{dc} \qquad (1)$$

where I is the inertia of the suspension plus the anchored specimen, θ is the angle of rotation of the suspension, t is the time, η' is the dynamic viscosity of the specimen, A is a geometrical factor, B is an instrument damping coefficient, G' is the dynamic shear modulus, k_0 is an instrument stiffness coefficient, k_i is the torque produced by unit current through the drive coil, and i_{dc} is the instantaneous current through the drive coil.

The inertia of a thin rectangular sample with one end anchored is given by

$$I_s = mc^2/36 \qquad (2)$$

where m is the mass of the sample and c is the large dimension of the specimen's cross section. In the apparatus described herein the inertia of the suspension is 18.5 g.-cm.^{2}; I_s is usually about 0.03 g.-cm^2 and can be neglected.

The damping coefficient of the instrument, B, includes air damping, eddy current damping within the drive coil wires themselves as they move in the magnetic field, and resistance damping caused by currents set up in the external circuit by the back EMF produced by the coil moving out of phase with the driving current. The former effects will probably be negligibly small; the latter effect can be significant and variable unless care is taken to minimize it, as can be done by having the coils "see" a large constant external resistance. (The frequencies involved are such that all impedances are almost purely resistive.) In the present instrument B is about 1 dyne-cm./rad./sec.

The stiffness coefficient of the instrument, k_0, includes not only the effects of the suspension wire, but also the effects of any magnetic impurities in the copper wiring of the drive coil, since these will, of course, cause the coil to seek some equilibrium position in the field. In this apparatus magnetic impurities of the order of 1 part in 50,000 are sufficient to make k_0 twice as great as would be the case in their absence. (Pugh[8] has recently presented some data on magnetic effects in 99.999% pure copper.) These impurities cause no difficulty if they are accounted for, but since even magnetic dust particles on the coil become important in a sensitive movement, k_0 should be

determined frequently. In this apparatus k_0 is about 250 dyne-cm./rad.

For a sinusoidal input current to the drive coil it can be shown that the dynamic shear modulus, G', and the dynamic viscosity, η', of the sample are given by:

$$G' = A\left[k_t\left(\frac{i_{dc_0}}{i_{cg_0}}\right)\left(\frac{i_{cg_0}}{\theta_0}\right)\cos\delta_1 - k_0 + I\omega^2\right] \tag{3}$$

$$\eta' = A\left[\frac{k_t}{\omega}\left(\frac{i_{dc_0}}{i_{cg_0}}\right)\left(\frac{i_{cg_0}}{\theta_0}\right)\sin\delta_1 - B\right] \tag{4}$$

where i_{dc_0} is the current amplitude in the drive coil, i_{cg_0} is the current amplitude in the current galvanometer, θ_0 is the amplitude of angular motion of the specimen (a maximum of 4° in this apparatus), δ_1 is the lag angle between input and output, and ω is the circular frequency. In calibrating the apparatus, I, k_0, and B can easily be found by well-known methods. The group $k_t(i_{cg_0}/\theta_0)(i_{dc_0}/i_{cg_0})$ includes the current-torque coefficient k_t and the quantities i_{dc_0}, i_{cg_0} and θ_0. If a 6 v. dry cell in series with a 1000 Ω resistance is used as a current source in place of the amplifier and the traces of θ and i_{cg} are equalized in a steady-state measurement in the absence of a sample by adjusting the various resistances of the impedance network, then i_{dc_0}/i_{cg_0} can be calculated and a value of k_t can be found which, although not truly the torque produced by unit current through the drive coil, is invariant as long as the magnetic field strength and the optical system remain unchanged. In such a measurement the electromagnetic torque is balanced by the torque resulting from twisting the suspension coil, so that

$$k_0 = k_t(i_{cg_0}/\theta_0)/(i_{dc_0}/i_{cg_0}) \tag{5}$$

No dynamic effects are involved and a precise measurement of k_t can easily be made.

IV. Experimental Results

A number of bulk polymers have been investigated in the apparatus. For purposes of demonstrating the type of data which has been obtained, the results of tests on three materials will be reported. These comprise limited measurements on steel and polyisobutylene and more extensive findings on poly(isopropyl methacrylate). Before

presenting these data, however, several things should be mentioned concerning the accuracy of the data and the selection of sample geometries.

The ratio of the amplitudes of the two traces can usually be determined within 1%, unless the sample is so stiff that its amplitude cannot be made roughly equal to the film half-width. The phase angle can be determined within about 1 degree. It will be recognized from an inspection of eqs. (3) and (4) that the accuracy of calculations of G' and η' will vary widely, depending upon the specimen, upon the care used to evaluate k_0, k_1, I, and upon the accuracy of the components of the impedance network. It is desirable to make the cross section of the specimen (relatively) large to avoid excessive tensile stresses; however, the dimensions should also be chosen so that the specimen is neither so stiff at low temperature that its twist amplitude cannot be made large enough for accurate measurement, nor so soft at high temperature that most of the rigidity of the system results from k_0. It is also essential, especially with soft materials, to make the ratio of sample length to sample width as large as possible in order to reduce the importance of any stresses caused by clamping; this point will be discussed in detail shortly. It may not be possible to satisfy all these requirements with a single specimen over large frequency and temperature ranges. With Plexiglas, for example, it has been desirable to introduce one change of sample geometry between 26 and 155°C.; however, for many samples a single specimen is sufficient. The specimens used to date have varied from 2 to 90 mils in thickness, from $^1/_4$ to $^1/_2$ in. in width, and from 1 to 3 in. in length.

Cold-rolled shim steel (0.0021 in. thick) was tested at room temperature. The real part of the complex shear modulus was found to be 11,200,000 psi at both 0.5 and 0.008 cycles/sec., in good agreement with values of the (static) shear modulus given in various engineering handbooks. No phase lag could be detected, indicating very low internal damping.

Measurements on a piece of poly(isobutylene) obtained through the courtesy of Dr. Lawrence A. Wood of the National Bureau of Standards gave, in our initial calculations, values of G' at 26°C. which were higher by an almost constant factor than those reported by Philippoff[5] on material from the same batch. The values of the loss factor, on the other hand, were in good agreement. This suggested

either an error in the measurement of the specimen's dimensions or an error caused by the sample holder constraining the movement of the cross sections at both ends of the specimens. The latter effect has apparently not been discussed in connection with the measurement of dynamic mechanical properties, and in this particular case was the major cause of discrepancies between the two sets of data. For this reason it will be discussed in greater detail. Timoshenko[6] has shown that if a rectangular sample is twisted by movements which in some fashion restrain the warping of the cross sections, the stiffness of the piece is increased, essentially because the normal stresses which restrain the warping also contribute to the strain energy of the bar when it is twisted. If, for example, a narrow rectangular specimen is twisted by a torque M at each end, with a torque $2M$ applied at the mid-section in the opposite sense, the mid-section, because of symmetry, cannot warp. The effective length of the specimen, l', is given by

$$l' = l\left(1 - \frac{\sqrt{5(1+\nu)}}{6}\frac{c}{l}\right) \tag{6}$$

where l is the actual length, ν is Poisson's ratio, and c is the width of the piece; c is assumed to be much greater than the thickness. Obviously, for long narrow specimens this effect is small. Since l/c for our poly(isobutylene) was only about 2.5, it seemed desirable to determine whether any analogous effects were important. We first examined a specimen of low-density polyethylene, on which we were working, and found no significant effects. We later tested a piece of the NBS poly(isobutylene) and indeed found a significant effect. In this latter test we varied l/c and calculated apparent values of G as a function of l/c at fixed frequency (1 cycle/sec.) and temperature. If we assume that

$$l' = l(1 - \psi\, c/l) \tag{7}$$

where ψ is a constant, then for any two tests

$$\frac{l_1'}{l_2'} = \frac{l_1\,(1 - \psi\, c/l_1)}{l_2\,(1 - \psi\, c/l_2)} = \frac{G_2 l_1}{G_1 l_2} \tag{8}$$

If we normalize a series of measurements with respect to test 1, then

$$G_1/G_n = (1 - \psi\, c/l_n)/K \tag{9}$$

where

$$K = 1 - \psi\, c/l_1 \tag{10}$$

The results of our tests are shown in Figure 4, from which it appears that $K \approx 0.91$ and $\psi \approx 0.45$. Considering that the sample was unclamped and reclamped after each change in length, it is gratifying

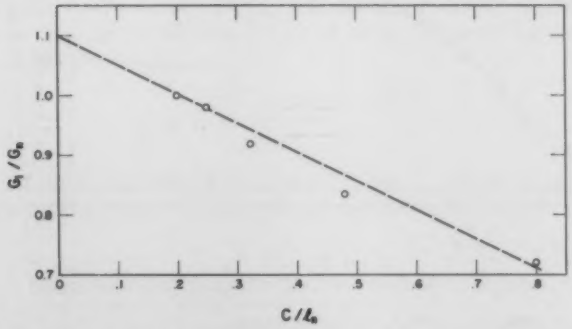

Fig. 4. Dependence of apparent shear rigidity upon specimen geometry for poly-(isobutylene).

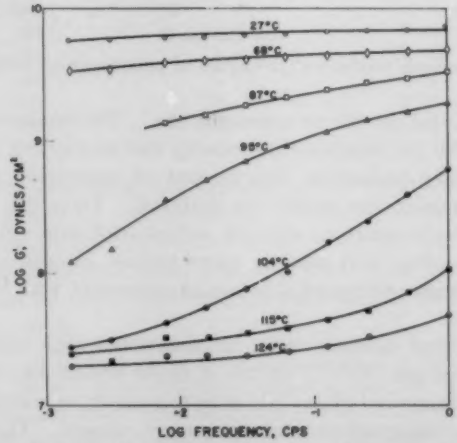

Fig. 5. Real part of complex shear modulus of poly(isopropyl methacrylate).

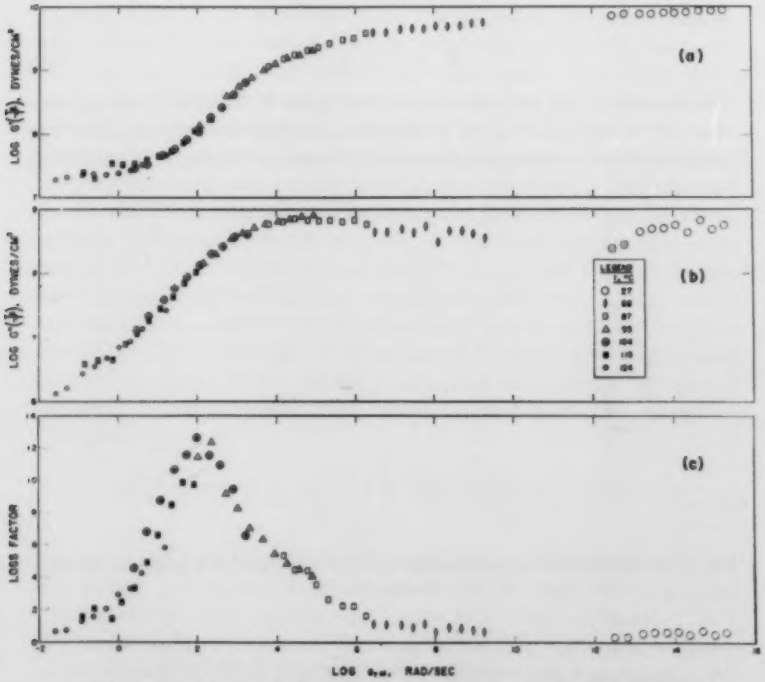

Fig. 6. Dynamic mechanical properties of poly(isopropyl methacrylate).

that the data fall so well on a straight line. The smaller effect of end clamping with polyethylene is probably due to the fact that, with a given clamping technique, the amount of constraint of the cross section is smaller the stiffer the material. Therefore, this source of error is most important with the softest materials. After correcting for this effect and making more precise measurements of the sample thickness, we found substantial agreement with the results of Philippoff.

Poly(isopropyl methacrylate), an amorphous bulk polymer whose glass temperature (81°C.) makes it quite convenient to study in both the rubbery and glassy states in this machine, was studied over fairly wide temperature and frequency ranges. The particular sample tested had a weight-average molecular weight of 320,000.

The real part of the complex shear modulus is shown at several temperatures in Figure 5. Figures 6a, b, and c show the real and imaginary parts of the reduced shear modulus and the loss factor as functions of the reduced frequency, $a_T\omega$. The real part of the complex modulus was given greater weight in determining the a_T's because of the higher accuracy of most of the data. By trial and error it was determined that if the characteristic temperature, T_s, of Williams[7] is chosen as 120°C., then good agreement is shown in the range of validity between values of a_T as predicted by the Williams-Landel-Ferry equation

$$\log a_T = \frac{-8.86\ (T - T_s)}{101.6 + T - T_s} \tag{11}$$

and the values of a_T found by matching the G' curves at different temperatures; a comparison of such values is given in Table I.

TABLE I
Comparison of a_T Values for Poly(isopropyl Methacrylate)

T, °C.	Log a_T from eq. (11)	Log a_T as used in Fig. 6
127	0	(0)
124	0.27	0.40
115	1.18	1.15
104	2.59	2.43
95	4.08	4.10
87	5.75	5.45
68	12.25	8.45
27	554	14.45

One expects increasing discrepancies at temperatures more than about 50°C. below T_s, and this indeed is found to be the case. However, the generally good agreement of the a_T's with those of eq. (11), as well as the other data mentioned, appears to demonstrate that the apparatus can be used to investigate materials in its design range without gross errors.

The authors wish to thank Dr. H. Markovitz and Mr. L. J. Zapas for their aid to the authors, Dr. B. S. Garrett for his continued interest, Mr. M. S. Bechta for aid in the mechanical design of the equipment, Mr. E. A. Taylor for aid in the amplifier design, and Mr. J. A. Shetter and Mrs. E. H. Cherry for collection of data presented herein.

References

1. Eirich, F. R., ed., *Rheology*, Vols. I and II, Academic Press, New York, 1957–1958.

2. Morrisson, T. E., L. J. Zapas, and T. W. DeWitt, *Rev. Sci. Instr.*, **26**, 357 (1955).

3. Lethersich, W., *J. Sci. Instr.*, **27**, 303 (1950).

4. Timoshenko, S., *Strength of Materials*, Part II, Van Nostrand, New York, 1941, pp. 298–304.

5. Philippoff, W., *J. Appl. Phys.*, **24**, 685 (1953).

6. Timoshenko, S., *Theory of Elasticity*, McGraw-Hill, New York, 1934, pp. 273–276.

7. Williams, M. L., *J. Phys. Chem.*, **59**, 95 (1955).

8. Pugh, E. W., *Rev. Sci. Instr.*, **29**, 1118 (1958).

Synopsis

An apparatus is described for low-frequency measurements (0.0004 to 1 cycles/sec.) of the dynamic mechanical properties of polymers. The apparatus is basically a modified version of the Morrisson-Zapas-De Witt machine at The Mellon Institute. The modifications consist principally in (*1*) using reflected light beams from a mercury arc source to trace both input and response curves on a photosensitive film, thus providing a common time base for recording without resorting to the use of any intermediate electrical system, and (*2*) using a constant impedance network to independently vary the recorded amplitude of the input and output traces, thus allowing accurate measurements of amplitude ratios over the entire frequency and temperature ranges (25–250°C.) without altering the geometry of the specimen. The calibration of the instrument and data treatment are discussed, and examples of the measurements made on solid samples are given.

TRANSACTIONS OF THE SOCIETY OF RHEOLOGY III, 41–59 (1959)

Stress Analysis for Linear Viscoelastic Materials*

E. H. LEE, J. R. M. RADOK,† and W. B. WOODWARD,‡ *Division of Applied Mathematics, Brown University, Providence, Rhode Island*

1. Introduction

In recent years methods have been developed for the determination of stress distributions in linear viscoelastic materials. Such solutions display features in marked contrast to the analogous distributions for elastic bodies, and these differences can have important significance technologically in the application of polymers. The purpose of this paper is to show that a variety of types of mathematical problems arise in determining stress distributions in linear viscoelastic bodies, and to present examples of two types of solution with comments on features which can be of significance in design. It is felt worthwhile to present such examples in detail, since the earlier literature has not discussed specific practical examples with consideration of design features.

The general problem of stress analysis is to determine the stress components $\sigma_{ij}(x_k,t)$ throughout a body, such as that shown schematically in Figure 1, when the loading and constraint of the surface are prescribed, as well as the body forces $f_i(x_k,t)$. Cartesian coordinates x_i are used, with i taking on the values 1, 2, and 3; the usual vector and tensor suffix notation are adopted. Thus, $\sigma_{ij}(x_k,t)$ signifies the variation of the stress components σ_{11}, σ_{12}, ..., as functions of position in the body (x_1, x_2, x_3) and the time t. Time arises in an essential way because of the viscoelasticity of the materials

* Sponsored under Department of Defense Contracts, NORD 11496 and 16471 between the Bureau of Ordnance, Navy Department, and Brown University.

† Present address: Department of Aeronautical Engineering and Applied Mechanics, Brooklyn Polytechnic Institute, Brooklyn, New York.

‡ Present address: Lincoln Laboratories, Massachusetts Institute of Technology, Lexington, Massachusetts.

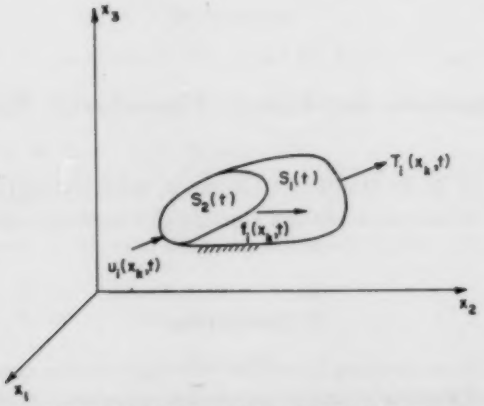

Fig. 1. Boundary conditions for the body V.

under consideration, and the boundary data prescribed are in general functions of time, as are the resulting dependent variables. This applies even for the quasi-static situation, for which inertia forces are negligible compared with applied forces. Figure 1 indicates that the boundary traction T_i is prescribed over the part S_1 of the surface S, and the displacement u_i over the part S_2, and that the regions S_1 and S_2 may vary with time. Other mixed combinations of traction components and displacement components can also be prescribed as in elasticity theory; for example: prescribed shear traction and normal displacement.

The stress components σ_{ij} must be chosen to satisfy the constitutive equations for the linear viscoelastic material under consideration. The analysis is here limited to infinitesimal strain, so that the strain components are represented in terms of the displacement vector u_i according to:

$$\epsilon_{ij} = 1/2[(\partial u_i/\partial x_j) + (\partial u_j/\partial x_i)] \tag{1.1}$$

For linear isotropic viscoelasticity, two independent pairs of viscoelastic operators are needed, analogously to the two independent elastic constants of isotropic elasticity. Choosing these to relate shear and dilatational behavior respectively, and writing s_{ij} and e_{ij} for the deviator or shear components of the stress and strain tensors, respectively, the constitutive equations take the form:

$$P(s_{ij}) = Q(e_{ij}) \tag{1.2}$$

$$P'(\sigma_{ii}) = Q'(\epsilon_{ii}) \tag{1.3}$$

where the operator pairs P,Q and P',Q' can take any of the various forms, differential, integral, or complex algebraic, by which linear viscoelastic relations can be represented,[1] and where the usual repeated suffix summation convention is utilized: $\sigma_{ii} = \sigma_{11} + \sigma_{22} + \sigma_{33}$.

The equations of motion must also be satisfied:

$$(\partial\sigma_{ij}/\partial x_j) + f_i = \rho(\partial^2 u_i/\partial t^2) \tag{1.4}$$

where ρ is the density and f_i the body force per unit volume.

In addition to the field equations, compatibility of the stress and displacement variables with the prescribed boundary conditions requires that:

$$T_i = \sigma_{ij}n_j \text{ on } S_1 \tag{1.5}$$

$$u_i \text{ prescribed on } S_2 \tag{1.6}$$

where n_j is the outward normal unit vector.

The eqs. (1.1) to (1.4) form a system of linear partial differential equations in the independent variables x_i and t. Boundary conditions are given by eqs. (1.5) and (1.6), and in general initial conditions over the body V at zero time will be required. Here consideration is limited to initially undisturbed bodies.

For the special circumstances that the form of the body V does not vary with time, apart from the infinitesimal displacements associated with the strain, and that the regions S_1 and S_2 over which load and displacement conditions are prescribed also are invariant with respect to time, application of the Laplace transform[2] removes the time from the equations and boundary conditions and reduces the viscoelastic problem to an equivalent elastic problem, known as the associated elastic problem.[3] This then brings to bear on the problem the extensively developed methods of the theory of elasticity, and Laplace inversion of any particular stress component so evaluated provides the stress distribution for the original viscoelastic problem. An example of this approach is given in Section 2 of this paper.

If the form of the body varies with time, such as the annihilation of material in a burning out rocket grain, this method does not apply since the Laplace transform is an integral over time from zero to

infinity, which is not defined for the part of the material which only exists for a finite time. Nor does the method apply if S_1 and S_2 vary with time, for then at a particular surface point the prescription of surface traction T_i, for example, will apply only up to a certain time t_1 when the boundary between S_1 and S_2 traverses the point, and thereafter u_i will be prescribed. Thus the Laplace transform, being an integral from zero to infinity in time, cannot be determined for either traction or displacement, one of which would be needed to specify the associated elastic problem.

When the Laplace transform method cannot be used, a tentative method of approach is available in terms of the sequence of elastic problems for the instantaneous boundary values at each time t, but a check by an alternative approach is called for. This can take the form of application of the Laplace transform in an inverse way when enough additional information has been deduced to make its application possible. Such an example is the solution of the contact problem for viscoelastic bodies.[5]

At the present time no general method of approach appears to be available when the Laplace transform is not applicable, but specialized problems can be treated by particular methods. An example is given in Section 3 of this paper by the determination of stresses in a thick walled cylinder of viscoelastic material subjected to internal pressure with annihilation of material associated with a continuously increasing inner radius.

2. Stresses in an Externally Reinforced Viscoelastic Cylinder

As an example which can be treated by application of the Laplace transform, consider the thick walled viscoelastic cylinder shown in

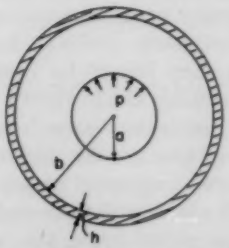

Fig. 2. Reinforced viscoelastic cylinder subjected to internal pressure.

Figure 2, reinforced by an external elastic sheet and subjected to internal pressure. The cylinder is assumed to be long, and the deformation plane strain with no axial motion. Inertia forces will be neglected, which will be permissible if the load durations considered are long compared with the time for stress wave propagation across the cylinder. The resulting quasi-static analysis is obtained by substituting $\rho = 0$ in eq. (1.4). Denoting the Laplace transform of a function $f(t)$ by $\bar{f}(p)$, where p is the transform parameter,[2] eq. (1.1) becomes:

$$\bar{\epsilon}_{ij}(x_k,p) = 1/2[(\partial\bar{u}_i/\partial x_j) + (\partial\bar{u}_j/\partial x_i)] \tag{2.1}$$

and eq. (1.4), for the case needed here of zero body forces and negligible inertia forces, becomes:

$$\partial\bar{\sigma}_{ij}/\partial x_j = 0 \tag{2.2}$$

The boundary conditions take the form:

$$\bar{T}_i = \bar{\sigma}_{ij}n_j \text{ on } S_1 \tag{2.3}$$

$$\bar{u}_i = \text{prescribed on } S_2 \tag{2.4}$$

The constitutive eqs. (1.2) and (1.3) are modified by application of the Laplace transform, since the operators become algebraic multipliers which are functions of the transform parameter p:

$$\bar{P}\bar{s}_{ij} = \bar{Q}\bar{e}_{ij} \tag{2.5}$$

$$\bar{P}'\bar{\sigma}_{ii} = \bar{Q}'\bar{\epsilon}_{ii} \tag{2.6}$$

For differential operators, which are associated with the common finite spring-dashpot models for viscoelastic materials, the $\partial/\partial t$ in the viscoelastic operators is simply replaced by p in the transformed operators, for initially undisturbed conditions.[2]

The system of equations and boundary conditions (2.1)–(2.6) constitutes the associated elastic problem for the determination of $\bar{\sigma}_{ij}(x_k,p)$. The usual elastic constants corresponding to eqs. (2.5) and (2.6) are the shear modulus:

$$G = \bar{Q}/2\bar{P} \tag{2.7}$$

and the bulk modulus:

$$K = \bar{Q}'/3\bar{P}' \tag{2.8}$$

The other corresponding elastic constants can be deduced in the usual way from these (ref. 6, p. 10), so that solutions in terms of, say, Young's modulus and Poisson's ratio can be utilized if this representation is more convenient. Bars will be retained over the elastic constants deduced from viscoelastic operators as a reminder of their significance. They represent transforms of the corresponding viscoelastic operators, for example, Young's modulus $\bar{E}$ is the quotient of the transformed operator pair which relates simple longitudinal stress and the corresponding strain for the viscoelastic body.

The particular problem of the thick cylinder under consideration can be solved directly in cylindrical polar coordinates (r,θ,z) in terms of the well known general Lamé solution (ref. 6, p. 56):

$$\sigma_{rr} = A' - (B'/r^2) \tag{2.9}$$

$$\sigma_{\theta\theta} = A' + (B'/r^2) \tag{2.10}$$

where A' and B' are constants in the elastic case or arbitrary functions of the transform parameter for the associated elastic problem. They are determined by the boundary conditions at the inner and outer radii, $r = a$, $r = b$, respectively. The internal pressure $\Pi(t)$ is prescribed, and for this traction eq. (2.3) takes the form

$$\bar{\Pi}(p) = -\sigma_{rr}, \qquad r = a \tag{2.11}$$

The boundary condition at $r = b$ must express the equilibrium between the stress in the reinforcement and the radial pressure on the cylinder, and the equality of the circumferential strain of the cylinder and the reinforcement in contact with it. The reinforcement is assumed to be thin so that membrane theory can be used with the neglect of bending influences. If $\bar{F}$ is the transformed circumferential tension in the reinforcement, then radial equilibrium at $r = b$ demands that:

$$\bar{F}d\theta = -\sigma_{rr}b\, d\theta \tag{2.12}$$

Using Hooke's law for the circumferential strain in the case of zero axial displacement (ref. 6, p. 23), and the suffix R for the elastic constants of the elastic reinforcing material of thickness h, the equality of the circumferential strain requires that:

$$\epsilon_{\theta\theta}(b,p) = \frac{\bar{F}}{h}\frac{(1-\nu_R^2)}{E_R} = \frac{\sigma_{\theta\theta}(1-\nu^2) - \nu(1+\nu)\sigma_{rr}}{\bar{E}} \tag{2.13}$$

where E is Young's modulus and ν Poisson's ratio. Note that because the reinforcement is elastic, E_R and ν_R are constants, and not functions of the parameter p. Elimination of $\bar{F}$ between eqs. (2.12) and (2.13) leads to the boundary condition:

$$\bar{\sigma}_{rr} = \bar{\sigma}_{\theta\theta} \frac{\alpha(1 - \bar{\nu}^2)}{\alpha\bar{\nu}(1 + \bar{\nu}) - \bar{E}}, \qquad r = b \tag{2.14}$$

where the constant $\alpha = E_R h/(1 - \nu_R^2)b$ contains the properties of the reinforcement. This is a more involved type of boundary condition than prescribed traction or displacement, but since it is the transform of a boundary condition in the viscoelastic case which does not change in form throughout the loading duration, it falls within the scope of the transform method of solution.

Substituting the boundary conditions (2.11) and (2.14) into the general solution, eqs. (2.9) and (2.10) permit A' and B' to be evaluated, giving the required particular solution:

$$\bar{\sigma}_{rr} = -\bar{\Pi} \frac{\dfrac{\alpha(1 - \bar{\nu}^2)}{\alpha\bar{\nu}(1 + \bar{\nu}) - \bar{E}} \left(\dfrac{b^2}{r^2} + 1\right) - \left(\dfrac{b^2}{r^2} - 1\right)}{\dfrac{\alpha(1 - \bar{\nu}^2)}{\alpha\bar{\nu}(1 + \bar{\nu}) - \bar{E}} \left(\dfrac{b^2}{a^2} + 1\right) - \left(\dfrac{b^2}{a^2} - 1\right)} \tag{2.15}$$

$$\bar{\sigma}_{\theta\theta} = \bar{\Pi} \frac{\dfrac{\alpha(1 - \bar{\nu}^2)}{\alpha\bar{\nu}(1 + \bar{\nu}) - \bar{E}} \left(\dfrac{b^2}{r^2} - 1\right) - \left(\dfrac{b^2}{r^2} + 1\right)}{\dfrac{\alpha(1 - \bar{\nu}^2)}{\alpha\bar{\nu}(1 + \bar{\nu}) - \bar{E}} \left(\dfrac{b^2}{a^2} + 1\right) - \left(\dfrac{b^2}{a^2} - 1\right)} \tag{2.16}$$

In order to evaluate the stress distribution for a particular example, the internal pressure is taken to be suddenly applied at $t = 0$, and maintained constant thereafter of magnitude Π_0, which determines:[2]

$$\bar{\Pi} = \Pi_0/p \tag{2.17}$$

The operators for a particular viscoelastic material for the cylinder must be inserted, and a material elastic in dilatation and behaving as a Maxwell body in shear is assumed, thus giving for the special cases of eqs. (1.2) and (1.3):

$$[A(\partial/\partial t) + B]\varepsilon_{ij} = (\partial/\partial t)e_{ij} \tag{2.18}$$

$$\sigma_{ii} = C\epsilon_{ii} \tag{2.19}$$

where A, B, and C are material constants. The shear behavior (2.18) corresponds to the Maxwell viscoelastic model shown in Figure 3. The corresponding transformed relations, equivalent to eqs. (2.5) and (2.6) are:

$$(Ap + B)\bar{s}_{ij} = p\bar{e}_{ij} \tag{2.20}$$

$$\bar{\sigma}_{ii} = C\bar{\epsilon}_{ii} \tag{2.21}$$

The equivalent $\bar{G}$ and $\bar{K}$ according to eqs (2.7) and (2.8) determine the corresponding $\bar{E}$ and $\bar{\nu}$ (ref. 6, p. 10) in the form:

$$\bar{E} = \frac{3Cp}{(2AC + 1)p + 2BC}, \qquad \bar{\nu} = \frac{(AC - 1)p + BC}{(2AC + 1)p + 2BC}$$

and substitution into eqs. (2.15) and (2.16) determines the transforms of the stresses for the particular problem considered:

$$\bar{\sigma}_{rr} = -\frac{\Pi_0}{p}\left[\frac{\left[\left(1 - \frac{b^2}{r^2} - \alpha A\right)\left(2AC + 1\right) - 3\alpha A\,\frac{b^2}{r^2}\right]p^2 + \left[\left(1 - \frac{b^2}{r^2}\right)2BC - \alpha B\left(3\,\frac{b^2}{r^2} + 4AC + 1\right)\right]p - 2\alpha B^2C}{\left[\left(1 - \frac{b^2}{a^2} - \alpha A\right)\left(2AC + 1\right) - 3\alpha A\,\frac{b^2}{a^2}\right]p^2 + \left[\left(1 - \frac{b^2}{a^2}\right)2BC - \alpha B\left(3\,\frac{b^2}{a^2} + 4AC + 1\right)\right]p - 2\alpha B^2C}\right] \tag{2.22}$$

$$\bar{\sigma}_{\theta\theta} = -\frac{\Pi_0}{p}\left[\frac{\left[\left(1 + \frac{b^2}{r^2} - \alpha A\right)\left(2AC + 1\right) + 3\alpha A\,\frac{b^2}{r^2}\right]p^2 + \left[\left(1 + \frac{b^2}{r^2}\right)2BC - \alpha B\left(-3\,\frac{b^2}{r^2} + 4AC + 1\right)\right]p - 2\alpha B^2C}{\left[\left(1 - \frac{b^2}{a^2} - \alpha A\right)\left(2AC + 1\right) - 3\alpha A\,\frac{b^2}{a^2}\right]p^2 + \left[\left(1 - \frac{b^2}{a^2}\right)2BC - \alpha B\left(3\,\frac{b^2}{a^2} + 4AC + 1\right)\right]p - 2\alpha B^2C}\right] \tag{2.23}$$

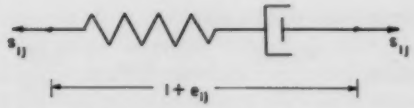

Fig. 3. Maxwell model for the assumed viscoelastic properties in shear.

Such a form of transform, consisting of the ratio of polynominals in p, can readily be inverted by the method of partial fractions[2] to give the variation of the stress distribution in the viscoelastic case. This procedure involves the evaluation of the roots of the quadratic denominator, which would lead to cumbersome expressions in the general algebraic form of eqs. (2.22) and (2.23), so that particular material constants have been substituted to permit numerical evaluation.

Typical values have been selected. The bulk modulus $K = C/3$ is taken to be the same as for water: 10^5 p.s.i. Young's modulus for instantaneous elastic response, which with K determines the constant A, is taken to be $E = 10^5$ p.s.i., and this corresponds to $A = {}^4/_3 \times 10^{-5}$. The only time which appears in the problem is the relaxation time of the Maxwell behavior, $\tau_0 = A/B$ time units, and so for convenience time measurement is taken in terms of this unit, so that $\tau_0 = 1$ and $A = B$. b/a is taken to be 2, and h/b to be ${}^1/_{32}$ (this corresponds roughly to $h = {}^1/_8''$ for $b = 4''$). The reinforcement is assumed to be steel with $E_R = 3 \times 10^7$ p.s.i., $\nu_R = 1/\sqrt{11}$, which determines $\alpha = 10^6$.

With these numerical values,

$$\vartheta_{rr} = -\frac{\Pi_0}{p}\frac{[333p^2 + 656p + 320] + (b^2/r^2)\,[147p^2 + 144p]}{921p^2 + 1232p + 320}$$

for example, which in terms of partial fractions can be written

$$\vartheta_{rr} = -\frac{\Pi_0}{p}\left[\left(.3616 + \frac{.005282}{p + .9849} + \frac{.2233}{p + .3528}\right) + \frac{b^2}{r^2}\left(1.596 - \frac{.001320}{p + .9849} - \frac{.05583}{p + .3528}\right)\right]$$

This can be inverted directly to give:

$$\sigma_{rr} = -\Pi_0 \left[\left\{ .3616 + \frac{.005282}{.9849} (1 - e^{-.9849t}) + \frac{.2233}{.3528} (1 - e^{-.3528t}) \right\} + \frac{b^2}{r^2} \left\{ .1596 - \frac{.001320}{.9849} (1 - e^{-.9849t}) - \frac{.05583}{.3528} (1 - e^{-.3528t}) \right\} \right]$$

with similar relations for $\sigma_{\theta\theta}$. These functions are plotted in Figures 4 and 5 to give the stress distributions as functions of the radius at several values of time.

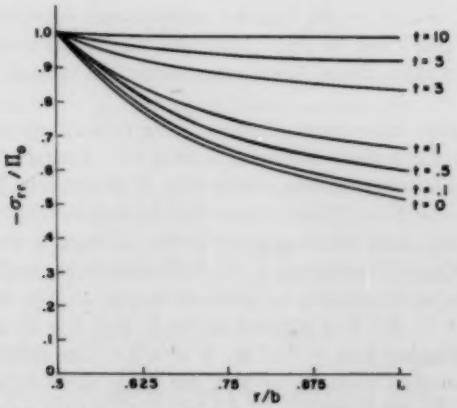

Fig. 4. Variation of the distribution of radial compressive stress.

It is seen that although the internal pressure Π_0 remains constant, the stress distribution for the viscoelastic cylinder varies very markedly with time. This is in sharp contrast with the elastic situation for which an invariant stress distribution would be obtained under constant pressure. In general the viscoelastic nature of a material causes variations of the stress distribution with constant surface loading.

Figure 4 shows that the radial compressive stress at the outside, $r = b$, increases gradually from about half the internal pressure to the full internal pressure for long durations of loading compared with the relaxation time of the material in shear. This is associated with the relaxation of the shear strength of the cylinder material, according to

its Maxwell behavior (Fig. 3), while it is constrained by the reinforcement. The shear strength relaxes to zero, and the viscoelastic material behaves as a liquid under uniform hydrostatic pressure so that the full internal pressure is transmitted to the reinforcement. The circumferential stress is then also uniform hydrostatic pressure, of magnitude Π_0. Since the tension in the reinforcement F is directly proportional to the external radial compressive stress in the cylinder according to eq. (2.12), F increases gradually on application of the constant internal pressure. Thus initially the viscoelastic cylinder supports part of the internal pressure, but this is gradually transferred to the steel reinforcement.

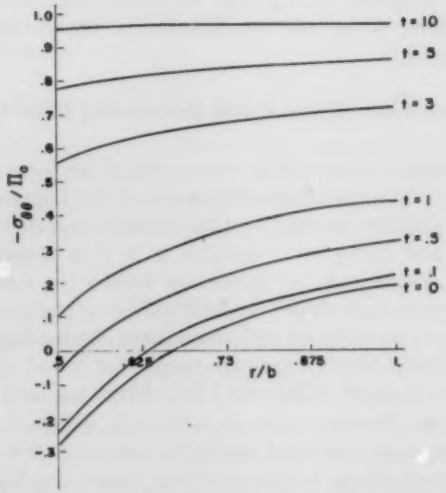

Fig. 5. Variation of the distribution of circumferential compressive stress.

Figure 5 shows that initially hoop tension occurs adjacent to the bore of the cylinder. The magnitude, and even the sign of this, depends on the stiffness of the reinforcement and the radius ratio b/a. This circumferential tension changes to compression as the pressure is maintained, and finally the limit of uniform hydrostatic compression is reached when the shear strength has relaxed to zero.

These features can have an important influence on the design of such a cylinder. If, for example, a pulse of pressure is to be applied

for a limited time, the delay in the buildup of tension in the reinforcement may be utilized to ease the design problem for the reinforcement by choosing the relaxation time of the cylinder material to prevent full transmission of the internal pressure before it decreases. The linearity of the problem permits the analysis for a pulse of stress to be obtained from the present solution by superposition.

The change to biaxial compression caused by the viscoelasticity of the cylinder material may be useful in preventing the initiation of fracture cracks. The initial hoop tensile stress could be reduced by applying the internal pressure gradually, and this again is a feature of viscoelastic response which provides freedom to meet design criteria which is not available in the case of elastic materials. It is the additional degree of freedom associated with the variation in time which permits this.

3. Stresses in a Cylinder with Annihilating Inner Radius

As an example of a viscoelastic stress analysis problem which is not amenable to treatment through application of the Laplace transform, the cylinder problem similar to that treated above, but with an annihilating inner radius: $r = a(t)$, $da/dt > 0$, is considered in this section. The problem is to be treated within the confines of infinitesimal displacement theory, and the motion of the inner boundary $r = a(t)$ is not to be confused with the particle motion there. At any time t_1 the material which initially corresponded to $r < a(t_1)$ has been annihilated, for example, burned and removed as gas, and the particle displacement at the boundary is $u(a(t_1),t_1)$ which is considered infinitesimal in magnitude and negligible compared with the radius $a(t_1)$. As pointed out in Section 1 of this paper, the Laplace transform cannot be used since material at radius r_1 only exists for a finite time t_1 given by $r_1 = a(t_1)$, so that the transform of stress or displacement at this radius is not defined. No general methods of attack on this kind of problem are at present available, so that a specialized procedure is sought.

In order that the direct approach detailed below can be applied, the problem is restricted to the situation, which is common for viscoelastic materials, in which shear strains dominate the deformation, so that dilatational strains can be neglected and the theory of incompressible motion applied. For the plane strain situation with

no axial motion, incompressibility prescribes the radial displacement to be of the form:

$$u(r,t) = k(t)/r \tag{3.1}$$

since with no volume change the outflow of material across each radius, $2\pi ru$, must be the same for all radii at a given instant t. $k(t)$ is an arbitrary function. Equation (3.1) corresponds to the strain components:

$$\epsilon_\theta = u/r = k(t)/r^2 \tag{3.2}$$

$$\epsilon_r = \partial u/\partial r = -k(t)/r^2 \tag{3.3}$$

The viscoelastic relation (1.2) can be conveniently written in terms of stress differences:

$$P(\sigma_\theta - \sigma_r) = Q(\epsilon_\theta - \epsilon_r) = Q(2k(t)/r^2) \tag{3.4}$$

For the coordinate system (r, θ, z) all shear components of stress and strain are zero by symmetry, so that the single suffix notation for components of stress and strain is satisfactory. In cylindrical coordinates, the equilibrium equation (1.4) without body force and inertia terms is:

$$r(\partial\sigma_r/\partial r) = \sigma_\theta - \sigma_r \tag{3.5}$$

so that σ_θ can be eliminated between eqs. (3.4) and (3.5) to give:

$$P(r(\partial\sigma_r/\partial r)) = Q(2k(t)/r^2) \tag{3.6}$$

The time operators and space derivative can be permuted since r and t are independent variables, and integration of eq. (3.6) with respect to r gives:

$$P(\sigma_r) = -Q(k(t))/r^2 + k_1(t) \tag{3.7}$$

where $k_1(t)$ is another arbitrary function of time. Equations (3.5) and (3.7) then give:

$$P(\sigma_\theta) = Q(k(t))/r^2 + k_1(t) \tag{3.8}$$

This general solution is analogous to the transform solution (2.9), (2.10), but contains the viscoelastic operators P and Q. As before the two arbitrary coefficients are determined by the boundary conditions at $r = a(t)$, and $r = b$.

The equilibrium condition for the reinforcement (2.12) applies for nontransformed variables, and the circumferential strain compatibility can be written down directly from (3.2):

$$\frac{k(t)}{r^2} = \frac{F}{h}\frac{(1 - \nu_R^2)}{E_R} \tag{3.9}$$

Combination of these leads to the boundary condition:

$$\frac{k(t)}{r^2} = -\frac{b}{h}\frac{(1 - \nu_R^2)}{E_R}\sigma_r, \qquad r = b \tag{3.10}$$

Elimination of σ_r between eqs. (3.7) and (3.10) determines $k_1(t)$ in terms of $k(t)$:

$$k_1(t) = -\frac{1}{b^2}\left(\frac{P}{C} - Q\right)(k(t)) \tag{3.11}$$

where $C = (b/h)(1 - \nu_R^2/E_R)$ is a constant expressing the properties of the reinforcement. This provides a new relation for the radial stress by substituting eq. (3.11) in eq. (3.7):

$$P(\sigma_r) = -\frac{Q(k(t))}{r^2} - \frac{1}{b^2}\left(\frac{P}{C} - Q\right)(k(t)) \tag{3.12}$$

From this $k(t)$ must be determined to satisfy the boundary condition at the surface of the cavity:

$$\sigma_r = -\Pi(t), \qquad r = a(t) \tag{3.13}$$

In general, this combination of relations to determine $k(t)$ is not easy to treat, since $p(\sigma_r)$ in eq. (3.12) is a time operator for fixed radius, and eq. (3.13) gives only the instantaneous value σ_r as the moving boundary passes through the radius $a(t)$. Thus the operator P cannot be applied directly to $\Pi(t)$.

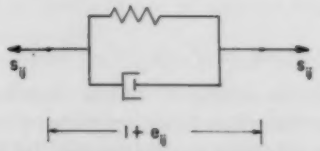

Fig. 6. The Kelvin or Voigt model for assumed viscoelastic properties in shear.

This difficulty does not arise in the case of the Kelvin delayed elastic material corresponding to the viscoelastic model shown in Figure 6, for then:

$$P = 1, \quad Q = H(\partial/\partial t) + J \tag{3.14}$$

where H and J are material constants. This case is considered below, and substitution of $-\Pi(t)$ on the left-hand side of eq. (3.12) for $r = a(t)$ gives a differential equation for the determination of $k(t)$:

$$H\left(\frac{1}{[a(t)]^2} - \frac{1}{b^2}\right)\frac{dk}{dt} + \left(J\left[\frac{1}{[a(t)]^2} - \frac{1}{b^2}\right] + \frac{1}{b^2C}\right)k = \Pi(t) \tag{3.15}$$

$k(t)$ is obtained from eq. (3.15) with the initial condition $k = 0$, since for the Kelvin material there is no instantaneous strain when the internal pressure is first applied. The relations detailed above then determine the entire stress and strain history for the viscoelastic cylinder.

For many choices of $a(t)$ it will be necessary to solve eq. (3.15) numerically, but a solution in terms of tabulated functions can be obtained by taking:

$$a(t) = a_0/(1 - \kappa t)^{1/2} \tag{3.16}$$

which approximates constant velocity annihilation for $r/a_0 < 2$. The corresponding displacement vs. time plots for various ratios b/a_0 are shown in Figure 7, where the time is measured as a proportion of the annihilation time t_0 for which $a(t_0) = b$. It is seen that for $b^2/a_0^2 = 2$, a significant approximation to constant velocity annihilation is achieved by this representation.

For this boundary motion, eq. (3.15) takes the form:

$$\frac{dk}{dt} + \left[\frac{1}{\tau_0} + \frac{1}{\tau_R\left(1 - \dfrac{t}{t_0}\right)}\right]k = \frac{\Pi(t)}{H\left(\dfrac{1}{a_0^2} - \dfrac{1}{b^2}\right)\left(1 - \dfrac{t}{t_0}\right)} \tag{3.17}$$

where $\tau_0 = H/J$ is the delay time for the Kelvin law (3.14) and $\tau_R = CH((b^2/a_0^2) - 1)$ has the dimensions of time and is associated with the viscosity of the cylinder material and the elasticity of the casing. It can thus be thought of as a retardation time associated with the casing.

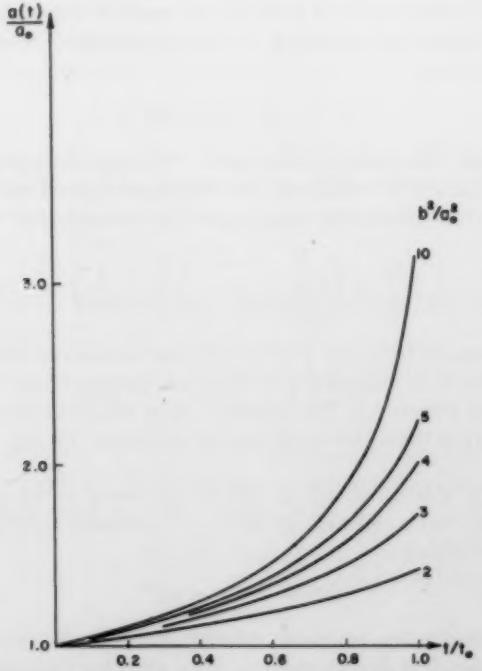

Fig. 7. Displacement vs. time plots for annihilation of the inner boundary according to eq. (3.16) for various ratios b^2/a_0^2.

Equation (3.17) can be integrated directly using the integrating factor:

$$e^{t/\tau_0}\left(1-\frac{t}{t_0}\right)^{-t_0/\tau_R}$$

which transforms the left-hand side into a complete differential, giving:

$$k(t)=\frac{e^{-t/\tau_0}\left(1-\dfrac{t}{t_0}\right)^{t_0/\tau_R}}{H\left(\dfrac{1}{a_0^2}-\dfrac{1}{b^2}\right)}\int_0^t\frac{\Pi(t)\,e^{t/\tau_0}}{\left(1-\dfrac{t}{t_0}\right)^{1+(t_0/\tau_R)}}\,dt \qquad (3.18)$$

For constant internal pressure $\Pi(t) = \Pi_0$, this integral can be evaluated in terms of the exponential integral tabulated in ref. 7 for integral values of t_0/σ_R. Intermediate results can then be obtained by interpolation.

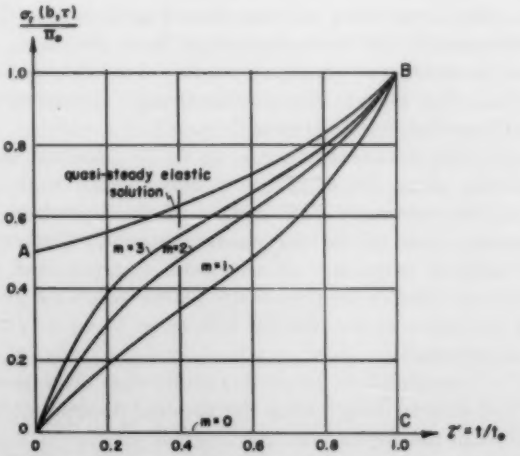

Fig. 8. Variation of the radial stress at the reinforcement with time for several values of the annihilation time.

The radial stress at $r = b$ determines the stress in the reinforcement, and is given by eq. (3.12) or eq. (3.9) and eq. (2.12), to be

$$\sigma_r = -k(t)/b^2C \tag{3.19}$$

The variation of $\sigma_r(b,\tau)$ as a proportion of the internal pressure Π_0 is shown in Figure 8, where τ is the time t expressed as a proportion of the annihilation time t_0. The calculation was carried out for equality of the delay time τ_0 of the cylinder material and the casing retardation time τ_R, and for several values of $m = t_0/\tau_R$. The curves of Figure 8 thus demonstrate the time histories of the stress in the reinforcement for different annihiliation times for a given cylinder and casing.

For m other than ∞, all curves in Figure 8 pass through the origin. This arises since the Kelvin material, Figure 6, does not exhibit instantaneous elastic response, so that on first application of the

pressure the displacement is zero instantaneously, and no stress is generated in the reinforcement. For $m \to \infty$, that is, long annihilation time, viscoelastic flow takes place for finite time t, but zero t/t_0, since $t_0 \to \infty$. Thus finite stress appears in the reinforcement while $t/t_0 = 0$.

For m other than zero, all curves in Figure 8 pass through B, which indicates the full internal pressure Π_0 on the casing at $t = t_0$, This must be so since no viscoelastic material is left inside the casing at this time. For $m = 0$, the solution changes discontinuously from C to B in Figure 8 as detailed below.

For very long annihilation time, $m \to \infty$, delayed elastic flow develops fully along OA in Figure 8, and at each time thereafter, because of the extremely slow motion of the boundary compared with the delay time of the viscoelastic material. Thus the Kelvin material behaves essentially as an elastic material, and the curve AB represents a series of quasi-static elastic solutions for different values of the radius of the internal hole given by eq. (3.16), with no other time influence.

For $m = 0$ annihilation occurs so rapidly that no retarded elastic flow has had time to occur before the material disappears, so that no stress occurs in the casing until the internal pressure Π_0 is applied to it at C, causing a discontinuous jump to B.

The curves of Figure 8 show that as the annihilation time is reduced, corresponding to decreasing m, or correspondingly as the delay time is increased, the buildup of stress in the reinforcement is less for a given proportion of burn out. This interplay of the viscoelastic characteristics of the material and the stress distribution because of time influences in the loading procedure offers the possibility of design choices to benefit from such influences. For example, in the practical case of rocket burn out, the gas pressure falls after reaching a maximum, and the delayed transmission of the internal pressure through the annihilating cylinder would provide a reduction in the maximum pressure for which the casing would have to be designed.

4. Discussion

The example detailed in Section 2 indicates the generality of approach which is possible for viscoelastic stress analysis problems which fall within the scope of the Laplace transform method of treat-

ment. Quite general viscoelastic operators can be accommodated to this procedure, with only the difficulty of increasing algebraic complexity, and full use can be made of results from the theory of elasticity. When this approach is not applicable, a general method of solution of the system of partial differential equations which represents the viscoelastic stress analysis problem is not at present available, and particular approaches lead to a variety of types of mathematical problems. The example given in Section 3 leads to a nonlinear differential equation, but more general operator equations will arise in other situations such as integro-differential equations, for which at the present time special approaches must be devised.

The examples evaluated show the influence of the material viscoelastic characteristics on the variation of stresses, and illustrate the bearing which this may have on the design of equipment using materials of this type.

References

1. Gross, B., *Mathematical Structure of the Theories of Viscoelasticity*, Hermann and Cie, Paris, 1953.

2. Carlslaw, H. S., and J. C. Jaeger, *Operational Methods in Applied Mathematics*, Oxford, 1941, or R. V. Churchill, *Modern Operational Mathematics in Engineering*, McGraw-Hill, New York, 1944.

3. Lee, E. H., *Quart. Appl. Math.*, **13**, 183 (1955).

4. Radok, J. R. M., *Quart. Appl. Math.*, **15**, 198 (1957).

5. Lee, E. H., and J. R. M. Radok, *The Contact Problem for Viscoelastic Bodies*, Brown University Report C11-47, 1959. To appear in *J. Appl. Mech.*

6. Timoshenko, S., *Theory of Elasticity*, McGraw-Hill, New York, 1934.

7. Jahnke, E., and F. Emde, *Tables of Functions*, Dover, New York, 1945.

Synopsis

The formulation of the theory for determining stress distributions in linear viscoelastic materials is presented. The particular situations in which the time variable can be removed and the problem transformed into an equivalent elastic problem by application of the Laplace transform are stated, and the difficulties to be expected when this is not possible are pointed out. An example of each type of problem is presented, showing the general approach available in the first case, and the special procedure which must be devised for the latter. The resulting variation of the stress-distributions with time under constant surface loading which is associated with the viscoelastic characteristics of the material is discussed from the standpoint of the flexibility it offers in the design of components containing such materials.

TRANSACTIONS OF THE SOCIETY OF RHEOLOGY III, 61–68 (1959)

The Concentration Dependence of the Newtonian Viscosity of Prolate Ellipsoids

JOHN G. BRODNYAN, *Rohm & Haas Company, Philadelphia, Pennsylvania*

The flow behavior of suspensions of rigid uncharged spherical particles has been investigated quite extensively both theoretically and experimentally. Einstein[1] theoretically determined the dependence of the relative viscosity of spheres on the volume fraction ϕ for dilute suspensions. Mooney[2] has extended this result to higher concentrations by a functional method. Mooney's equation:

$$\eta_{rel} = \exp\left\{\frac{2.5\phi}{1 - k\phi}\right\} \tag{1}$$

reduces to Einstein's equation at low concentrations and does successfully fit the experimental data over the whole range of concentration with the proper choice of k. The crowding factor k is an interaction constant. Mooney has shown that it is most probably equal to 1.35 or less in the case of polydispersity. An upper limit of 1.91 is expected.

All the data[3] readily available to the author on the viscosity of spheres has been plotted in Figure 1. Mooney's equation with various values of k is drawn on this graph. It is seen that this equation, and therefore the functional method, has been successful in extending Einstein's equation.

The flow behavior of ellipsoids has not been so extensively studied. Very little data for concentrated suspensions is available. However, there have been a number of theories proposed for the dependen e of the relative viscosity of dilute suspensions of ellipsoids on the volume fraction and axial ratio (p). These equations, which follow, are dealt with in more detail in Frisch and Simha's review.[4]

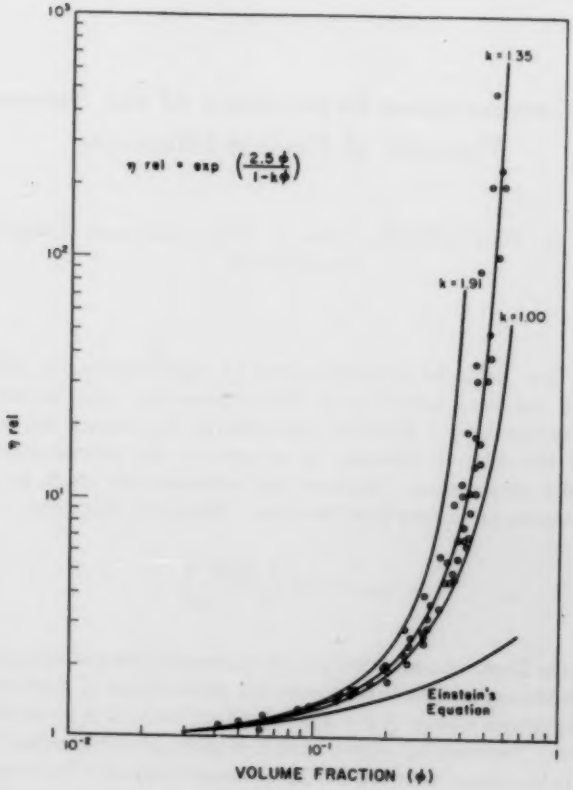

Figure 1.

$$\eta_{rel} = 1 + 2.5\phi + \frac{32}{15\pi}\left(\frac{1}{p} - 1\right)\phi - 0.628\,\frac{(1/p) - 1)}{(1/p) - 0.75}\,\phi \qquad 0 < p < 1 \quad (2)$$

$$\eta_{rel} = 1 + 2.5\phi + 0.4075(p-1)^{1.508}\phi \qquad 1 < p < 15 \quad (3)$$

$$\eta_{rel} = 1 + 1.6\phi + \frac{p^2}{5}\left[\frac{1}{3(\ln 2p - 1.5)} + \frac{1}{\ln 2p - 0.5}\right]\phi \qquad p > 15 \quad (4)$$

$$\eta_{rel} = 1 + {}^{14}/_{15}\phi + \frac{p^2}{5}\left[\frac{1}{3(\ln 2p - k)} + \frac{1}{\ln 2p - k + 1}\right]\phi \qquad p > 5 \quad (5)$$

In general the equations are of the form:

$$\eta_{rel} = 1 + k_1\phi + k_2 f(p)\phi \qquad (6)$$

Equations (2), (3), and (4) were derived by Kuhn and Kuhn[5] while eq. (5) was derived by Simha.[6] These equations are analogous to Einstein's equation, having been derived for infinite dilution, and reduce to it for $p = 1$.

The most interesting problem is the viscous behavior at finite concentrations. Therefore, an attempt has been made to extend the "dilute solution" theories to high concentrations using the method Mooney found useful in treating the problem of spheres in concentrated solutions.

Conditions to be Fulfilled and Assumptions

In attacking this problem we should expect the following conditions to be fulfilled:

(*a*) The final viscosity should be independent of the sequence of stepwise additions of partial volume fractions of the ellipsoids to the suspension.

(*b*) The equation should reduce to one of the four dilute solution equations as ϕ approaches zero.

(*c*) The equation should reduce to Mooney's equation for $p = 1$.

In the following derivation the following assumptions are made: (*a'*) The only interaction is that due to crowding, i.e., only first-order interactions are to be considered. (*b'*) The ellipsoids have a constant axial ratio p.

Derivation

Assume the ellipsoids are added in two volume fractions ϕ_1 and ϕ_2. The addition of the first fraction will increase the viscosity by a factor $H(\phi_1, p) = \eta_1/\eta_0$ where H must reduce to eq. (6) at low values of ϕ_1. The second fraction gives an increase again; $H(\psi_{21}) = \eta_2/\eta_1$. In this case the first solution acts as the solvent. Due to the crowding effect, i.e., the interaction, the volume fraction available to ϕ_2 is reduced to $1 - k\phi_1$. Therefore, ψ_{21} has the form $h(\phi_2, p)/1 - k\phi_1$.

However, the ϕ_2 volume fraction mutually crowds the ϕ_1 volume giving $H(\phi_1, p) = H(\psi_{12})$ and $\psi_{12} = h(\phi_1, p)/1 - k\phi_2$. Next we must consider the fact that the ϕ_1 and ϕ_2 volume fractions have each ellipsoids interact with the rest of the members of its own volume fraction. This means that $\psi_{21} = h(\phi_2, p)/1 - k(\phi_1 + \phi_2)$ or $\psi_{21} = h(\phi_2, p)/1 - k\phi$. In the same way $\psi_{12} = h(\phi_1, p)/1 - k\phi$.

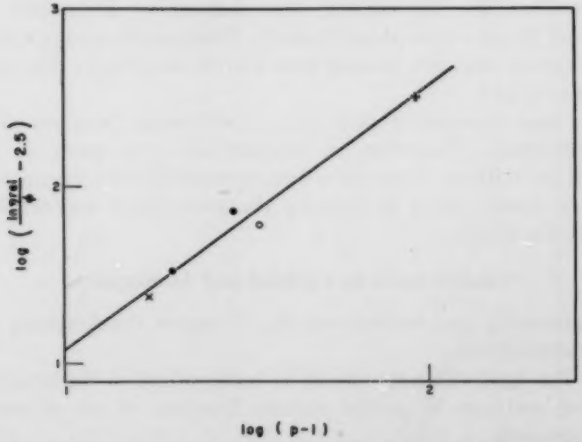

Fig. 2. (●) M. A. Lauffer, *J. Am. Chem. Soc.*, **66**, 1188 (1944). (○) M. A. Lauffer and W. M. Stanley, *Chem. Revs.*, **24**, 303 (1940). (×) G. Oster, P. M. Doty, and B. H. Zimm, *J. Am. Chem. Soc.*, **69**, 1193 (1947). (+) J. T. Yang, *J. Am. Chem. Soc.*, **80**, 1783 (1958).

Since the product $H(\psi_{12})H(\psi_{21})$ is the relative viscosity of the suspension of total concentration $(\phi_1 + \phi_2)$ we have:

$$H(\phi_1 + \phi_2, p) = H(\psi_{12})H(\psi_{21}) = H\left(\frac{h(\phi_1, p)}{1 - k\phi}\right) H\left(\frac{h(\phi_2, p)}{1 - k\phi}\right)$$

The above equation is satisfied by:

$$H(\phi, p) = \exp\left\{\frac{h(\phi, p)}{1 - k\phi}\right\} \tag{7}$$

Also it is seen that ϕ must be present only to the first power.

If $h(\phi, p) = k_1\phi + k_2 f(p)\phi$, then eq. (7) reduces to the general form of the dilute solution theories as ϕ approaches zero. Also, if

$f(p) = 0$ when $p = 1$, and $k_1 = 2.5$, Mooney's equation is the limiting case for $p = 1$ and all our initial conditions are fulfilled.

If we assume for simplicity $k_2 f(p)$ to be of the form $a(p - 1)^b$, which is the same as eq. (3), we can plot $(\ln \eta_{rel}/\phi) - 2.5$ vs. $(p - 1)$ on a log-log plot and obtain b from the slope and a from the intercept. This was done for the experimental data[7,8] available to the author and is given in Figure 2. The final empirical result is then:

$$\eta_{rel} = \exp\left\{\frac{2.5\phi + 0.399(p - 1)^{1.48}\phi}{1 - k\phi}\right\} \tag{8}$$

The values for the constants are very close to those calculated by Kuhn and Kuhn. In fact the values compared in Table I are seen to agree within 2%.

TABLE I

Constants	Experimental values	Calculated values
a	0.399	0.4075
b	1.48	1.508

Comparison with Experimental Data

The data on poly-γ-benzyl-L-glutamate solutions given by Yang[8] are probably the best to use for comparison with eq. (8). This is true for three reasons: (*1*) his material has been proven essentially monodisperse; (*2*) his data are shown experimentally to give viscosities in the Newtonian region and this has not been shown for the other data; and (*3*) his data have also been taken in a higher range of volume fractions where we would notice deviations from dilute solution behavior.

From his reported molecular weight and the known density and width of the particles an axial ratio of 93.3 was computed. In Figure 3 the lines for three equations with p equal to 93.3 have been plotted as well as Yang's data. The equations plotted are eq. (4), the result if eq. (4) had been treated in the manner given above in the derivation, and eq. (8).

It can be seen that eq. (8) fits the data better than either of the other two equations and is certainly much better than the dilute solution eq. (4). However, the fit is far from exact. Nothing has

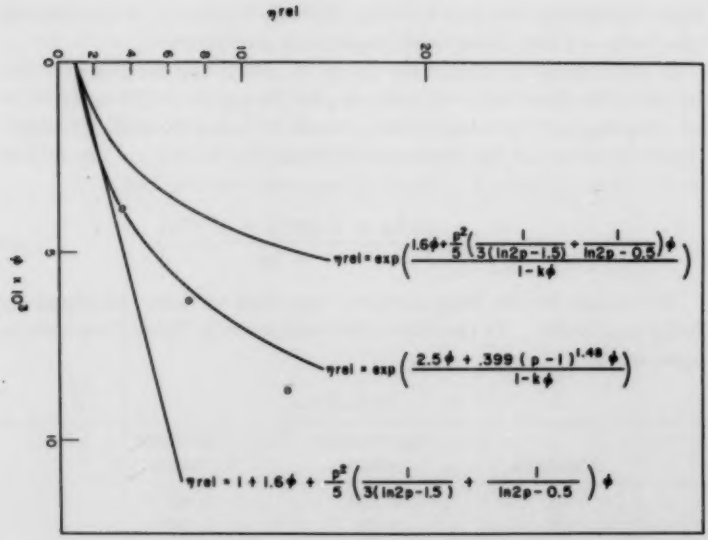

Figure 3.

been said about the value of k used, because the volume fractions are so small that it would not have mattered if we neglected consideration of the excluded volume effect.

Evaluation of k

As we go from spheres of axial ratio one to ellipsoids of axial ratio greater than one, it becomes obvious that the cubic close packing assumed by Mooney to obtain $k = 1.35$ is no longer possible. However, as the concentration of a suspension of ellipsoids increases, we would expect an ordering to take place, with the ellipsoids lining up with their long axes parallel. In fact, Vold[9] showed theoretically that this is the case if van der Waals forces are the chief forces of interaction. We could not expect as dense packing as would occur with spheres but a possible picture can be visualized in Figure 4. In this case $p = 1/b$. The volume of a unit cell would be b^2l, and we see that one ellipsoid should be contained in this cell (four quarter ellipsoids). The volume of this ellipsoid would be $(\pi/6)b^2l$. There-

fore, the volume fraction taken up by the ellipsoids when we approach densest packing would be: $\pi/6 = \phi_{max}$.

Since $k = 1/\phi_{max}$ we have $k = 1.91$ for ellipsoids with a large value of p. However, we have seen that for $p = 1$ we have a value of k equal to 1.35. We, therefore, expect k to approach 1.91 rapidly and asymptotically as p increases.

Discussion

The choice of $k_2 f(p)$ and the form of the equation seem to be correct as a first approximation. However, the experimental viscosity does not seem to increase quite as fast as eq. (8) would predict. It is not quite clear what alterations have to be made in the theory, and any modification will have to await further experimental data. Similarly the choice of k will also have to rest on experimental proof unavailable at present, but 1.91 probably will suffice as a first approximation.

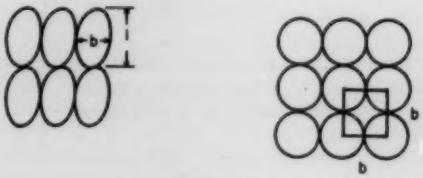

Figure 4.

Since Yang[8] has shown that the viscosity of rigid ellipsoids as a function of rate of shear is given by Scheraga's[10] numerical tabulation of the Jeffery-Peterlin-Saito treatment, the viscosity of a concentrated solution of ellipsoids may now be determined to a first approximation knowing only the axial ratio p and the volume fraction ϕ. The rotary diffusion constant can be estimated from Perrin's[11] equations if the length of the major axis is known.

References

1. Einstein, A., *Ann. Physik*, **17** (4), 549 (1905).
2. Mooney, M., *J. Colloid Sci.*, **6**, 162 (1951).
3. Robinson, J. V., *Trans. Soc. Rheology*, **1**, 15 (1957). S. H. Maron, B. P. Madow, and I. M. Krieger, *J. Colloid Sci.*, **6**, 584 (1951). S. H. Maron and S. M. Fox, *J. Colloid Sci.*, **10**, 485 (1955). S. H. Maron and A. E. Levy-Pascal,

J. Colloid Sci., **10,** 494 (1955). S. H. Maron and R. J. Belner, *J. Colloid Sci.*, **10,** 523 (1955).

4. Frisch, H. L., and R. Simha, in *Rheology*, Vol. 1, F. Eirich, ed., Academic Press, New York, 1956, Chap. 14.

5. Kuhn, W., and H. Kuhn, *Helv. Chim. Acta.*, **28,** 97 (1945). W. Kuhn, H. Kuhn, and P. Buchner, *Ergeb. exakt. Naturw.*, **25,** 1 (1951).

6. Simha, R., *J. Phys. Chem.*, **44,** 25 (1940); *J. Chem. Phys.*, **13,** 188 (1945).

7. Lauffer, M. A., and W. M. Stanley, *Chem. Revs.*, **24,** 303 (1939). M. A. Lauffer, *J. Am. Chem. Soc.*, **66,** 1188 (1944). G. Oster, P. M. Doty, and B. H. Zimm, *J. Am. Chem. Soc.*, **69,** 1193 (1947).

8. Yang, J. T., *J. Am. Chem. Soc.*, **80,** 1783 (1958).

9. Vold, M., *J. Colloid Sci.*, **9,** 451 (1954).

10. Scheraga, H. A., *J. Chem. Phys.*, **23,** 1526 (1955).

11. Perrin, F., *J. phys. radium*, **5** (7), 497 (1934).

Synopsis

Kuhn and Kuhn's theory for the viscosity of ellipsoids in dilute solutions has been extended to concentrated solutions using Mooney's functional method. The resulting equation is:

$$\eta_{rel} = \exp\left\{\frac{2.5\phi + 0.399(p-1)^{1.48}\phi}{1 - k\phi}\right\}$$

The constants 0.399 and 1.48 were obtained from the available experimental data and are found to be within 2% of the theoretical values. The dependence of the relative viscosity on volume fraction (ϕ) is seen to agree with the experimental results presented by Yang.

TRANSACTIONS OF THE SOCIETY OF RHEOLOGY III, 69–80 (1959)

An Analysis of an Absolute Torsional Pendulum Viscometer

ELLIOT A. KEARSLEY, *National Bureau of Standards, Washington, D.C.*

Introduction

At present, the only accurate absolute method of measuring the viscosity of Newtonian liquids is based on Poiseuille flow through capillaries. In fact, accuracy better than 0.1% requires such elaborate care that only the viscosity of water has been directly measured with this accuracy. Viscosities of other fluids are customarily measured with relative viscometers calibrated either directly or indirectly against water.

It is of interest to develop an independent absolute method of measuring viscosity of Newtonian fluids comparable in accuracy to the technique of Poiseuille flow, i.e., a method such that all errors can be bounded in some practical sense not involving comparison with fluids of known viscosity.

A viscometer originally considered by Helmholtz[1] consists of a spherical shell suspended from a torsion wire and filled with fluid to be tested. The sphere is excited in torsional oscillation and the subsequent motion observed. The liquid filling the shell will affect the oscillation in two ways: (*1*) damping will be enhanced due to consumption of mechanical energy by viscous heating of the liquid; (*2*) the period of the torsional pendulum will be lengthened by the inertial effects of the liquid carried along with the shell.

In principle, a measurement of either the period or the damping of the torsional oscillation will determine the viscosity of the fluid. Practically, the values of the various parameters of the pendulum—torque constant, radius of shell, mass of shell, density of fluid—will determine which measurement specifies the viscosity with greater accuracy. Although torsional pendulum viscometers have been used

in the past,[2] they have always been designed with parameters such that the damping rather than the period was a sensitive function of the viscosity of the test fluid. In view of the highly developed methods of measuring time intervals now available, it appears that the measurement of period might be the more precise method. This paper reports on an investigation now in progress whose goal is an answer to the following question: What should be the values of the design parameters of an oscillating sphere viscometer such that a measurement of period will give the most precise absolute value of viscosity for test fluids of a certain nominal viscosity range?

Calculation of the Viscous Torque

The calculation of the period as a function of the viscosity of the fluid is done in two steps: (*1*) the fluid flow problem is solved and the viscous torque on the shell is calculated; (*2*) the calculated viscous torque is inserted into the dynamic equation of the shell and the motion of the shell is then found.

Figure 1 is a schematic diagram of the pendulum with the spherical coordinates used in the flow problem indicated. The flow problem is solved in the approximation of small angle of rotation of the shell so that quadratic inertial terms can be ignored. The physical meaning of this approximation is that the effects of fluid flow in planes containing the axis of rotation of the pendulum are ignored. If the pendulum is to serve as an absolute viscometer, this error must subsequently be estimated.

The Navier-Stokes equation in spherical coordinates, ignoring quadratic inertial terms and taking account of symmetry, is

$$\frac{\partial w}{\partial t} = \nu \left\{ \frac{1}{r^2} \frac{\partial}{\partial r} \left(r^2 \frac{\partial w}{\partial r} \right) + \frac{1}{r^2 \sin \theta} \frac{\partial}{\partial \theta} \left(\sin \theta \frac{\partial w}{\partial \theta} \right) - \frac{w}{r^2 \sin^2 \theta} \right\} \quad (1)$$

where w is the fluid velocity perpendicular to planes containing the axis of rotation (the ϕ component of velocity), and ν is the kinematic viscosity. This is a linear homogeneous equation in w and the time dependence can be separated out by assuming*

$$w = ve^{i\Omega t} \quad (2)$$

* As is usual, when real physical quantities are set equal to complex expressions, the real part of the complex expression is implied. Notice that Ω is in general a complex quantity.

The boundary conditions applicable are then

$$v = i\Omega\Theta R \sin\theta, \qquad \text{when } r = R \tag{3}$$

v is continuous and finite within the sphere, Θ is the angle through which the sphere is turned from equilibrium at $t = 0$.

The solution of this boundary value problem is

$$v = \frac{i\Omega\Theta R}{x^2} \frac{\sin zx - zx\cos zx}{\sin z - z\cos z} \tag{4}$$

$$z = i\sqrt{i\Omega/\nu}\, R, \qquad x = r/R$$

The complex parameter z is closely related to boundary layer thickness.

Finally the viscous torque due to this flow pattern acting on the shell is

$$L = -(8/3)\pi R^3 \mu i\Omega\Theta e^{i\Omega t}\left(\frac{z^2 \sin z}{\sin z - z\cos z} - 3\right) \tag{5}$$

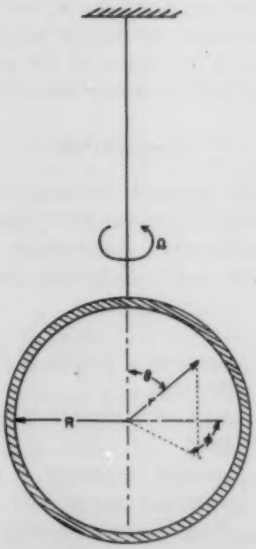

Fig. 1. The spherical coordinates used in the flow problem.

where μ is the coefficient of viscosity; that is, density times kinematic viscosity.

The Dynamic Equation of the Shell

The dynamic equation of the shell is obtained by equating the torques acting on the shell to the rate of change of angular momentum of the shell, viz.:

$$I\Omega^2\Theta e^{i\Omega t} = K\Theta e^{i\Omega t} + L \tag{6}$$

where I is the moment of inertia of the shell and K is the torque constant of the suspension wire. Substitution of eq. (5) into eq. (6) and some manipulation results in the following equation,

$$-I\Omega^2 + i\Omega(8/15)\pi R^5\mu z^2\left(\frac{5}{1 - z\ \mathrm{ctg}\ z} - \frac{15}{z^2}\right) + K = 0 \tag{7}$$

Up to this point the analysis has not been anything new. The remaining problem, to solve this equation for Ω, is in a sense only arithmetic. Because Ω is contained in z, this is a complex transcendental equation in Ω. Previous authors have developed various approximate solutions of this equation valid for certain ranges of the parameters, but in general not valid for values of the parameters such that a measurement of period will accurately determine the viscosity.

Computations

Before setting up the equation for solution on a computer, it is advisable to put it in nondimensional form so as to reduce the number of computational parameters. Accordingly, Ω is broken up into real and imaginary parts and the following quantities are defined:

$$\Omega = (2\pi/T) + i\delta$$

$I_0 = (8/15)\pi R^5\rho$	moment of inertia of fluid in rigid body rotation	
$\alpha = I/I_0$	ratio of moments of inertia of shell to fluid	
$\omega_0 = \sqrt{K/I}$	circular frequency of empty shell	(8)
$\tau = (\sqrt{\alpha}\ \omega_0/2\pi)T$	dimensionless period	
$\eta = \nu/R^2\sqrt{\alpha}\ \omega_0$	dimensionless viscosity	
$D = \delta T/\pi$	decrement per period	

Using these definitions the computational problem reduces to finding a one-parameter family of curves. In particular, after defining a new function

$$\Phi(z) = \frac{5}{1 - z\text{ctg } z} - \frac{15}{z^2} \tag{9}$$

eq. (7) can be written in extremely compact form,

$$\Phi(z) = \alpha + 1/\eta^2 z^4 \tag{10}$$

Mathematically, it is necessary to study the function $\Phi(z)$ and then to look for roots of eq. (10). For given values of α and η, eq. (10) defines certain complex values of z. Then,

$$\begin{aligned} \alpha &= \frac{\text{Im } (z^4\Phi(z))}{\text{Im}(z^4)} \\ 1/\eta^2 &= \text{Re}(z^4\Phi(z)) - \alpha\text{Re}(z^4) \\ 1/\tau &= -\eta\text{Im}(z^2) \\ D &= 2\frac{\text{Re}(z^2)}{\text{Im}(z^2)} \end{aligned} \tag{11}$$

in which Re and Im mean "the real part of" and "the imaginary part of," respectively.

For a given set of parameters, α and η, there is one primitive complex root of the equation and an infinity of real roots. The former corresponds to a damped oscillation and the latter to purely damped components of the motion. The complex root determines the period of the oscillation, and the real roots are of interest only in that they may affect the experimental measurement of period by causing a "zero drift" error.

In practice, the IBM 704 computer was used in the following way. First various complex values of z were inserted in eqs. (11) and the associated parameters were computed. After sufficient data were developed in this way, it was possible to make a good guess at the roots of eq. (10). The procedure was then reversed; values of α and η and an estimated root, z, were fed to the computer. The root z was then corrected by Newton's method and then τ, D, etc. were calculated. A typical line of output from the computer contained columns labelled α, η, Re(z), Im(z), τ, D.

Figure 2 graphs some results of the computations, τ as a function of η for various values of α. As might be expected, τ ranges from $\sqrt{\alpha}$ for vanishing η to $\sqrt{\alpha + 1}$ for infinite η, corresponding respectively to the periods of the empty shell and the shell and fluid rotating as a rigid body. Figure 3 is included for completeness, and shows the decrement per period as a function of η for various values of α. The fact that the decrement for α equals zero approaches a finite limit for vanishing viscosity is a mathematical phenomenon due to the fact that D is not an analytic function of either α or η about the point $\alpha = \eta = 0$. For $\alpha = 0$ and vanishing viscosity the period becomes infinite and the energy loss per unit time vanishes in such a way that the product is finite. The slightest inertia of the shell will have a dominant effect for small enough viscosity, so that for any finite α the energy loss per period will vanish for vanishing viscosity. Figure 4 shows the damping against the logarithm of η and illustrates this fact more clearly.

Figure 5 shows the dimensionless period as a function of log η for various values of α. Notice that, independent of α, there is a flattening of the curve for η between 10^{-1} and 10^{-2}.

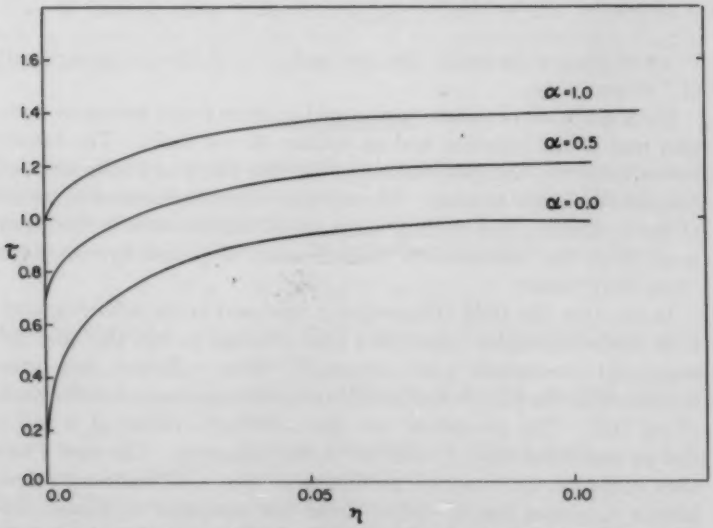

Fig. 2. Dimensionless period as a function of dimensionless viscosity for three values of ratios of moments of inertia, α.

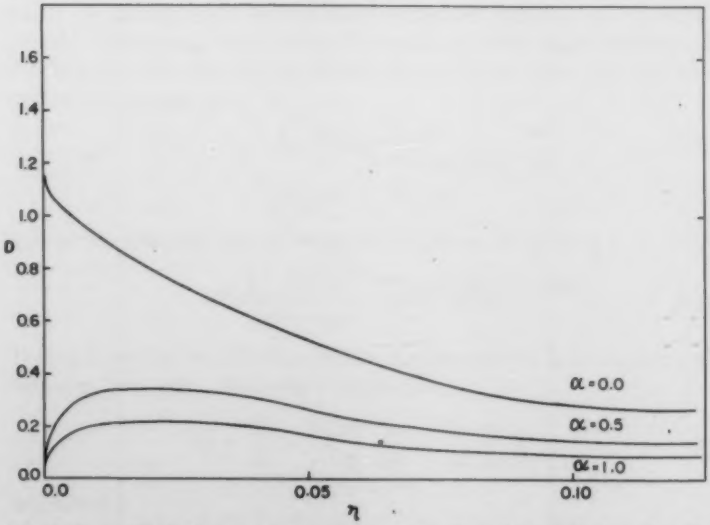

Fig. 3. Logarithmic decrement in nepers as a function of dimensionless viscosity for three values of α.

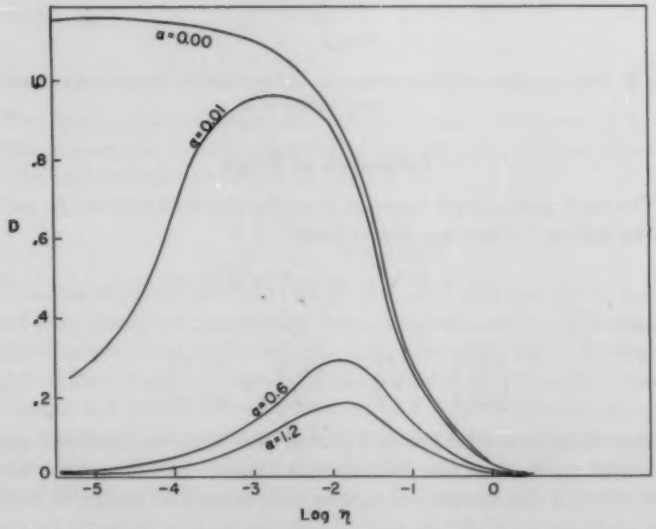

Fig. 4. Logarithmic decrement in nepers as a function of the logarithm of dimensionless viscosity for four values of α.

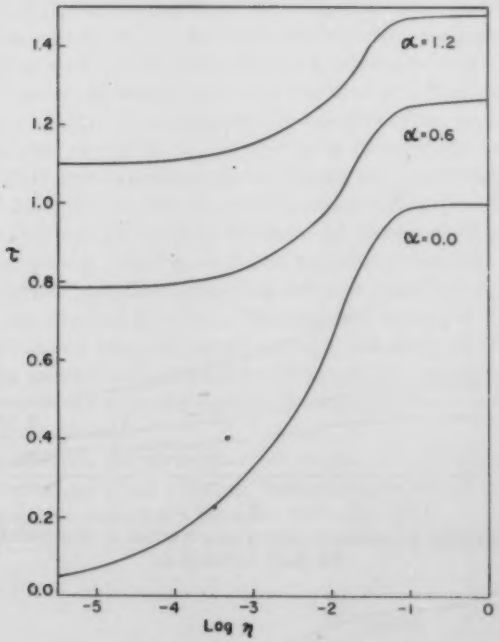

Fig. 5. Dimensionless period as a function of logarithm of dimensionless viscosity for three values of α

Estimation of Errors

The most crucial error seems to be in the determination of the radius of the sphere. From eq. (8) we have,

$$\nu = R^2\sqrt{\alpha}\,\omega_0\eta = R^2\sqrt{K/I_0}\,\eta \tag{12}$$

Hence

$$\left(\frac{\partial \nu}{\partial R}\right)_\tau = \left(\frac{2}{R} - \frac{\partial I_0/\partial r}{2I_0} + \frac{\partial \eta}{\partial R}\frac{1}{\eta}\right)\nu \tag{13}$$

In this notation a subscript on a partial derivative indicates the quantity held constant as the derivative is taken. In taking the partial derivative of the moment of inertia with respect to radius, it is nec-

essary to specify how the moment of inertia actually will be computed. Since the inside radius of a sphere is difficult to measure, it is best to find the mass of the fluid by weighing and then calculate the moment of inertia from

$$I_0 = (2/5)MR^2 \tag{14}$$

Then,

$$\partial I_0/\partial R = 2I_0/R \tag{15}$$

To calculate $\partial\eta/\partial R$ it is easiest to transpose eq. (8) to give

$$T = \frac{2\pi}{\sqrt{\alpha}\,\omega_0}\,\tau = 2\pi\sqrt{I_0/K}\,\tau \tag{16}$$

Taking a derivative of this equation with respect to R and holding T constant, one gets, after some substitutions,

$$0 = \frac{1}{R} + \frac{1}{\tau}\left(\frac{\partial\tau}{\partial\eta}\frac{\partial\eta}{\partial R} - \frac{2\alpha}{R}\frac{\partial\tau}{\partial\alpha}\right) \tag{17}$$

and hence,

$$\frac{\partial\eta}{\partial R} = \frac{2\alpha(\partial\tau/\partial\alpha) - \tau}{R(\partial\tau/\partial\eta)} \tag{18}$$

Finally,

$$\frac{R}{\nu}\left(\frac{\partial\nu}{\partial R}\right)_\tau = \left(1 + \frac{2\alpha(\partial\tau/\partial\alpha) - \tau}{\partial\tau/\partial\log\eta}\right) \tag{19}$$

This is an equation for the ratio of relative errors in ν and R using a measurement of period to determine viscosity. A similar equation for the ratio of relative errors in ν and T is,

$$\frac{T}{\nu}\left(\frac{\partial\nu}{\partial T}\right)_R = \frac{\tau}{\partial\tau/\partial\log\eta} \tag{20}$$

The quantities on the right of eqs. (19) and (20) can all be calculated graphically or numerically from Figures 2 and 4. The ratio of relative errors in ν and R is sensibly 2 for η less than 10^{-1}; for higher values it rises rapidly. The ratio of relative errors in ν and T has a minimum as a function of η for fixed α. $\Delta T_{\min}(\alpha)$ determines a curve in the τ,η plane which is shown in Figure 6, superimposed on the curves of Figure 5. Also shown are contours for $(T/\nu)(\partial\nu/\partial T)_R$ equal to 10 and 30.

A further error calculation has yet to be completed; the uncertainty in viscosity due to the effects of secondary flow. As was pointed out earlier, the inclusion of quadratic inertial terms in the Navier-Stokes equation leads to fluid flow in planes through the axis of rotation of the pendulum (see Fig. 7). This in turn has a second-order effect on the torque by distorting the boundary layer of fluid and therefore introduces a correction term to eq. (5).

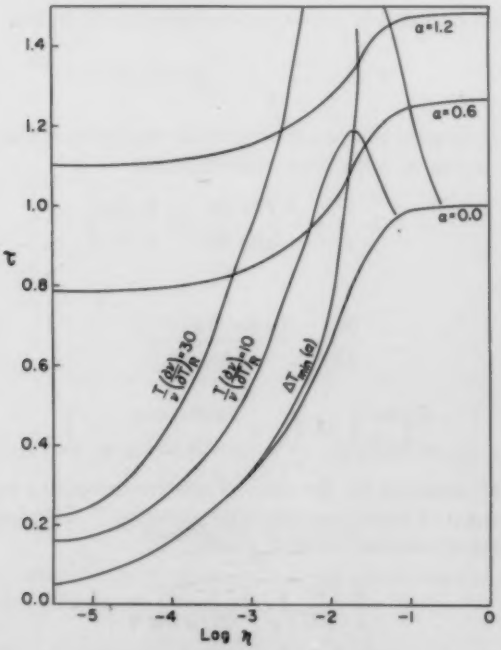

Fig. 6. The curve determined by minimum ratio of relative errors in period and viscosity and two curves of constant ratio of relative errors in period and viscosity superimposed on Fig. 5.

Carrier and DiPrima[3] have calculated a correction term for the torque on a sphere in torsional oscillation immersed in fluid. The same technique can be applied to the interior flow problem of interest here. This calculation is now in progress, and although it is clear

that an exact solution to the problem is virtually impossible, the analysis can be used to give an upper bound on the correction term.

By analogy to the Carrier and DiPrima problem, it can be argued that the correction term to the torque will be proportional to the square of the amplitude of the oscillation and will be a monotonically increasing function of the radius of the sphere. These considerations alone are enough to show the qualitative effect of the secondary flow correction.

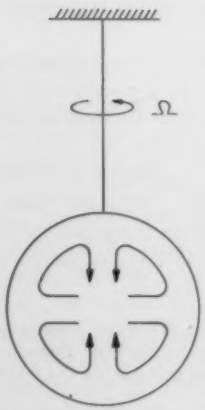

Fig. 7. Secondary flow in the spherical torsional pendulum viscometer.

It was mentioned earlier that eq. (10) defines a set of purely damped components of motion as well as a damped oscillation. Experimentally, the former will appear as a zero-point drift in measuring the period of the oscillation. In practice, it will be necessary to allow these components to become ignorably small before beginning to measure the period. Because the oscillating component of motion is itself damped, the initial amplitude of motion must be large enough to allow a practical determination of period after this waiting period. The initial amplitude of the oscillation must, therefore, be a compromise—large enough for an accurate period measurement, small enough to keep the secondary flow correction within bounds. In general, the larger the ratio of moments of inertia, α, the smaller the damping of the oscillation and the easier this compromise is to make.

Determination of Best Parameters

The question of the best set of parameters for the torsional pendulum viscometer is now beginning to unravel. The following procedure can be adopted to answer the question.

(*1*) From the studies of relative error, a best point (point of minimum error) can be found on the τ,η plane of Figure 6.

(*2*) Equations (8) are then sufficient when combined with an estimate of viscosity and density of the test fluid to select a set of physical parameters such that τ,η, and α correspond to the best point determined by step (*1*).

(*3*) Various practical requirements must then be reviewed and may force some modification of the choice of operating point. Typical of the practical requirements are reasonable radius of sphere, and reasonable strength of suspension.

Finally, although the problems of thermostating, air resistance, damping in suspension, etc., have not been discussed here, it is clear that they must be considered in a practical design of a torsional pendulum viscometer. They do not appear to be insurmountable problems.

Dr. Andreas Schopf of The American University and Mr. Stanley Prusch of the Computation Section of the National Bureau of Standards contributed the formulation and coding of the problem for the IBM 704.

References

1. Helmholtz, H., *Wissenschaftliche Abhandlung*, J. A. Barth, Leipzig, 1882, p. 172.

2. Andrade, E. N., and Y. S. Chiong, *Proc. Phys. Soc.* (*London*), **48**, Part I, 247 (1936).

3. Carrier, G. F., and R. C. DiPrima, *J. Appl. Mech.*, **23**, 601 (1956).

Synopsis

Both the period and decrement of a hollow sphere, filled with fluid and used as a torsional pendulum, depend on the viscosity of the fluid. It appears that a measurement of period might give an absolute measure of viscosity comparable in accuracy to measurements by Poiseuille flow. The relative errors in viscosity due to relative errors in measurement of period and radius of sphere are calculated. A technique is described for selecting the best set of physical parameters for such a viscometer. Final results await the solution of a problem in secondary flow.

TRANSACTIONS OF THE SOCIETY OF RHEOLOGY III, 81–93 (1959)

Viscoelastic Behavior of Polyethylene and Polypropylene

JOSEPH A. FAUCHER, *Research Department, Union Carbide Chemicals Company, South Charleston, West Virginia*

There have been frequent statements in the literature to the effect that the method of reduced variables, which has been so successful with amorphous materials, is inadequate to describe the mechanical behavior of crystalline polymers. These objections rest largely on two grounds: first, that the structure of crystalline polymers changes with temperature (so that the convenient time-temperature equivalence is invalid), and second, that these materials are nonlinear in their viscoelastic behavior. Although these objections are well-founded, the result has been that the mechanical behavior of crystalline polymers has been left in a purely empirical state. In order to escape from this undesirable situation, we have tried to retain the essential features of reduced variables by determining under what range of conditions the theory might be valid for these materials. This paper is a description of these conditions and a summary of results obtained for the particular cases of polyethylene and polypropylene.

With respect to the first objection above it is known that many crystalline polymers maintain the same structure over a fairly wide temperature range: i.e., their per cent crystallinity vs. temperature curves have a long plateau and break over rather sharply near the melting point; consequently, if one stays in the plateau region the first objection will not apply. Two samples of polyethylene were used for the present study: DYNH, a low-branched material, and Marlex-50, which is essentially linear. Their crystallinity-temperature curves are given in Figure 1 (data derived from density measurements). The plateau for Marlex-50 extends as far as 70°C., while for DYNH it is somewhat less, reaching to about 20 or 30°C. Similar

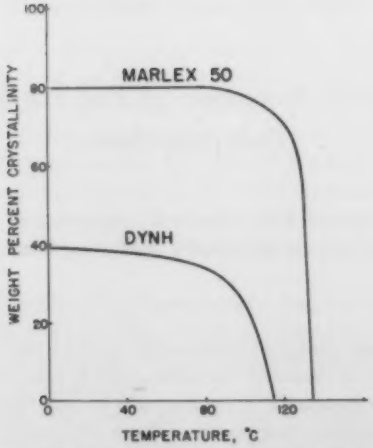

Fig. 1. Crystallinity-temperature curves for polyethylene.

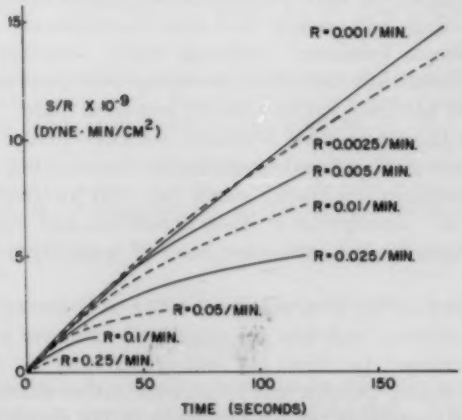

Fig. 2. S/R vs. time. Marlex-50 at 40°C.

measurements were not made on polypropylene, but it is clear from the Arrhenius plot of Figure 12 that the plateau extends to nearly 120° in this case.

The second objection—that of nonlinearity—can be met by a restriction of another kind, namely in the amount of strain. Under

sufficiently low strain any material behaves linearly. In this connection Alfrey[1] has pointed out a convenient means of testing for linear behavior. It is based on the following formula for stress relaxation which can be derived from the "infinite Maxwell Model":

$$S(t) = R\int_{-\infty}^{+\infty} xH(x)(1 - e^{-t/x})d \ln x \qquad (1)$$

where S is the time-dependent stress, R is the rate of strain, and $H(x)$ is the distribution of relaxation times. It is clear that S/R is a function of time only. Consequently, from a series of stress-time curves at various strain rates one should be able to plot S/R vs. time and obtain a single master curve. No data of this kind for crystalline polymers have appeared in the literature, so Marlex-50 was tested at a number of strain rates varying from 0.1 to 25%/min. The plot of S/R vs. time in Figure 2 shows that a single curve is not even approximately realized. The curve at 0.1%/min. strain rate has the least total strain and hence best represents the "ideal" master curve, if one indeed exists. It is clear that the larger the absolute strain, the greater is the deviation from the ideal curve. Even the values at 1% strain (e.g., 60 sec. on the 1% curve) are appreciably off. Accordingly, relaxation data for Marlex-50 were taken at a maximum of 0.5% strain. From the figure it is apparent that at this low strain deviations from the master curve will be quite small. For DYNH a similar series of curves shows that significant deviations do not occur till 1% strain is reached; this material is only about half as crystalline as Marlex-50. The stress relaxation data shown below for DYNH were taken at 1% strain. Polypropylene was not tested in the manner just described, but was assumed to be similar to Marlex in this respect. The relaxation data for it were taken at 0.5% strain.

Experimental

The polyethylene samples used were Marlex-50 and DYNH; both are commercially produced and have been frequently described in the literature. Crystalline polypropylene was prepared in the laboratory using a Ziegler-type catalyst; its density was 0.912. Assuming values of 0.936 for crystalline polypropylene and 0.850 for amorphous polypropylene, this material has a weight per cent crystallinity of about 75%. The "amorphous" sample used for comparison was made by taking a low-crystalline polypropylene and extracting it successively

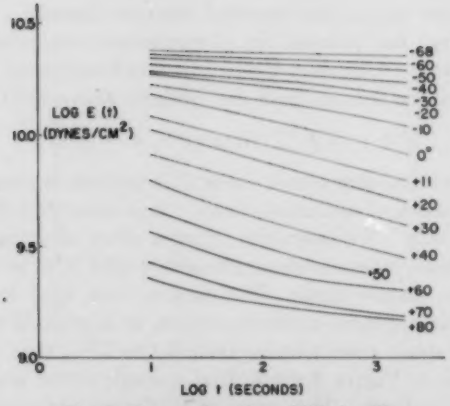

Fig. 3. Stress relaxation of Marlex-50.

with acetone (to remove oils) and ethyl ether. The fraction dissolving in ethyl ether was precipitated by methanol, vacuum dried, and made into plaques. Its density was 0.856, indicating a crystallinity of about 8%.

The mechanical properties of these materials were investigated by the method of stress relaxation. A sample of known dimensions was extended at about 5%/min. to a total strain of 0.5% (1% for DYNH) on the Instron tester and held while the stress was measured over a time of 10 to 2000 sec. This was carried out at 10° intervals from −60° to above 100°C. The tensile modulus $E(t)$ can then be calculated by:

$$E(t) = S(t)\, l/A\, \Delta l \tag{2}$$

where $S(t)$ is the measured stress in dynes, A is the cross-sectional area in sq. cm., l is the sample length and Δl is the extension. The data for the four materials used are shown in Figures 3–6.

The time-temperature equivalence which has been applied to amorphous polymers[2,3] relates $E(t)$ at two different temperatures by:

$$(T_0/T)E_T(a_T t) = E_{T_0}(t) \tag{3}$$

where T_0 is an arbitrary standard temperature and $(a_T t)$ is the "reduced" time. The factor T_0/T is introduced to correct for the effect

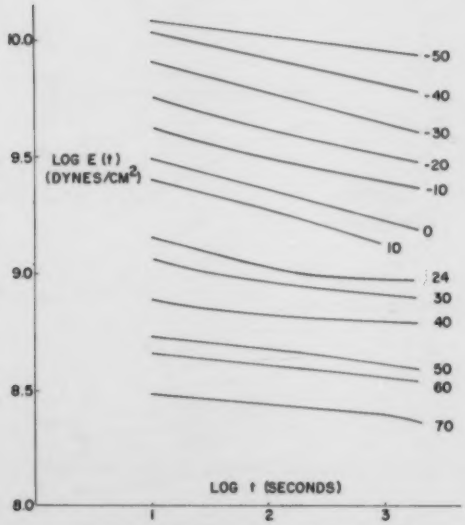

Fig. 4. Stress relaxation of DYNH.

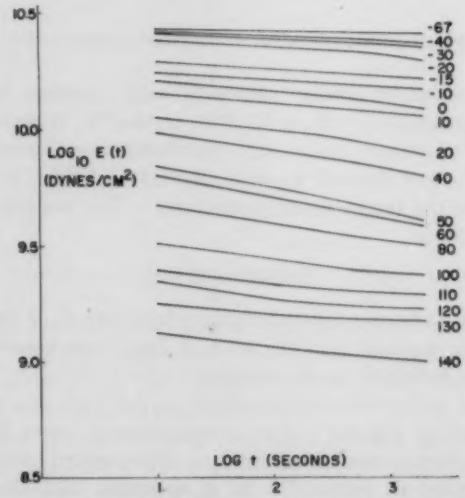

Fig. 5. Stress relaxation of crystalline polypropylene.

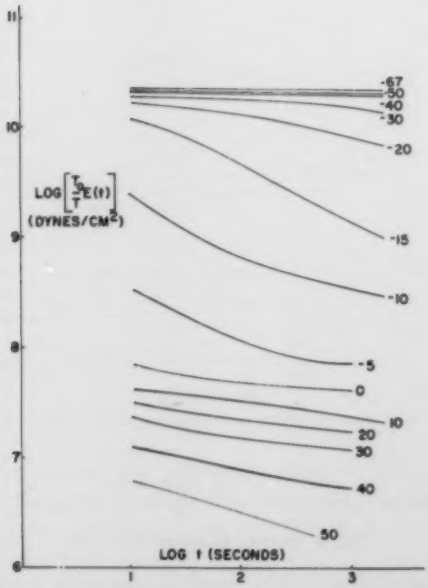

Fig. 6. Stress relaxation of amorphous polypropylene.

of rubber elasticity which increases with absolute temperature. Since our materials are about 75–80% crystalline, it is not at all clear that rubber elasticity makes any contribution in this case. Consequently, we have decided to omit this factor (which is not a large correction in the temperature range here). The temperature reduction used then is

$$E_T(a_T t) = E_{T_0}(t) \tag{4}$$

(For the case of amorphous polypropylene the T_0/T factor has, of course, been retained, and the data of Fig. 6 are corrected by this amount as is indicated on the ordinate.)

When the temperature reduction is carried out, one converts the series of lines in Figures 3–6 to a single master curve in each case. These relaxation curves, using 20°C. as the standard temperature, are shown together in Figure 7. It is apparent that the crystalline materials have very similar relaxation behavior; indeed, polypro-

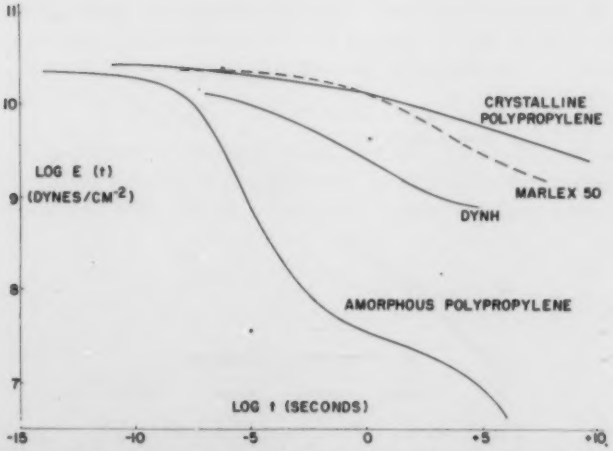

Fig. 7. Relaxation curves of polyethylene and polypropylene at 20°C.

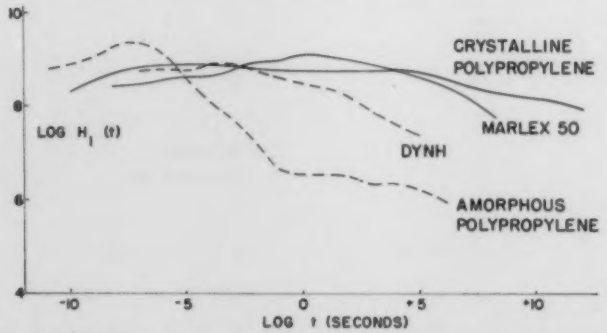

Fig. 8. Distribution of relaxation times for polyethylene and polypropylene.

pylene and Marlex-50 are nearly indistinguishable over a long range of times. On the other hand, amorphous polypropylene has a relaxation curve much like polyisobutylene, which has been rather thoroughly investigated in recent years.[4]

From the relaxation curve we can calculate the distribution of relaxation times, $H(t)$, which is defined by the integral equation:

$$E(t) = \int_{-\infty}^{+\infty} H(x)e^{-t/x}d \ln x \qquad (5)$$

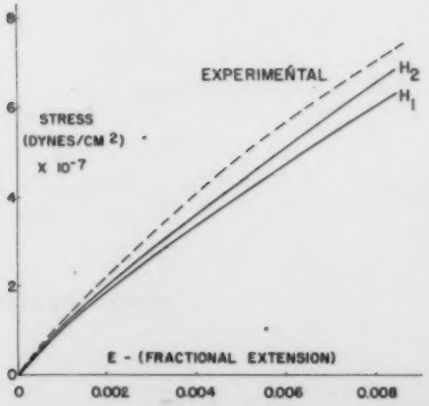

Fig. 9. Stress-strain curves of Marlex-50 at 20°C.

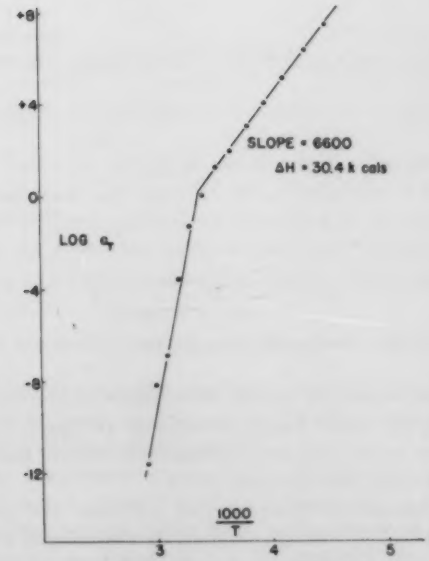

Fig. 10. Shift factors for DYNH.

The symbols used throughout this paper are those proposed by the Committee on Nomenclature of the Society of Rheology.[5] $H(t)$ can be derived from experimental data by the relation:

$$H_1(t) \cong -E(t)\ (d \log E/d \log t) \tag{6}$$

where the subscript 1 denotes a first approximation. The curves of $\log H(t)$ vs. $\log t$ are shown in Figure 8; as expected, the crystalline polymers are all quite similar. Apparently such flat curves extending

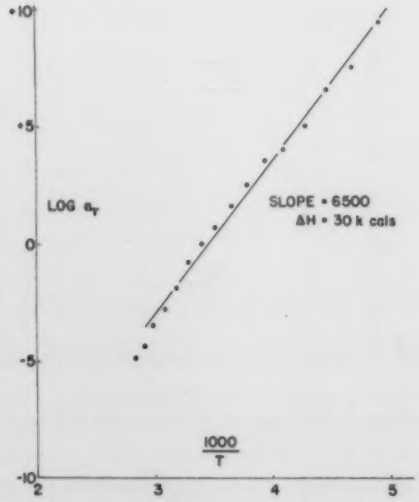

Fig. 11. Shift factors for Marlex-50.

over many decades of log time are characteristic of crystalline materials; at present there is no theory to predict this behavior. On the other hand, amorphous polypropylene shows the well-known slope of $-1/2$ in the transition region ($\log t = -6$ to 0) required by the Rouse theory,[6] while the tailing off at higher time seems to indicate considerable polydispersity in the sample.[7]

Since relaxation spectra of crystalline polymers are still rather novel, it seemed desirable to test the distribution function just obtained in some manner. This was done in the case of Marlex-50

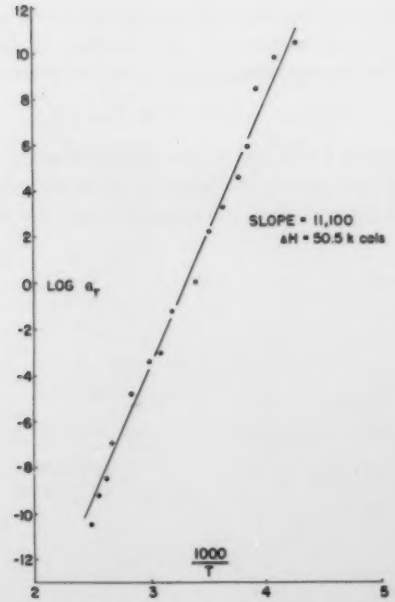

Fig. 12. Shift factors for crystalline polypropylene.

using the spectrum to calculate a stress-strain curve according to the equation:

$$S(\epsilon) = R \int_{-\infty}^{+\infty} xH(x)\,(1 - e^{-\epsilon/Rx}) d \ln x \qquad (7)$$

where ϵ is the fractional strain and R is the strain rate. To perform the integration an average value of H was taken in each decade of log time. The results with $H_1(t)$ as given by eq. (6) were compared with an experimental stress-strain curve at 1%/min. strain rate. The agreement was not very impressive, so a second approximation to $H(t)$ was made according to:

$$H_2(t) = -E \frac{d \log E}{d \log t} + \gamma E \left(\frac{d \log E}{d \log t} \right)^2 + \frac{\gamma E}{2.303} \frac{d^2 \log E}{d \log t^2} \qquad (8)$$

(ref. 8, eq. 20) where γ is Euler's constant, $\gamma = 0.5772$. The second approximation gives a better calculated stress-strain curve, as can be

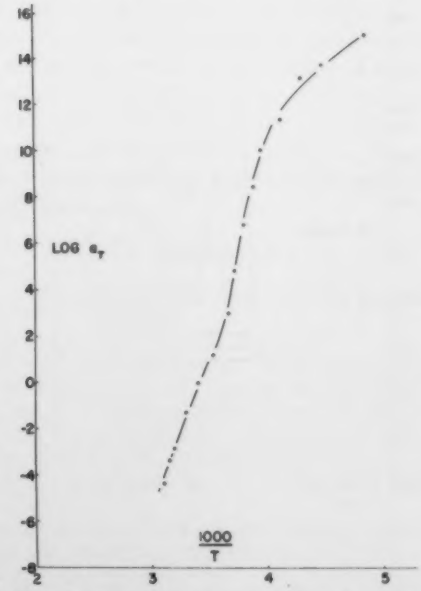

Fig. 13. Shift factors for amorphous polypropylene.

seen in Figure 9. A third-order approximation would probably give a still better result, but the data hardly warrant such tedious calculations. The point is, that since we have used data from −70 to +70°C. to get the calculated curve, it seems that the time-temperature equivalence concept does indeed apply in this case.

As is well known, the magnitude of the a_T shift factors can be used to determine the activation energy of the stress relaxation process. In Figures 10–12 are shown the plots of log a_T vs. $1/T$ for the crystalline polymers DYNH, Marlex-50, and polypropylene. In each case a reasonable straight line is obtained. The slopes of these lines (times $2.303R$) give the heats of activation—about 30 kcal. for polyethylene and 50 kcal. for polypropylene. For amorphous polymers this activation energy is for a process of viscous flow; at present it is not clear just what process is involved with the crystalline materials. An elucidation of this point would go far to explain the rather large difference in activation energy of polypropylene and polyethylene, as

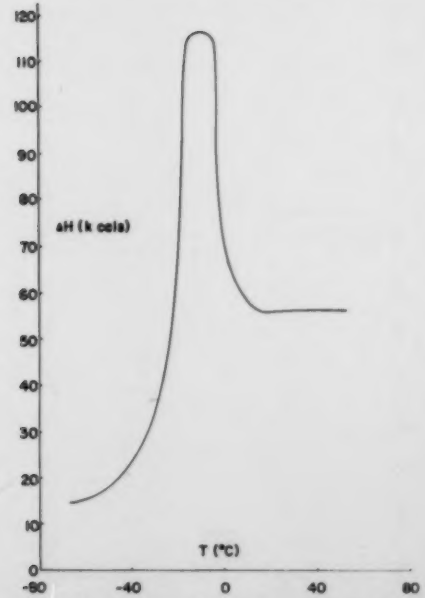

Fig. 14. Activation energy of flow for amorphous polypropylene.

well as the rather interesting fact that DYNH and Marlex-50 have the same activation energy, although their crystallinities differ by a factor of 2.

It should be noted for the polyethylenes that deviations from the straight-line plot begin to occur at those temperatures where crystallinity starts to decrease, i.e., about 30°C. for DYNH and 80°C. for Marlex-50. For polypropylene, deviations begin at about 130°, indicating that the crystallinity stays constant up to this point, although this was not actually verified by density measurements.

The log a_T vs. $1/T$ curve for amorphous polypropylene is shown in Figure 13, and the heat of activation derived therefrom is given in Figure 14. The maximum observed at -10 to $-20°$ probably represents the glass transition for this material.

In conclusion its seems appropriate to mention the work of Kê on polycrystalline aluminum between 150 and 225°C.[9] in which the method of stress relaxation was used with very small strains. The mas-

ter relaxation curve obtained was very similar to our Figure 7 (Marlex-50 and crystalline polypropylene) and the plot of log a_T vs. $1/T$ yielded a straight line whose slope indicated an activation energy of about 34 kcal. It seems likely that the relaxation curves of Figure 7 (excepting amorphous polypropylene) are typical of crystalline materials generally and are quite insensitive to details of chemical structure, unless these latter may influence the position of the curve on the log E and log t axes.

References

1. Alfrey, T., *Mechanical Behavior of High Polymers*, Interscience, New York, 1948, pp. 186 ff.
2. Ferry, J. D., *J. Am. Chem. Soc.*, **72**, 3746 (1950).
3. Andrews, R. D., N. Hofman-Bang, and A. V. Tobolsky, *J. Polymer Sci.*, **3**, 669 (1948). R. D. Andrews and A. V. Tobolsky, *J. Chem. Phys.*, **13**, 3 (1945).
4. Catsiff, E., and A. V. Tobolsky, *J. Appl. Phys.*, **25**, 145 (1954).
5. Leaderman, H., *Trans. Soc. Rheol.*, **1**, 213 (1957).
6. Rouse, P. E., *J. Chem. Phys.*, **21**, 1272 (1953).
7. Tobolsky, A. V., A. Mercurio, and K. Murakami, *J. Colloid Sci.*, **13**, 196 (1958).
8. Andrews, R. D., *Ind. Eng. Chem.*, **44**, 707 (1952).
9. Kê, T., *Phys. Rev.*, **71**, 533 (1947).

Synopsis

An attempt is made to apply the theory of reduced variables to the crystalline polymers polyethylene and polypropylene. It appears that this can be done if suitable restrictions are made in temperature range and amount of strain. Data were obtained by the method of stress relaxation. Curves at different temperatures can be superposed to give a single master curve, and the shift factors so obtained fall on a straight line in an Arrhenius plot. The distributions of relaxation times are calculated for both polymers and are found to be very similar. The two are compared with amorphous polypropylene, whose behavior is much like polyisobutylene.

TRANSACTIONS OF THE SOCIETY OF RHEOLOGY III, 95-99 (1959)

Thermodynamics of Transport Processes in Liquids

R. E. NETTLETON,* *Department of Chemistry, The Rice Institute, Houston, Texas*

To discuss momentum and energy transport in an infinite, isotropic, non-uniform fluid, it is convenient to divide the fluid into sub-macroscopic volume elements, each containing several million molecules. The non-equilibrium state of one such volume element, hereafter called the "system," is described by the local density and temperature and by additional variables which fall into two classes. Type I variables describe the degrees of advancement of chemical reactions,[1] the occupation numbers of internal rotational and vibrational levels, degree of molecular association, and local concentration of free volume. Type II variables are the space-gradients of the temperature T and Eulerian velocity of flow, $\mathbf{u}$, and first and higher time derivatives of these variables. A non-equilibrium thermodynamic treatment using Type I variables has recently been given by Davies,[2] while Prigogine (see ref. 3, chapter 7) has developed the thermodynamics of continuous systems, using Type II. We shall show that these two descriptions are related through the equations giving the rates of change of Type I variables in such a way that in the limit of low frequency, the first of these two descriptions reduces to the second.

The demonstration of this result employs the Onsager-Casimir reciprocity theorem.[3] This theorem asserts that when the irreversible part of the rate of entropy production is given by a sum of products of fluxes J_i and conjugate forces X_i and no magnetic field is present, then in the linear force-flux equations $J_i = \sum_j L_{ij} X_j$, we have $L_{ij} =$

* Present address: Mineral Products Division, National Bureau of Standards, Washington, D. C.

L_{ji} whenever the corresponding forces X_i and X_j are both odd or even with respect to time reversal, while $L_{ij} = -L_{ji}$ when one force is odd and the other even. Proof of this theorem[3-5] from the principle of microscopic reversibility assumes the J_i are time derivatives of Onsager variables which vanish in equilibrium and that the X_i are linear sums of such variables. We shall proceed to interpret thermodynamically the relaxation-rate equations which can be derived from physical models of the system on the basis of the fact that they contain terms having a mathematical form analogous to that usually assumed for the J_i and X_i.

We consider first a model for shear relaxation. Frenkel[6] proposed that a liquid should behave like an elastic solid when sheared sufficiently rapidly so that the molecules have no time to rearrange themselves through viscous flow. Thus we can envisage the system divided into many microscopic subregions, in some of which the molecular planes are sheared and in some of which the shear has relaxed, and introduce a strain tensor $\epsilon^i{}_j$ to represent the average elastic strain over all subregions. $\epsilon^i{}_j$ relaxes to a diagonal tensor with the Maxwell relaxation time τ_1 as the system approaches mechanical equilibrium, and thus $\sigma^i{}_j \equiv \epsilon^i{}_j - {}^1/_3\epsilon^\alpha{}_\alpha\,\delta^i{}_j$ relaxes to zero. This fact can be represented by the equation:

$$\dot{\sigma}^i{}_j = -\frac{1}{\tau_1}\,\sigma^i{}_j + B^i{}_j \tag{1}$$

The tensor $B^i{}_j \equiv {}^1/_2\{\nabla\mathbf{u} + \overline{\nabla\mathbf{u}}^i\}^i{}_j - {}^1/_3\nabla\cdot\mathbf{u}\delta^i{}_j$ is the divergenceless rate-of-deformation. If all variables vary with time as $e^{i\omega t}$, $\dot{\sigma}^i{}_j$ and $B^i{}_j$ are both proportional to ω, so that as $\omega \to \infty$, the middle term in eq. (1) is negligible and $\dot{\sigma}^i{}_j = B^i{}_j$, in accord with Frenkel's hypothesis, which is thus seen to demand the presence of the term $B^i{}_j$. To examine the significance of this term, we must make a thermodynamic interpretation of all the terms in eq. (1). Since $\sigma^i{}_j$ is an Onsager variable, we interpret the components of $\dot{\sigma}^i{}_j$ as thermodynamic fluxes, by analogy with the general theory discussed above. We suppose that the term linear in $\sigma^i{}_j$ is proportional to a thermodynamic force $\Omega^i{}_j = -\sigma^i{}_j/\mu_1\tau_1$ conjugate to $\dot{\sigma}^i{}_j$, μ_1 being a phenomenological coefficient.

The thermodynamic interpretation just made allows us to apply the Onsager theorem, provided we make the additional assumption that the rate of entropy production contains the term $\Omega^i{}_j\,\dot{\sigma}^j{}_i$, a sum of

products of the fluxes and forces identified in eq. (1). From the Onsager theorem, since the flux $\dot{\sigma}^i{}_j$ depends linearly on $-B^i{}_j$ which is thermodynamically conjugate to the pressure $P^i{}_j$ divided by the number density n, and which is odd with respect to time reversal, then $P^i{}_j$ must depend linearly on $\Omega^i{}_j$ according to the equation:

$$P^i{}_j = P\delta^i{}_j + n\Omega^i{}_j \tag{2}$$

where P is thermodynamic pressure given by the equilibrium equation-of-state.

Since $\Omega^i{}_j$ is proportional to the divergenceless elastic strain tensor, eq. (2) indicates that the shear modulus of the liquid is: $\lambda_2 = n/\mu_1\tau_1$. As $\omega \to 0$, $\dot{\sigma}^i{}_j \to 0$, and $\Omega^i{}_j \to -B^i{}_j/\mu_1$. Substitution of this result into eq. (2) shows that the low frequency shear viscosity η is:

$$\eta = {}^1/_2\lambda_2\tau_1 \tag{3}$$

Thus we see how $P^i{}_j$ in general depends on the Type I variable $\Omega^i{}_j$ but at low frequencies depends on the Type II variable $B^i{}_j$, the transport coefficient η being determined from our thermodynamic interpretation of eq. (1).

One can calculate τ_1 with the aid of a recent theory by Mooney[7] and λ_2 from the expression $\rho c^2 = B_\infty + {}^2/_3\lambda_2$ for the velocity c of longitudinal hypersonic acoustic waves, were ρ is the mass density. B_∞ is the high-frequency bulk modulus, discussed below. The velocity c in turn can be calculated from the thermal conductivity with the aid of a theory of heat conduction due to Debye,[8] which assumes that it is the high-frequency sound waves which carry thermal energy throughout the fluid. Calculated values of τ_1 and $2\eta/\lambda_2$ have been found to agree as to order-of-magnitude in carbon tetrachloride, acetone, and chloroform.[9]

To calculate B_∞, we must discuss the relaxation of compressional stress, which we do in a manner mathematically analogous to the discussion of shear relaxation. In non-associated liquids, sound absorption is attributable to a lag in the energy transfer between translational and vibrational degrees of freedom.[10] If ζ is the fraction of molecules in the system in the lowest excited vibrational level, ζ will relax to an equilibrium function $\zeta^0(\rho,T)$ of the density, ρ, and temperature with a relaxation time τ_2 which can be calculated from a theory of Schwarz and Herzfeld.[11] If $\xi \equiv \zeta - \zeta^0$, the

Onsager variable ξ will relax to zero, which can be expressed mathematically by the equation:

$$\dot{\xi} = -\frac{1}{\tau_2}\xi + \Gamma \nabla \cdot \mathbf{u} \tag{4}$$

The presence in eq. (4) of the term linear in $\nabla \cdot \mathbf{u} = -\dot{\rho}/\rho \equiv -\dot{s}$, s being the condensation, is explained by considering the limiting form of eq. (4) for frequencies $\omega >> \tau_2^{-1}$. At such frequencies, ζ has no time to relax and thus assumes a fixed value, ζ_0. Under these conditions if wave propagation is adiabatic, then $\xi = \zeta_0 - \zeta^0 = -(\partial\zeta^0/\partial s)_\sigma s$, σ being the entropy per molecule. Since $\dot{\xi}$ and $\dot{s}$ are both proportional to ω, we find that when $\omega >> \tau_2^{-1}$, $\xi = -\Gamma s$, so that $\Gamma = (\partial\zeta^0/\partial s)_\sigma$. The presence of the term in $\nabla \cdot \mathbf{u}$ also suggests a thermodynamic interpretation of the terms in eq. (4), analogous to that made for the terms in eq. (1). We can suppose that $\dot{\xi}$ is a flux and that $\Phi \equiv -\xi/\mu\tau_2$ is the conjugate force, $\mu(\rho,T)$ being a phenomenological coefficient. If the rate of entropy production is assumed to contain the term $\Phi\dot{\xi}$, we can apply the Onsager theorem to eq. (4) and conclude that because the rate equation for $\dot{\xi}$ is linear in $-\nabla \cdot \mathbf{u}$, the diagonal elements in $P^i{}_j/n$ must be linear in Φ, i.e., that:

$$\bar{P} = P + n\Gamma\Phi = P - n\,\Gamma\xi/\mu\tau_2, \; \bar{P} \equiv {}^1/_3\, P^\alpha{}_\alpha \tag{5}$$

If we put $\dot{\xi} = i\omega\xi$ in eq. (4), solve for ξ, and substitute in eq. (5), we obtain the complex bulk modulus $B(\omega)$:

$$B(\omega) = B_\sigma + \frac{i\omega n\Gamma^2/\mu}{1 + i\omega\tau_2} \tag{6}$$

where B_σ is the equilibrium adiabatic bulk modulus. When $\omega >> \tau_2^{-1}$, eq. (6) reduces to $B_\infty = B_\sigma + n\Gamma^2/\mu\tau_2$. As $\omega \to 0$, we obtain the bulk viscosity $\eta_0 \equiv \lim_{\omega\to 0} Im[B(\omega)/\omega] = n\Gamma^2/\mu$. These results have been used to calculate both B_∞[9] and η_0[12] for non-associated liquids, the calculated results being in qualitative agreement with experiment despite the fact that most liquids exhibit a distribution of relaxation times. Such a distribution gives rise to a whole set of normal coordinates obeying rate equations mathematically similar to eq. (4), while $B(\omega)$ contains a linear sum of complex terms like the term on the right in eq. (6), there being one term in the sum for

each relaxation time. A thermodynamic treatment of systems having many relaxation times has been developed.[12]

The author gratefully acknowledges support from a research grant made by the Robert A. Welch Foundation.

References

1. Prigogine, I., and R. Defay, *Chemical Thermodynamics*, Longmans Green, New York, 1954.
2. Davies, R. O., *Repts. Progr. Phys.*, **19**, 326 (1956); see pp. 350 ff.
3. DeGroot, S. R., *Thermodynamics of Irreversible Processes*, North-Holland, Amsterdam, 1951.
4. DeGroot, S. R., and P. Mazur, *Physica*, **23**, 73 (1957).
5. Van Kampen, N. G., *Physica*, **23**, 707, 816 (1957).
6. Frenkel, J., *Kinetic Theory of Liquids*, Dover, New York, 1955, p. 196 f.
7. Mooney, M., *Trans. Soc. Rheol.*, **1**, 63 (1957).
8. Debye, P., in *Vorträge über die kinetische Gastheorie*, Teubner, 1914, pp. 46–60.
9. Nettleton, R. E., *Phys. Fluids*, **2**, 256 (1959).
10. Compare T. A. Litovitz, *J. Chem. Phys.*, **26**, 469 (1957).
11. Schwarz, R. N., and K. I. Herzfeld, *J. Chem. Phys.*, **22**, 767 (1954).
12. Nettleton, R. E., *J. Acoust. Soc. Am.*, **31**, 557 (1959).

Synopsis

Two types of variables are distinguished in the local description of a non-uniform fluid. Type I variables determine the molecular structure of the fluid and degrees of advancement of chemical reactions, while Type II variables are the gradients of temperature and velocity which appear in the hydrodynamic description of a continuous fluid. The rate equations for Type I variables also depend on Type II variables, so that at low acoustic frequencies one can solve for the former in terms of the latter. When specific terms in the rate equations are identified as forces or fluxes in the sense of irreversible thermodynamics, one can use Onsager's theorem to calculate the dependence of the pressure on Type I variables, which in turn enables one at low frequencies to determine the dependence of pressure on the fluid velocity gradient and to calculate the shear and bulk viscosities.

TRANSACTIONS OF THE SOCIETY OF RHEOLOGY III, 101–112 (1959)

Secondary Stresses in Anisotropic Amorphous Media

CHARLES MACK, *Research Department, Imperial Oil Limited, Sarnia, Ontario, Canada*

I. Introduction

The presence of secondary stresses was first observed by Poynting,[1] who found that steel and copper wires elongated and increased in volume when subjected to a torsional torque. This result is not in accord with the predictions of the classical theory of elasticity. Secondary stresses have also been demonstrated in liquids under laminar flow conditions by Weissenberg. Their effect is easily shown with solutions of high polymers. If a cylinder is rotated in such a solution, the liquid will creep up along the rotating cylinder, the more so the greater the speed of rotation. A simple liquid would be thrown off the rotating cylinder if the centrifugal forces were great enough. Such behavior indicates that, besides a shearing stress, there is a normal stress parallel to the cylinder axis, which is a tensile stress.

In deriving a theory of secondary stresses, Weissenberg[2] assumed that such liquids have elastic properties. He associated the secondary stresses with the shear modulus and the shearing stress with the viscosity. Mooney[3] treated the problem in a similar manner with the difference that he applied his theory of nonlinear "superelasticity" to the elastic behavior.[4]

Rivlin[5] discarded elastic effects altogether and postulated that the stress components on an element of the material depend only on the state of flow. He associated the shearing stress with the viscosity and the normal stresses with a "normal stress coefficient" which has the dimensions of viscosity. A similar treatment was given by Reiner.[6]

To test the various theories, Roberts[7] measured the normal stresses produced in a series of Newtonian and non-Newtonian liquids. He

found one normal stress to be a tension. The other two were found to be equal. The normal stress difference was proportional to the shearing stress, within the experimental error, at values up to 10^3 dynes/cm.^{2}, in agreement with Weissenberg's theory, but in disagreement with the theories of Mooney, Rivlin, and Reiner. At greater values of the normal stress difference, the results were incompatible with all theories. Philippoff[8] has discussed various theories and has partly confirmed Roberts' results by data obtained on polyisobutylene solutions.[9]

Although these experiments prove the existence of secondary stresses, they do not indicate whether their presence is associated with the elastic or viscous behavior of liquids. What is known is that secondary stresses are absent in deformed isotropic bodies. They must, therefore, be associated with anisotropic behavior as a result of deformation, irrespective of whether the deformation is elastic or viscous.

Since most industrially important materials are anisotropic or become so during deformation, the secondary stresses will, in the following, be treated for anisotropic systems in general. The treatment in three dimensions is confronted with difficulties. For reasons of simplification, the case of simple shear will be considered, which reduces the problem to a two-dimensional one. Since the relations between stress components and strain or strain rate components are not known, the motion of an element relative to rotating axes is considered. This procedure eliminates strains or strain rates, and results in a representation of forces in terms of stress components and inertial forces only, which applies to any kind of deformation, whether elastic or time-dependent, and can be compared with experimental results.

II. Stress Distribution in Anisotropic Bodies under Plane Shear

The stress components in an isotropic body under simple shear consist of the shearing stress, τ, acting tangentially on the shear plane, and an arbitrary hydrostatic pressure, p, normal to the plane (Fig. 1). The stress on the plane is

$$s = -p + \tau \tag{1}$$

By superimposing on this a system of secondary stresses, we obtain the stress distribution in an anisotropic body, as shown in Figure 2. A circle inscribed in the plane *ABCD*, with the coordinate axes as

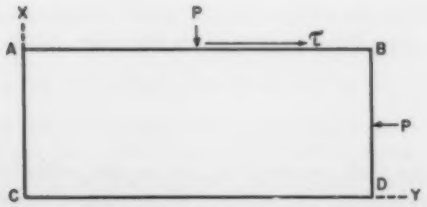

Fig. 1. Stress in isotropic body under simple shear.

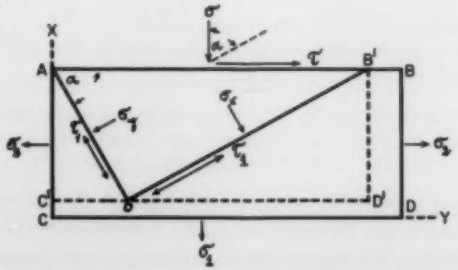

Fig. 2. Stress distribution in anisotropic body under simple shear.

diameters, is changed on deformation into an ellipse, the principal axes of which are the shortened and lengthened diameters of the original circle. Let AO and OB' coincide with the directions of the axes of the ellipse; the secondary stresses can then be imagined to arise from a rotation of the coordinate axes. Considering only a state of stress, they refer to the axes of the stress ellipsoid.

In addition to the hydrostatic pressure and shearing stress, we have the stresses σ_y and σ_x normal to the planes AO and OB'. The latter are associated with the principal stresses σ_2 and σ_1 normal to the planes bounded by the coordinate axes. The condition of anisotropy requires that $\sigma_y \neq \sigma_x$ and $\sigma_2 \neq \sigma_1$. The oblique planes are further subjected to tangential stresses which are equal and are denoted by the secondary shearing stress τ_1. The resultant of the secondary stresses is a stress component σ acting normal to the plane AB but making an angle α with the direction of OB'. With this term the stress for the condition of plane shear becomes

$$s_d = \sigma + \tau \tag{2}$$

which is similar to eq. (1), but σ is a stress deviator.

For the correlation of the various stress components, we consider the condition of equilibrium of forces in the prism AOB', and

$$\begin{aligned} \sigma \cos \alpha - \tau \sin \alpha &= \sigma_y \cos \alpha + \tau_1 \sin \alpha \\ \sigma \sin \alpha + \tau \cos \alpha &= \sigma_x \sin \alpha + \tau_1 \cos \alpha \end{aligned} \tag{3}$$

Multiplying the first equation by cos α, the second by sin α, and adding the results gives σ in terms of the secondary stresses:

$$\sigma = \sigma_x \sin^2 \alpha + \sigma_y \cos^2 \alpha + \tau_1 \sin 2\alpha \tag{4}$$

Multiplication of the first eq. (3) by sin α and the second by cos α gives, on addition and subtraction of the results, the following expressions for σ and τ:

$$\sigma = {}^1/_2 (\sigma_x + \sigma_y) + \tau_1 / \sin 2\alpha - \tau \cot 2\alpha \tag{5}$$

$$\tau = {}^1/_2 (\sigma_x - \sigma_y) \sin 2\alpha + \tau_1 \cos 2\alpha \tag{6}$$

In order to express σ_x and σ_y in terms of the principal stresses σ_1 and σ_2, which can be experimentally determined, the same operation is applied to the equilibrium of forces in the prisms $OC'A$ and $OD'B'$, and we have the following relations:

$$\begin{aligned} \sigma_x &= -p + {}^1/_2 (\sigma_1 + \sigma_2) + \tau_1 \cot 2\alpha \\ \sigma_y &= -p + {}^1/_2 (\sigma_1 + \sigma_2) - \tau_1 \cot 2\alpha \\ \tau_1 &= -{}^1/_2 (\sigma_1 - \sigma_2) \sin 2\alpha \end{aligned} \tag{7}$$

$$\sigma_x + \sigma_y = \sigma_1 + \sigma_2 - 2p; \quad \sigma_x - \sigma_y = 2\tau_1 \cot 2\alpha$$

$$\sigma_1 - \sigma_2 = (\sigma_1 + \sigma_2) \cos 2\alpha$$

With these terms eqs. (5) and (6) become

$$\sigma = {}^1/_2 (\sigma_1 + \sigma_2 - 2p) - \tau \cot 4\alpha \tag{8a}$$

$$\sigma = \sigma_2 - p - \tau \cot 2\alpha \tag{8b}$$

$$\sigma = \sigma_1 - p + \tau \tan 2\alpha \tag{8c}$$

$$\tau = 2\tau_1 \cos 2\alpha = (\sigma_1 - \sigma_2) \sin 2\alpha \cos 2\alpha \tag{9}$$

For the conditions chosen, there is no external pressure or tension applied, and the principal stresses can be either independent of the hydrostatic pressure, or one of the principal stresses can be equal to it. Hence

for $\sigma_2 = p$: $$\sigma = \tau \cot 2\alpha \tag{10a}$$

for $\sigma_1 = p$: $$\sigma = \tau \tan 2\alpha \tag{10b}$$

$$\sigma = -\tau(\operatorname{cosec} 4\alpha \sec 2\alpha + \cot 4\alpha) - p \tag{10c}$$

where the last equation is obtained by combining eq. (8a) with eq. (9) and the last of eq. (7). The point O in Figure 2 on rotation describes a curve, the slope of which is determined by the trigonometric functions of eqs. (10).

Introducing eqs. (10) into eq. (2) gives the stress in terms of the shearing stress alone for the various conditions. The equations describe a state of plane stress and refer to the undeformed state. Strains, however, are associated with the deformed state. Both states are identical if the deformations are infinitesimal, or if the body is isotropic. This condition does not hold for larger strains in anisotropic bodies, and for a complete description of the state, the stresses have to be related to the deformed state.

III. Stress in Relation to the Deformed State

For the anisotropic case, the strain components can be obtained in a manner similar to the stress components by replacing the angle α by α', the angle associated with the deformational rotation of the coordinate axes. Let ϵ, ϵ_1, ϵ_2, e, and γ be the strain components and shear associated with σ, σ_1, σ_2, p, and τ, respectively; then the strains corresponding to the stresses in eqs. (10) are

for $\epsilon_2 = {}^1/_2 e$: $$\epsilon = -\gamma \cot 2\alpha' \tag{11a}$$

for $\epsilon_1 = {}^1/_2 e$: $$\epsilon = \gamma \tan 2\alpha' \tag{11b}$$

for the general case: $$\epsilon = \gamma(\operatorname{cosec} 4\alpha' \sec 2\alpha' + \cot 4\alpha) \tag{11c}$$

These equations, or their counterparts in terms of strain rates, hold only in special cases. From the standpoint of generalization, nothing is gained by such a procedure, since a given stress component can produce, in the extreme case, all of the strain components. In addition, the relationships between the stress and strain components are not known. This difficulty is overcome by superimposing upon the stress system the rotating axes of the strain ellipsoid, in a manner similar to that followed for the treatment of the secondary stresses. For the solution of this condition, use is made of the equations of motion.

For the case considered, the shearing stress τ acts in the y direction, and the normal stress σ in the x direction. Since the normal stress is a function of the shearing stress, we can generalize by setting $\sigma = \tau f(\alpha)$ and the equation of motion becomes

$$\partial\tau/\partial y + \partial\tau f(\alpha)/\partial x - \rho g = \rho\ddot{x} \tag{12}$$

where ρ = mass per unit volume and $\ddot{x} = \partial\dot{x}/\partial t$ is the acceleration in the x direction. The term ρg is the body force per unit volume and is written here as the product of density and acceleration due to gravity. Multiplication by ∂y gives this equation in terms of forces per unit area instead of gradients, and

$$\partial\tau + \partial\tau f(\alpha)/(\partial x/\partial y) = \rho(\ddot{x} + g)\partial y \tag{13}$$

The derivative $\partial x/\partial y$ arises from the rotation and is, therefore:

$$(\partial x/\partial y)_{\text{rot}} = {}^1/_2(\partial x/\partial y - \partial y/\partial x) \tag{14}$$

A point (x,y) on rotation describes a curve, the slope of which is $\partial x/\partial y$. Rotating the axes counter-clockwise through an angle $\beta = 90° - \alpha$ (see Fig. 2) gives:

$$(\partial x/\partial y)_\beta = {}^1/_2(\tan\beta - \cot\beta) = -\cot 2\beta = \cot 2\alpha' \tag{15}$$

During this rotation ∂x increases and ∂y decreases. As the angle 2β increases from 90° to 180°, $\cot 2\beta$ increases from zero to infinity. This is equivalent to a tension in the x direction in the absence of forces in the y direction, and corresponds therefore with the condition $\sigma_2 - p = 0$.

A clockwise rotation produces a curve which is normal to that of eq. (15) and

$$(\partial x/\partial y)_{90+\beta} = -1/\cot 2\alpha' = -\tan 2\alpha' \tag{16}$$

Here ∂x decreases as a result of a tension in the y direction, and $\sigma_1 - p = 0$. Where both rotations are operative, we obtain a curve intermediate in position between the two described; hence

$$(\partial x/\partial y) = {}^1/_2(\cot 2\alpha' - \tan 2\alpha') = \cot 4\alpha' \tag{17}$$

Generalizing by setting $\partial x/\partial y = f(\alpha')$, eq. (13) becomes

$$\partial\tau + \partial\tau f(\alpha)/f(\alpha') = \rho(\ddot{x} + g)\partial y = \rho(\ddot{x} + g)\partial x/f(\alpha')$$

Both functions $f(\alpha)$ and $f(\alpha')$ vary with stress and rotation. With $f(\alpha)/f(\alpha')$ being constant, integration gives

$$\tau + \tau f(\alpha)/f(\alpha') = \int \rho(\ddot{x} + g)\partial x/f(\alpha') = F_i \qquad (18)$$

This equation describes the dynamics of a particle relative to rotating axes. We have then the shearing stress τ, the force per unit area acting tangentially on the original frame of reference, and a force, described by the integral, which is the sum of the inertial force and body force (or combined inertial force, for short) per unit area with accelerations relative to the rotated coordinates. The difference between these forces is the apparent force $\tau f(\alpha)/f(\alpha') = \sigma/f(\alpha')$, which also acts on the rotated frame.

Combining eqs. (15–17) with eqs. (10) gives

$$\text{for } \sigma_2 = p: \qquad \tau - \tau \cot 2\alpha/\cot 2\alpha' = F_i$$

$$\text{for } \sigma_1 = p: \qquad \tau - \tau \tan 2\alpha/\tan 2\alpha' = F_i \qquad (19)$$

for the general case:

$$\tau - \tau\,(\operatorname{cosec} 4\alpha \sec 2\alpha + \cot 4\alpha)/\cot 4\alpha' = F_i$$

On substituting the generalized function $f(\alpha)/f(\alpha')$ by b, these equations reduce to

$$\tau = b\tau + (1 - b)\tau \qquad (20)$$

where $(1 - b)\tau$ is the combined inertial force per unit area. This equation holds also if b is replaced by a variable b' varying with the stress.

Equations (19) and (20) represent the equilibrium between all the forces acting on a system and are, therefore, applicable to any kind of deformation whether elastic or time-dependent. As such, they are incomplete, in that they do not refer to stress-strain relations. However, since they contain secondary effects resulting from the rotation of the cordinate axes, they can be applied to the tangential components of stress and deformation which are obtained from experiment. This procedure will be described for non-Newtonian flow.

IV. Non-Newtonian Viscosity and Anisotropic Behavior

Viscosity measurements are often carried out so that the tangential shearing stress is known and the resulting rate of deformation is measured, or by applying a given rate of deformation and measuring the resulting shearing stress. The direction of this rate of deformation coincides with that of the tangential shearing stress, and the

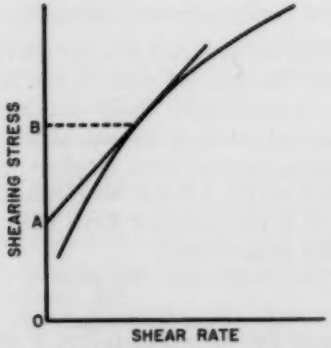

Fig. 3. Relationship between shearing stress and shear rate for non-Newtonian flow.

rate of deformation is proportional to the shear rate in the same frame of coordinates.

Non-Newtonian viscosity varies with the shearing stress or with the shear rate. This variable viscosity is often expressed as an "apparent viscosity," shearing stress over shear rate, in analogy with Newtonian viscosity. Actually, non-Newtonian viscosity is determined by the tangent to a point of the shearing stress-shear rate curve (Fig. 3). The tangent intersects the shearing stress axis at point B dividing the stress into two parts, an apparent stress AB and an intercept OA. These parts are, according to eq. (20), the apparent stress $b\tau$ and the intercept $(1 - b)\tau$. The non-Newtonian viscosity is then

$$\eta' = d\tau/d\dot{\gamma} = b\tau/\dot{\gamma} \tag{21}$$

Substituting for b the trigonometric functions from eqs. (19a) and (19b) gives

for $\sigma_2 = p$: $$\eta' = \tau \cot 2\alpha/\dot{\gamma} \cot 2\alpha' \tag{22}$$

for $\sigma_1 = p$: $$\eta' = \tau \tan 2\alpha/\dot{\gamma} \tan 2\alpha' \tag{23}$$

These relationships show that non-Newtonian viscosity, in contrast to Newtonian viscosity, is determined solely by the secondary stress components, $\tau \cot 2\alpha$ and $\tau \tan 2\alpha$ and the secondary strain rate components, $\dot{\gamma} \cot 2\alpha'$ and $\dot{\gamma} \tan 2\alpha'$.

It will be seen that these strain rates correspond to the secondary strains given in eqs. (11a and 11b), and $\eta' = \sigma/\dot{\epsilon}$. It follows also

that for cot $2\alpha <$ cot $2\alpha'$ and tan $2\alpha <$ tan $2\alpha'$, b is smaller than 1, and the shearing stress-shear rate curve is concave towards the shear rate axis. In the reverse case, b is larger than 1, and the curve is convex toward the abscissa. For the general case we have from eqs. (19)

$$\eta' = d\tau/d\dot{\gamma} = \tau(\text{cosec } 4\alpha \sec 2\alpha + \cot 4\alpha)/\dot{\gamma} \cot 4\alpha' \qquad (24)$$

It can be reasonably assumed that at low shear rates the directions of stress and deformation coincide. In this case $\alpha = \alpha'$, and the viscosity according to eqs. (22 and 23) will be constant, which has been verified by experiment (e.g., reference 9). This viscosity is, however, not Newtonian in the strict sense of the word, since it is still the result of secondary stresses and strain rates, and may be termed "equilibrium viscosity." A liquid with such a viscosity still shows the Weissenberg effect, which would be absent in a Newtonian isotropic liquid.

The three equations for non-Newtonian viscosity represent three different kinds of behavior under shear. In the case of eq. (22), the secondary stress effect results in a positive pressure normal to the direction of shear, and the Weissenberg effect is positive. Where eq. (23) holds, this pressure acts in the direction of shear and the Weissenberg effect is negative. This effect works in both directions for the general case of eq. (24) and is more difficult to demonstrate.

Integration of eq. (21) with b = constant gives

$$\tau/\tau_0 = (\dot{\gamma}/\dot{\gamma}_0)^b \qquad (25a)$$

where τ_0 and $\dot{\gamma}_0$ refer to the upper limits of the region with equilibrium viscosity. In the absence of this limit, the equation may be written as follows:

$$\tau = B\dot{\gamma}^b \qquad (25b)$$

where B is a constant. This equation has been empirically derived by de Waele,[10] Farrow and Lowe,[11] and W. Ostwald.[12]

Although $\dot{\gamma}$ is a tangential shear rate, it is not the same as for Newtonian flow. However, with the aid of eq. (25a), the velocity gradient can be correlated with the stress gradient for any experimental shear condition.

An interesting case with a variable value of b is obtained when the product of shearing stress and the variable b is constant: $b'\tau = b\tau_0$. The coefficient of non-Newtonian viscosity is then

$$\eta' = d\tau/d\dot{\gamma} = b'\tau/\dot{\gamma} = b\tau_0/\dot{\gamma}$$

and is a function of the shear rate alone but independent of the stress. Integration yields

$$\exp[(\tau - \tau_0)/\tau_0] = (\dot{\gamma}/\dot{\gamma}_0)^b \tag{26}$$

which has also been given by Ludwik.[13]

If the volume of a non-Newtonian liquid remains constant during the shearing operation, the viscosity remains a shear viscosity. However, when accompanied by volume changes, non-Newtonian viscosity can be divided into a shear viscosity associated with the secondary shearing stress τ_1 and a volume viscosity in terms of the principal stresses in accordance with eqs. (8) and (9).

For the evaluation of the trigonometric functions of α and α', it is necessary to measure the normal stress which according to eq. (10) is $\sigma = \tau f(\alpha)$. With the knowledge of α and b, which is obtained from the flow diagram, the angle α' can be calculated. Since α' is associated with the deformation, its knowledge permits the calculation of the flow birefringence (see Peterlin[14]).

The association of non-Newtonian viscosity with anisotropic behavior leads to a new interpretation of the work function. The area under the curve of Figure 3 represents the work per unit volume per second, and for the case where the shearing stress is a power function of the shear rate according to eq. (25), is

$$W' = \int \tau d\dot{\gamma} = \frac{1}{1+b}\,\tau\dot{\gamma} \tag{27}$$

The shearing stress is the sum of two components as shown by eq. (20), and the work function can be also divided into two parts

$$W' = \frac{b}{1+b}\,\tau\dot{\gamma} + \frac{1-b}{1+b}\,\tau\dot{\gamma} = \frac{b}{1+b}\,\tau\dot{\gamma} + \int \rho(\ddot{x}+g)\partial x d\dot{\gamma}/f(\alpha') \tag{28}$$

The first term on the right side of the equation represents the work per unit volume per second due to the secondary stresses, and the second term, containing the inertial and body forces, is dissipated into heat. For the Newtonian case, this work is $W' = {}^1/_2\tau\dot{\gamma}$, and is completely dissipated.

Similarly for non-Hookean elasticity, the work per unit volume is

$$W = \frac{1}{1+b}\tau\gamma = \frac{b}{1+b}\tau\gamma + \int \rho(\ddot{x} + g)\partial x d\gamma / f(\alpha') \qquad (28)$$

For the case of Hookean elasticity this work is $W = {}^1/_2\tau\gamma$ and represents only the potential energy. The inclusion of the kinetic energy in the work for non-Hookean elasticity indicates that the latter can be associated with time effects.

V. Stress Distribution in Anisotropic Bodies under Tension and Compression

For the condition of tension or compression, the stress distribution as shown in Figure 2 is also valid after omitting the shearing stress τ. With σ_1 being the principal tensile or compressive stress, the stress becomes in analogy with eq. (2):

$$s_d = \sigma_1 + \sigma \qquad (29)$$

The normal stress component σ is defined by eq. (4). Omitting the hydrostatic pressure, since it does not contribute to the deformation, we have from eqs. (7)

$$\begin{aligned} \sigma &= {}^1/_2(\sigma_1 + \sigma_2) + {}^1/_2(\sigma_1 - \sigma_2)\cos 4\alpha \\ \sigma &= \sigma_2 \sin^2 2\alpha + \sigma_1 \cos^2 2\alpha \end{aligned} \qquad (30)$$

From eqs. (7) we have in addition

$$\sigma_1 - \sigma_2 = (\sigma_1 + \sigma_2)\cos 2\alpha$$

hence

$$\sigma_2 = \sigma_1 \tan^2\alpha$$

which simplifies the second of eqs. (30) as follows:

$$\sigma = \sigma_1(\cos^2 2\alpha + \sin^2 2\alpha \tan^2 \alpha) = \sigma_1(1 - \sin 4\alpha \tan \alpha) \qquad (31)$$

The principal stress σ_1 acts in the x direction and the normal component in the y direction, and eq. (18) becomes for the case of compression or tension with $(1 - \sin 4\alpha \tan \alpha)\partial x/\partial y = \text{constant}$:

$$\sigma_1 - \sigma_1(1 - \sin 4\alpha \tan \alpha)\cot 4\alpha' = \int \rho(\ddot{x} + g)\partial y \cot 4\alpha' \qquad (32)$$

The coefficient of traction, corresponding to non-Newtonian viscosity, is consequently

$$\mu' = d\sigma_1/d\dot{\epsilon}_1 = \sigma_1(1 - \sin 4\alpha \tan \alpha)\cot 4\alpha'/\dot{\epsilon}_1 \qquad (33)$$

Since for a given value of σ_1 the trigonometric functions of α and α' have different values for tension and compression, the results show that non-Newtonian liquids have different rheological properties under shear, tension, and compression, respectively, as should be the case for anisotropic bodies.

References

1. Poynting, J. H., *Proc. Roy. Soc.* (*London*), **A82,** 546 (1909); **A86,** 534 (1912).
2. Weissenberg, K., *Nature*, **159,** 310 (1947); *Proc. Intern. Congr. Rheol.*, North Holland, Amsterdam, 1949.
3. Mooney, M., *J. Colloid Sci.*, **6,** 96 (1951).
4. Mooney, M., *J. Appl. Phys.*, **11,** 582 (1940).
5. Rivlin, R. S., *Proc. Roy. Soc.* (*London*), **A193,** 260 (1948); **A200,** 168 (1950).
6. Reiner, M., *Am. J. Math.*, **70,** 433 (1948).
7. Roberts, J. E., *Proc. Intern. Congr. Rheol., 2nd Congress, Oxford, 1953*, Butterworth, London, 1954.
8. Philippoff, W., *Trans. Soc. Rheol.*, **1,** 95 (1957).
9 Brodnyan, J. G., F. H. Gaskins, and W. Philippoff, *Trans. Soc. Rheol.*, **1,** 109 (1957).
10. de Waele, A., *J. Oil & Colour Chemists' Assoc.*, **4,** 33 (1923).
11. Farrow, F. D., and G. M. Lowe, *J. Textile Inst.* **14T,** 414 (1923).
12. Ostwald, W., *Kolloid-Z.*, **36,** 99 (1925).
13. Ludwik, P., *Elemente der Technologischen Mechanik*, Springer, Berlin, 1909.
14. Peterlin, A., and R. Signer, *J. Polymer Sci.*, **12,** 45 (1954).

Synopsis

Secondary stresses have been the subject of several investigations since their presence was first demonstrated by Weissenberg in liquids during laminar flow. They have been associated with elasticity by some investigators, and with viscous effects by others. In these theories, secondary stresses are assumed to arise from the deformation or rate of deformation in otherwise isotropic bodies. Since most industrially important materials are not isotropic, a theory of secondary stresses is given for anisotropic behavior in general. It is shown that non-Newtonian viscosity is the direct outcome of secondary stresses, and their importance for rheological behavior is discussed. In relating secondary stresses with non-Hookean elasticity, it is found that this type of elasticity is also associated with time effects.

TRANSACTIONS OF THE SOCIETY OF RHEOLOGY III, 113–136 (1959)

Volume Changes and Dewetting in Glass Bead–Polyvinyl Chloride Elastomeric Composites Under Large Deformations*

THOR L. SMITH,† *Jet Propulsion Laboratory, California Institute of Technology, Pasadena, California*

INTRODUCTION

Elastomeric materials loaded with inert filler have rheological properties which, on the one hand, are qualitatively like those of unfilled polymeric materials, but which, on the other hand, are unique to filled systems. Their stress-strain curves usually have several distinct regions which are similar to those for certain unfilled polymeric materials. The curves have an initial region in which the stress increases with strain, and here the modulus depends primarily on the amount of filler and the properties of the binder. In the second region, the stress may be roughly independent of the strain or may increase at a rate markedly less than that in the initial region. The transition between these two regions may be either gradual and hardly perceptible or sharp, with a well-defined yield point. Thus, in these two regions, the stress-strain curves may be like those for typical unfilled rubbers or for plastics, or they may resemble the curves for rubbers at low temperatures, which cold-draw or neck. In the third region the stress increases more rapidly with strain than in the second region and continues to increase until the specimen breaks; again, this is similar to what is observed for certain plastics and rubbers. Thus, both filled and unfilled systems can have sigmoidal stress-strain curves which may or may not have distinct yield points.

* This paper presents the results of one phase of research carried out at the Jet Propulsion Laboratory, California Institute of Technology, under sponsorship of the Department of the Army, Ordnance Corps (Contract No. DA-04-495-Ord 18).

† Present address: Stanford Research Institute, Menlo Park, California.

However, filled systems, and especially those in which the binder wets, but does not react chemically with the filler, exhibit the sigmoidal-type stress-strain curve for different reasons than do rubbers and plastics. In filled systems, the binder adheres to the filler initially, which reinforces or strengthens the system. However, in the transition and second regions of the stress-strain curve, adhesive bonds between the filler and binder break, a process called dewetting, and vacuoles form around the filler particles. After the adhesive bonds are essentially all broken, a further increase in strain only stretches the binder further and enlarges the vacuoles.

Perhaps the best method for studying dewetting is to measure the volume of the filled system as a function of elongation. When an unfilled rubber is stretched, its volume remains essentially constant, provided crystallization does not occur. However, when a filled system is stretched, and vacuoles form, the volume increase may be large: e.g., 50 to 100%, or possibly more. The measurement of this volume increase by means of a sensitive dilatometer can give a precise value for the elongation at which the dewetting begins, and possibly that at which it is complete.

Additional information can be derived from a study of the volume changes. Since the data show precisely the elongation at which adhesive failure begins, methods for modifying the adhesive strength can be investigated. Further, the temperature dependence of the adhesive strength can be studied by carrying out tests at different temperatures. If certain assumptions are made, an estimate can be obtained of the elongation of the binder between adjacent filler particles at the time when dewetting occurs. This result, when combined with the stress-strain properties of the unfilled binder, gives an indication of the stress required to break the adhesive bonds.

Relatively few dilatometric studies have been made of the volume changes that occur during the stretching of filled materials. Holt and McPherson[1] made a careful study of the stretching of unfilled vulcanized rubber and the volume changes resulting from crystallization; also, a few studies were made of a gum stock filled with whiting and a carbon black. These investigations were extended by Jones and Yiengst,[2] who studied the volume changes that occurred when various pigmented-rubber systems were stretched in a dilatometer similar to one used by Holt and McPherson. More recently, some data were obtained in a similar manner by Bryant and Bisset[3] for

several filled rubber vulcanizates. Prior studies relating to vacuole formation in filled rubbers were made by Schippel,[4] Green,[5] Vogt and Evans,[6] and DePew and Easley.[7]

The present study was made to extend previous work and to obtain data at several temperatures. Filled systems composed of small glass beads dispersed in a polyvinyl chloride–dioctyl sebacate rubber were stretched in a dilatometer at 0, 25, and 50° C. Less precise data were also obtained by stretching specimens and measuring the change in their width and length. A simple equation was derived to relate the volume fraction of filler to the yield strain obtained from the dilatometric data.

EXPERIMENTAL

A. Materials

(1) *Glass Beads*

The glass beads were obtained from the Minnesota Mining and Manufacturing Company; their No. 1160 beads were used in nearly all the composites studied. These beads were essentially spherical and were analyzed for size and polydispersity by means of a Micromerigraph. The beads had a weight-average diameter of approximately 40 μ, and about 94 wt.-% of the beads had diameters between 20 and 60 μ.

Limited studies were made with beads Nos. 118, 116, 114, and 112. From rough Micromerigraph data, it appeared that these beads had weight-average diameters of about 50, 80, 105, and 140 μ, respectively. (The size of the No. 112 beads was not measured, but a diameter of 140 μ was assumed after comparing data supplied by the manufacturer with measurements obtained on the Micromerigraph for beads Nos. 118, 116, and 114.)

(2) *Elastomer*

The elastomer was prepared from equal weights of a polyvinyl chloride plastisol (Geon 121) and dioctyl sebacate and contained 2.5% lead stearate as stabilizer. To obtain a uniform dispersion, the solids were slowly added to the dioctyl sebacate while it was stirred mildly by a Brookfield counter-rotating stirrer. The mixture was then vigorously stirred for 10 min. by the Brookfield stirrer running at a

high speed. The resulting dispersion was cast into trays, degassed for about 30 min. (or until no more gas was evolved), and then cured for about 1 hr. at 180° C. The cured sheets, about $^1/_8$ in. thick, were visibly homogeneous and completely bubble-free.

(3) *Composites*

In preparing the glass-bead composites, the polyvinyl chloride dispersion was mixed as described above, and then degassed. The glass beads were next added slowly while the dispersion was stirred at low speed. The resulting mixture was cast into trays, degassed, and then cured.

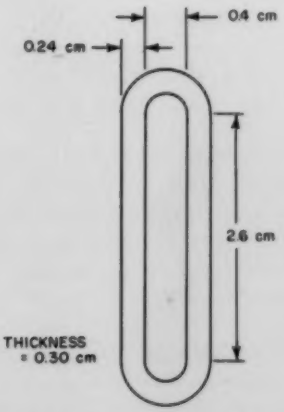

Fig. 1. Elongated-ring specimen used in dilatometer.

In addition to sheets of the composites, elongated ringlike specimens were prepared for testing in the dilatometer. The shape and dimensions of the rings are shown in Figure 1. Specimens of this shape were chosen in preference to circular rings, since they could be stretched in the dilatometer without first being flattened, which might disrupt some adhesive bonds between the beads and binder. The rings were prepared by casting the uncured composite into an open mold machined in a small block of aluminum. After the dispersion was poured into the mold, it was degassed again; the excess was then scraped from the surface of the mold, and the mold was placed on a

hot plate to effect cure. Highly uniform rings, which ordinarily differed in weight by less than 5%, were prepared in this way.

One disadvantage of rings is that the strain in a stretched specimen is not uniform, since the outside of the ring is elongated more than the inside. The rings used had an outside-to-inside-circumference ratio of about 1.23; therefore, the average circumference was used to calculate an average strain or extension ratio from the extension of a ring.

The cured composites were essentially free of voids, as determined by density measurements, and the beads appeared to be uniformly dispersed. However, composites prepared from beads Nos. 112 and 116 had a thin resin-rich surface, which indicated that these beads had settled somewhat after mixing.

The densities of representative samples of the composites prepared with No. 1160 beads were obtained by hydrostatic weighing. These values are compared in Table I with the theoretical densities calculated from density values of 2.39 and 1.135 g./ml. for the beads and the elastomeric binder, respectively. The calculated and measured

TABLE I
Experimental and Calculated Densities of Composites Containing No. 1160 Glass Beads

Glass-bead content, wt.-%	Glass-bead content, vol.-%	Density, g./ml.		
		Experimental	Calculated	Difference
25	13.7	1.273	1.308	−0.035
50	32.2	1.355	1.541	−0.186
60	41.5	1.645	1.657	−0.012
70	52.5	1.840	1.794	0.046
75	58.9	1.895	1.875	0.020
80	65.4	1.975	1.955	0.020

densities agreed within a few per cent, except for the composite having 50 wt.-% beads. The reason for this disagreement is not known; it probably is the result of some error, since no other evidence was obtained which indicated voids in any samples for which data are reported. (Densities were measured on only one set of samples, and many samples were prepared during the study.)

(4) *Polyurethane Foam Rubber*

To prepare the foam, a castable polyurethane elastomer filled with 59% by volume of a water-soluble inorganic salt was first prepared. About 70% of the salt had an average particle diameter of 150 μ, and 30% had an average diameter of 15 μ. The foam was obtained by extracting the salt from the filled elastomer with boiling water. The foam was dried carefully and chemically analyzed to verify that the salt had been extracted completely.

B. Apparatus and Procedure

(1) *Dilatometer*

A dilatometer was constructed which was similar to the one used by Holt and McPherson[1] and by Jones and Yiengst.[2] It consisted of a metal tube which had rubber O-rings and screw caps on each end. A piece of drill rod passed completely through the metal tube and screw caps. Inserted in each screw cap was a threaded stuffing box, which prevented leakage of the dilatometer fluid and yet allowed the rod to be moved up and down. The metal tube had a side arm, to which a calibrated glass capillary and an auxiliary reservoir were attached. To hold the ring test specimen in the dilatometer, a metal hook was attached on the inside, near the top of the metal tube, and a similar hook was attached to the drill rod.

In making measurements, the top screw cap was removed, and a ring specimen was hung over the hook attached to the inside of the metal tube. The screw cap was then replaced, and the dilatometer was filled with water from the auxiliary reservoir. A small vent hole in the upper screw cap permitted the escape of any trapped air, after which the vent hole was plugged, and the auxiliary reservoir was isolated from the main part of the apparatus. To test for leaks, the water level in the capillary was observed while the drill rod was moved down and up. The drill rod was next moved to the appropriate position and then rotated until its attached hook moved inside the ring and was in the same vertical plane as the upper hook. The rod was slowly moved down until fiducial marks on the exposed portion of the rod and on a reference rod indicated that the ring was snugly fitted between the hooks and ready to be tested. Next, the rod was moved down stepwise to stretch the ring. After each step, the water level

in the capillary was read, and the position of the fiducial mark on the rod was measured by a cathetometer. This procedure was continued until the ring had been stretched about 200%.

Some data were obtained with another dilatometer, which was similar except that the tube was made of Lucite tubing, rather than metal. In this dilatometer, the extension of the ring could be observed visually. Occasionally, the extension of a ring was measured directly by the cathetometer, and the results agreed closely with values obtained from the fiducial mark on the rod. However after two Lucite tubes had cracked, the tube was replaced by a metal one.

To obtain data at 0, 25, and 50° C., the dilatometer was placed in a water bath controlled to ±0.1° C. or less. A few runs were made at −19° C.; in these, a silicone fluid was substituted for water as the confining liquid in the dilatometer. Accurate temperature control of the thermostat was always maintained in order to prevent small temperature fluctuations during an experiment from changing the water level in the capillary.

(2) *Dimension Measurements*

Some studies were made by measuring the elongation and width of rectangular tensile specimens which were stretched stepwise. Bench marks were inked on a specimen, and the separation of these marks was measured by a cathetometer after each incremental elongation of the specimen. The width of the specimens was measured by a micrometer. Although this simple procedure is not as precise as the dilatometric method, it provided reasonably accurate data.

THEORETICAL

A. Poisson's Ratio

The deformation of an elastic material in pure homogeneous strain may be characterized by three principal extension ratios. For example, suppose that an undeformed rectangular parallelepiped, having length L_0, width W_0, and thickness T_0, is deformed by loads applied perpendicularly to its opposite faces. The resulting deformation is given by the principal extension ratios $\lambda_1 = L/L_0$, $\lambda_2 = W/W_0$, and $\lambda_3 = T/T_0$, where L, W, and T are the new length, width, and thickness. Thus, the volume change is given by the relation

$$V/V_0 = \lambda_1\lambda_2\lambda_3 \tag{1}$$

where V and V_0 are the volumes of the deformed and undeformed material.

When an isotropic material is subjected to tension or compression, λ_2 equals λ_3. If no volume change occurs, the following relation holds:

$$1 = \lambda_1\lambda_2^2 \tag{2}$$

This leads to the equation

$$d\lambda_2/d\lambda_1 = -\lambda_2/2\lambda_1 = d\epsilon_w/d\epsilon_1 \tag{3}$$

where ϵ_w is the lateral strain, and ϵ_1 is the longitudinal strain. According to classical elasticity, based on small-deformation theory, Poisson's ratio ν equals $-d\epsilon_w/d\epsilon_1$, and eq. (3) shows that this ratio varies with the extension, even though it is assumed that no volume change occurs. However, eq. (3) can be integrated to give

$$\ln \lambda_2/\ln \lambda_1 = -1/2 \tag{4}$$

where $\ln \lambda_2$ and $\ln \lambda_1$ are the Hencky, or logarithmic, lateral and longitudinal strains. Thus, Poisson's ratio, defined in terms of the logarithmic measure of strain, is independent of the extension and equals $^1/_2$, provided that the volume remains constant.

Poisson's ratio, defined in terms of logarithmic strain,* is a convenient number to use in specifying volume changes that occur when an elastic material is subjected to large deformations. The volume change that occurs during a tensile or compressive deformation is given by the following equation, derived by differentiating eq. (1) after noting that λ_2 equals λ_3:

$$\frac{d \ln V/V_0}{d \ln \lambda_1} = 1 + 2\frac{d \ln \lambda_2}{d \ln \lambda_1} = 1 - 2\nu \tag{5}$$

where Poisson's ratio ν, which may be a function of λ_1, is defined as follows:

$$\nu = -d \ln \lambda_2/d \ln \lambda_1 \tag{6}$$

* Certain valid reasons are recognized for not defining Poisson's ratio in terms of logarithmic strain. However, Poisson's ratio defined in terms of logarithmic strain is used in this paper only as a convenient index for rate of volume change, even though some other name should, perhaps, be given to this quantity.

B. Yield Strain

Certain filled elastomers, like glass bead–polyvinyl chloride composites, can be stretched to a limited extent without showing any appreciable volume change. However, at a reasonably well-defined yield strain, dewetting occurs, and the volume of the sample increases continuously with further stretching. The yield strain can be related to the volume fraction of filler by an equation based on certain simplifying assumptions.

Consider a unit cube of an elastomer filled with n^3 spherical particles, each having a radius r and a modulus which is large compared with that of the elastomeric binder. Assume that these spheres are uniformerly dispered, and that their centers lie in a cubic close-packed array: i.e., if the radius of each sphere were enlarged until all spheres touched, a cubic close-packed array would result.

Now consider a line through the centers of the n spheres in one row. The length of the line is unity, the fraction of the line occupied by spheres is $2rn$, and the fraction occupied by binder is d_0. Thus,

$$2rn + d_0 = 1 \tag{7}$$

The volume fraction of spheres V_f can be shown, by considering the geometrical properties of cubic close-packed arrays, to be

$$V_f = \frac{4\sqrt{2}}{3}\pi (rn)^3 \tag{8}$$

By combining eqs. (7) and (8), the following expression is obtained:

$$\left(\frac{3\sqrt{2}}{\pi}\right)^{1/3} V_f^{1/3} + d_0 = 1 \tag{9}$$

If the cube containing the filler is stretched a distance Δl, and if dewetting does not occur, then the following equation can be written:

$$1.105 V_f^{1/3} + d_0 + \Delta l = 1 + \Delta l \tag{10}$$

where $1.105 = (3\sqrt{2}/\pi)^{1/3}$. Equation (10) can be rearranged to give

$$1.105 V_f^{1/3} + (1 + \epsilon_r)\, d_0 = 1 + \epsilon \tag{11}$$

where ϵ_r is the strain in the binder between adjacent spheres and equals $\Delta l/d_0$, and ϵ is the strain imposed on the unit cube and equals Δl.

Now, by substituting in eq. (11) the value of d_0 given by eq. (9), the following relation is obtained:

$$\epsilon = \epsilon_r (1 - 1.105 V_f^{1/3}) \tag{12}$$

This equation gives ϵ/ϵ_r (the ratio of the over-all strain imposed on the sample to the strain in the binder along the line between the centers of adjacent spheres) in terms of the volume fraction of spheres. Now, assume that dewetting occurs when ϵ_r reaches a critical value $\epsilon_{r,c}$, which is assumed to be independent of the amount of filler. Thus, the observed yield strain ϵ_c is given by the equation

$$\epsilon_c = \epsilon_{r,c} (1 - 1.105 V_f^{1/3}) \tag{13}$$

When no filler is present, this equation shows that $\epsilon_c = \epsilon_{r,c}$, and, when V_f equals 0.74 (the volume fraction of spheres in a cubic close-packed array), that $\epsilon_c = 0$.

RESULTS AND DISCUSSION

A. Preliminary Studies

A tensile specimen of the polyurethane foam rubber was stretched in incremental steps, and the width and per cent elongation were measured for elongations up to about 50%. Figure 2 shows that -log W/W_0 is directly proportional to log L/L_0, and that Poisson's ratio is 0.362. When similar measurements were made on a polyurethane elastomer, Poisson's ratio was found to be 0.50 over the entire range of extensions covered. The behavior of the foam is like that of a filled elastomer after dewetting is complete, in that Poisson's ratio is independent of extension.

Similar measurements were made on specimens of the polyvinyl chloride composites containing 13.7, 32.2, 41.5, and 58.9 vol.-% glass beads. (These volume per cents, and others given in this paper, were calculated from the known weight per cents of binder and glass beads.) The data from these preliminary tests are shown in Figures 3 and 4; data on the unfilled polyvinyl chloride elastomer are also included in Figure 3. In small deformations, Poisson's ratio for all polyvinyl chloride composites is 0.50, within the experimental error, and, for the unfilled elastomer, it is 0.50 over the entire range of extensions (i.e., 0 to 200%). For the composites, however, dewetting begins at some

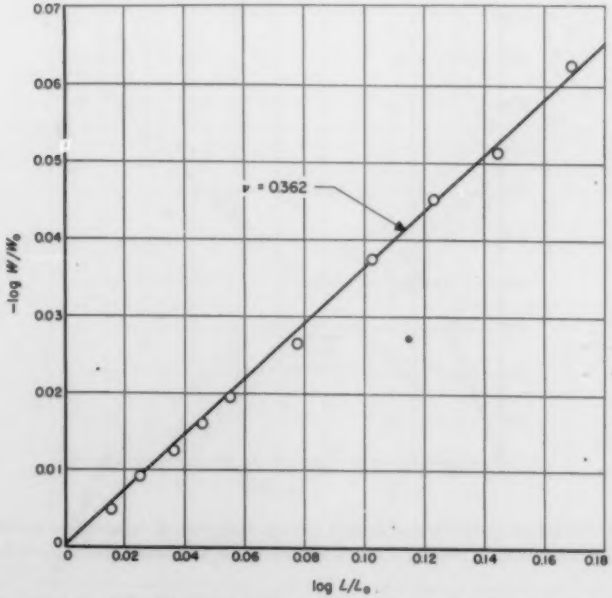

Fig. 2. Variation in width and length during extension of foam-rubber specimen.

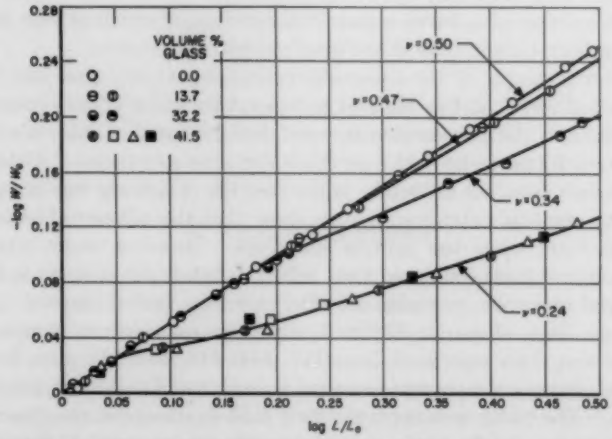

Fig. 3. Variation in width and length during extension of glass-bead composites.

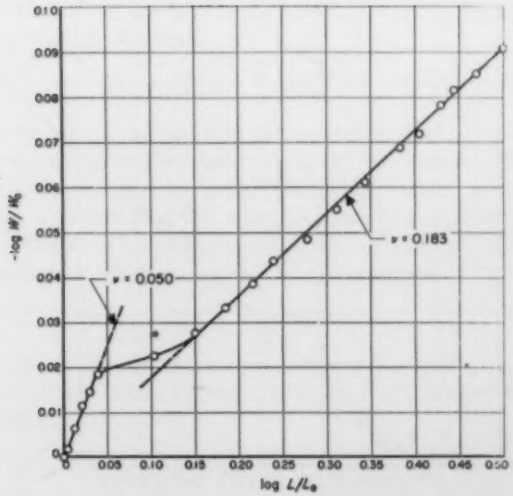

Fig. 4. Variation in width and length during extension of composites containing 58.9% glass beads. (Legend on first section of curve should read: $\nu = 0.500$.)

critical extension; after a transition region, -log W/W_0 again increases linearly with log L/L_0, but at a reduced rate. The slope of the final linear portion of a curve equals Poisson's ratio, which is seen to increase from 0.24 to 0.50 as the glass content is decreased.

After a sample of the composite containing 41.5% glass had been stretched 200%, it was allowed to recover to within 3% of its initial length, and the measurements were then repeated. Poisson's ratio was now found to be 0.24 over the entire extension range. Although this result does not definitely prove that the dewetting was complete during the first extension, it does show that the adhesive bonds did not re-form when the sample recovered. However, some qualitative observations indicated that adhesive bonds can re-form in a recovered specimen, provided a sufficiently long period elapses.

Some data, shown in Figure 5, were also obtained on composites containing 52.5 vol.-% of Nos. 112, 114, 116, and 118 glass beads. Again, Poisson's ratio was constant at both small and large deformations. The value was approximately 0.50 in small deformations and 0.172 in large deformations, even though the composites contained

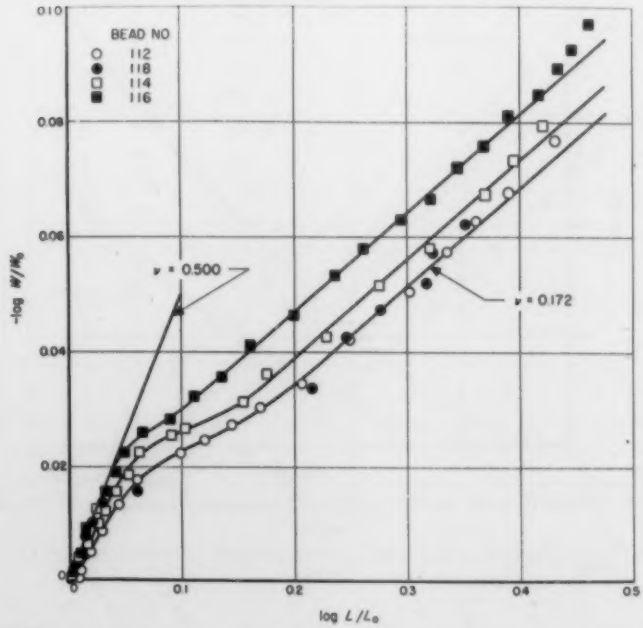

Fig. 5. Variation in width and length during extension of composities containing 52.5% glass beads of different sizes.

different-sized beads. The composites had different yield values, although the values obtained are not very accurate. In general, yield values are not very reproducible, but Poisson's ratio in large deformations is usually reproducible.

B. Dilatometric Studies

More precise and extensive data on Poisson's ratio and the yield strain were obtained by use of the dilatometer. First, an unfilled polyvinyl chloride ring was elongated to 150% in incremental steps in the dilatometer. The volume increase observed was exceedingly small, approximately 0.23%, and gave a Poisson's ratio of about 0.499. This value is in close agreement with the value of 0.500 reported by Holt and McPherson[1] for vulcanized natural rubber at extensions up

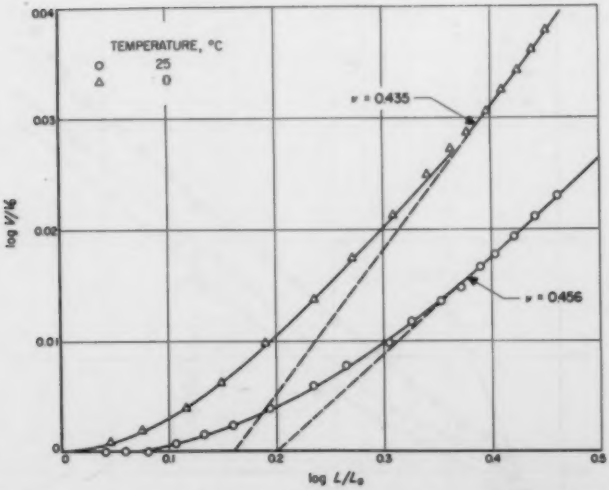

Fig. 6. Volume increase during extension of composites containing 13.7% glass beads.

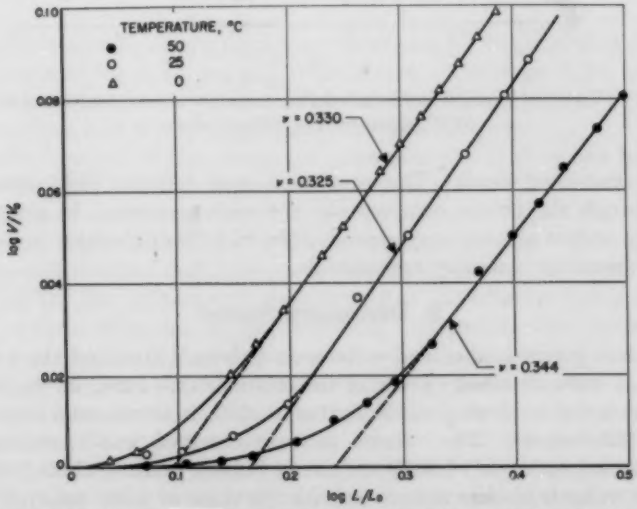

Fig. 7. Volume increase during extension of composites containing 32.2% glass beads.

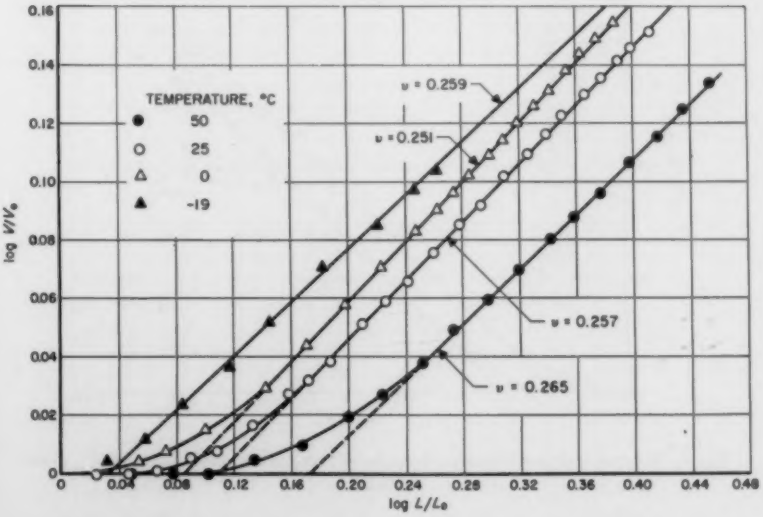

Fig. 8. Volume increase during extension of composites containing 41.5% glass beads.

to 300%. Other experiments made on the unfilled polyvinyl chloride elastomer, stretched to 200% and more, also showed essentially no volume changes. It is thus concluded that, when the binder itself is extended, volume changes do not occur (at least not at 25° C.) either because of formation of voids or resulting from crystallization.

Volume changes as a function of extension were measured dilatometrically for the composites containing 13.7, 32.2, 41.5, and 52.5 vol.-% glass. Measurements were made at 0, 25, and 50° C. for the composites containing 32.2% glass; the composites having 13.7 and 52.5% glass were tested at only two temperatures; and the composite containing 41.5% glass was tested at −19° C., in addition to the three other temperatures. Ordinarily, duplicate experiments were made, but only the results of single experiments are shown in Figures 6 to 9, plotted as $\log V/V_0$ vs. $\log L/L_0$.

These figures show that the data from any experiment can be divided into three sections, similar to those in Figures 3 to 5. In the first section, which is for small deformations, little or no volume in-

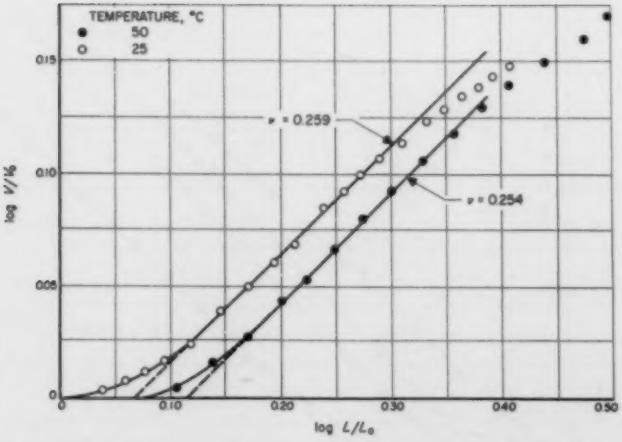

Fig. 9. Volume increase during extension of composites containing 52.5% glass beads.

crease occurs as a specimen is extended. The next section is the transition region, in which dewetting of the filler occurs, and the volume increases at a progressively increasing rate as the sample is extended. In the final section, the dewetting is believed to be complete and log V/V_0 increases linearly with the logarithmic strain. Figure 9 shows that the rate of volume increase drops off at high extensions. This behavior is believed to result from water in the dilatometer diffusing into the vacuoles or other defects in the stretched specimen.

By the use of eq. (5), Poisson's ratio was calculated from the slope of the linear section of a curve. The linear section was also extrapolated to zero volume change to obtain a yield strain. Values for Poisson's ratio and the yield strain are presented in Table II, together with the values for Poisson's ratio which were obtained in the preliminary experiments by measuring the width and length of a specimen. At −19° C., Poisson's ratio and the yield strain for the 41.5%-glass composite were 0.259 and 0.08, respectively. The data in Table II show that the duplicate values for Poisson's ratio are in close agreement, and that the values obtained from the preliminary experiments agree closely with those obtained dilatometrically, except for the composite containing 52.5% glass. Within the experimental

TABLE II
Poisson's Ratio and Yield Strain for Glass-Bead Composites

Glass-bead content			Poisson's ratio ν				Yield strain ϵ_y		
Bead No.	wt.-%	vol.-%	0°C.	25°C.	50°C.	~25°C.[a]	0°C.	25°C.	50°C.
1160	25	13.7	0.435	0.456	—	0.47	0.44	0.58	—
			0.432	0.463	—		0.45	0.75	—
			—	0.419	—		—	0.68	—
1160	50	32.2	0.330	0.325	0.344	0.34	0.24	0.46	0.73
			0.326	0.313	—		0.25	0.57	—
			—	0.310	—		—	0.50	—
1160	60	41.5	0.234	0.268	0.265	0.24	0.24	0.23	0.49
			0.251	0.257	0.275		0.19	0.31	0.35
1160	70	52.5	—	0.259	0.254	0.16	—	0.17	0.30
			—	0.265	—		—	0.09	—
			—	0.256	—		—	0.12	—
1160	75	58.9				0.19		0.10[b]	
112	70	52.5				0.172		0.08[b]	
114	70	52.5				0.172		0.10[b]	
116	70	52.5				0.172		0.12[b]	
118	70	52.5				0.172		0.06(?)	

[a] Preliminary data obtained by measuring the width and length of stretched specimens.

[b] Yield strains obtained from interpolated "break-away" points in Figs. 4 and 5.

error, Poisson's ratio is probably independent of temperature, although the data suggest that it may increase slightly with temperature. Although the data on a single ring specimen are very precise, the reproducibility of results on identically prepared ring specimens is not accurately known. Thus, it is believed that the variation in Poisson's ratio may be partly due to slight variations in specimen density, which would indicate the existence of microscopic voids in the specimens, and partly due to nonuniform dispersion of the beads in the different specimens. The small experimental error in obtaining the strain in a ring, partly due to the use of fiducial marks outside the dilatometer, would not affect Poisson's ratio, although it would lead to error in the yield strain.

Table II shows that the yield strain depends rather strongly on temperature, although its reproducibility is poor. The poor reproducibility is not unexpected, since dewetting is a sensitive and highly rate-dependent process. Small differences in the microscopic

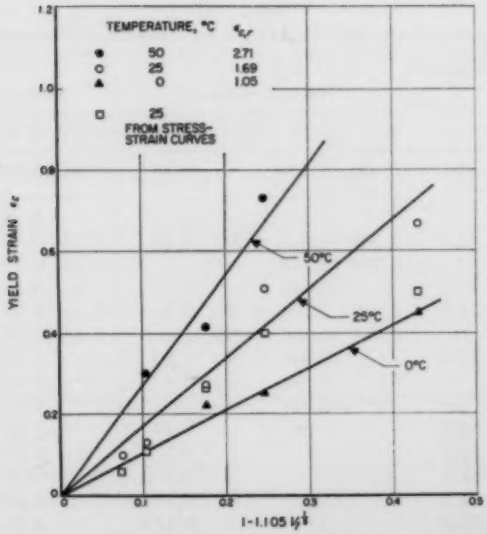

Fig. 10. Variation of yield strain with volume fraction of glass beads.

structure or mechanical treatment of a specimen can easily cause marked variations of the strain range in which dewetting occurs. However, the temperature dependence of the yield strain is expected, since the modulus of the binder is temperature-dependent.

To show how accurately eq. (13) predicts the variation of the yield strain with the volume fraction of filler, average values of the yield strain ϵ_c are plotted against $1 - 1.105V_f^{1/3}$ in Figure 10. This figure also shows yield strains at 25° C. obtained from stress-strain curves measured on the Instron tester at a strain rate of 0.6 min.$^{-1}$. The stress-strain curves had two near-linear portions: at strains somewhat less and strains somewhat greater than the yield strain. These linear portions were connected either by a curve of gradually decreasing slope or by a curve which passed through a maximum; the latter type of curve was like those for plastics which cold-draw. From both types of curves, the yield strain was obtained by extrapolating both linear portions until they intersected.

Although the points in Figure 10 scatter considerably, the lines drawn are reasonably consistent with the data and have slopes of

1.05, 1.69, and 2.77 at 0, 25, and 50° C., respectively. These slopes, according to eq. (13), should equal $\epsilon_{c,r}$, the strain of the binder between adjacent particles immediately preceding adhesion failure. From the stress-strain curves for the unfilled binder, it was found that these strains correspond to stresses of 550, 470, and approximately 430 p.s.i. at 0, 25, and 50° C., respectively. Thus, the adhesion force appears to show little or no temperature dependence.

C. Stress-Strain Behavior

Only limited stress-strain data were obtained on the composites and unfilled binder. However, some data measured on the Instron tester at 25° C. are given in Table III. This table gives the yield

TABLE III
Tensile Data for Glass-Bead Composites at 25°C.

Glass-bead content, vol.-%	σ_c, p.s.i.	ϵ_c	E_0, p.s.i.	E_a, p.s.i.	$E_a(V_b - 0.26)^{-1}$
13.7	230	0.50	450	285	473
32.2	240	0.40	580	140	334
41.5	146[a]	0.26[a]	560	114	351
52.5	90[a]	0.11[a]	820	94	437
58.9	63[a]	0.06[a]	1050	76	503

[a] Obtained by double extrapolation, as explained in text.

stress σ_c, the yield strain ϵ_c, the initial modulus E_0, and the modulus after yield E_a; the latter modulus was taken as the slope of the linear portion of the σ–ϵ curves after yield. (Values of σ_c and ϵ_c for the three composites having the most filler were obtained by interpolation, as explained previously.) It is seen that the yield stress and strain decreases, and the initial modulus increases, with filler content; however, the modulus does not increase very rapidly, considering the large variation in filler content.

The modulus after yield decreases with filler content, as expected, since now the filler only dilutes the binder and has no reinforcing effect. If it is assumed that the filler only dilutes the binder, it seems reasonable to suggest that E_a is proportional to $V_b - 0.26$, where V_b is the volume fraction of binder. The factor 0.26 is introduced, since if the spheres were monodisperse, the maximum volume fraction of

spheres would be 0.74, and thus 0.26 would be the minimum fraction of binder that could be present in a well-consolidated composite. The assumption that E_a is proportional to $V_b - 0.26$ means that E_a is zero when V_b equals 0.26, which seems reasonable. With these several assumptions, the following equation results:

$$E_a = 1.35E_b(V_b - 0.26) \tag{14}$$

where E_b is the modulus of the unfilled binder. Values of $E_a(V_b - 0.26)^{-1}$, given in the last column of Table III, are seen to be relatively constant: none vary by more than 20% from the average, which is 420. When this average value is divided by 1.35, a value of 310 p.s.i. is obtained for the modulus of the unfilled binder, which compares favorably with an experimental value of 386.

Tensile data for the composite having 32.2% filler and the modulus for the unfilled binder, as measured at a strain rate of 0.6 min.$^{-1}$ and at a series of temperatures, are given in Tables IV and V. The data

TABLE IV
Temperature Dependence of Mechanical Properties for the Composite Containing 32.2% Glass Beads

Temperature, °C.	$\sigma_{e'}$ p.s.i.	ϵ_e	E_0, p.s.i.	E_a, p.s.i.
−40	220	0.07	3200	660
−23	240	0.15	1500	360
− 7	240	0.24	975	240
− 1	280	0.30	905	184
27	240	0.40	580	140
43	168	0.52	320	115
60	73	0.32	225	116

TABLE V
Temperature Dependence of the Modulus for the Unfilled Binder

Temperature, °C	E_b, p.s.i.
−48	2800
−34	1580
4	585
27	386
49	230
71	132

given in Tables III to V depend on the strain rate, sometimes markedly. The most marked dependence on strain rate is shown by the section of the stress-strain curve for a composite in the yield or dewetting region. Since a complete study was not made, the effect of the strain rate and the reproducibility of the tensile data are not accurately known.

An analysis of E_0 and E_a in Table IV and of E_b in Table V for the unfilled binder shows that these three quantities have the same temperature dependence. Since these quantities are determined by the properties of the binder, this behavior is expected. However, the yield stress in Table IV appears independent of temperature within experimental error, with the exception of values at 43 and 60° C. This temperature insensitivity implies that the filler-binder adhesive strength is temperature-independent. A similar conclusion was reached, but in a different way, by analysis of the data in Figure 10.

D. Comparison With Literature Data

Bryant and Bisset[3] made an interesting study of vulcanizates which contained up to 55% by volume of mineral fillers having particle size greater than 1 μ (apparently in the range 20 to 40 μ). They measured stress-strain curves and volume changes that occurred when specimens were extended in a dilatometer. These investigators also studied the effect of per cent filler, particle size (over a rather limited

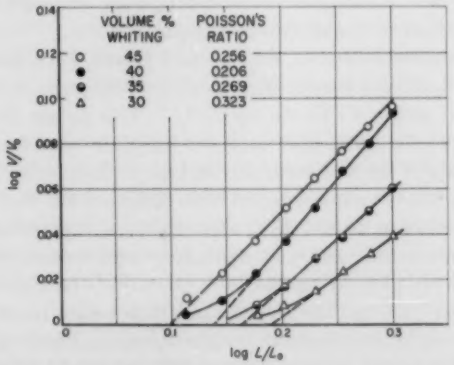

Fig. 11. Replotted data of Bryant and Bisset for a pale crepe vulcanizate containing different amounts of whiting.

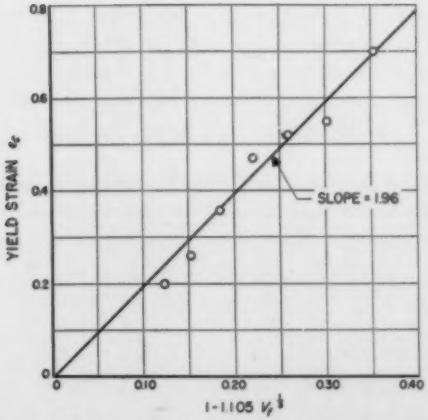

Fig. 12. Variation of yield strain with volume fraction of whiting in pale crepe vulcanizates.

range), degree of cure, and wetting agents for pale crepe and GR-S vulcanizates loaded with whiting and other mineral fillers. Qualitatively, their results are similar to those reported here for the glass-bead composites, except that they often found an extended plateau in the stress-strain curve following the initiation of dewetting. When this occurred, the dewetting extended over a larger range of strain than that found for the glass-bead composites, although the length of the plateau decreased with increasing particle size.

The dilatometric data of Bryant and Bisset for a pale crepe vulcanizate containing between 30 and 45% whiting are shown in Figure 11, replotted as log V/V_0 vs. log L/L_0. This figure shows that the Bryant and Bisset data, like those for the glass-bead composites, can be characterized by the constant values of Poisson's ratio listed in Figure 11. Yield values ϵ_e were also obtained for the vulcanizates containing between 20 and 45% whiting by extrapolating their linear curves of volume change vs. elongation to zero volume change. The yield values are plotted against $1 - 1.105V_f^{1/3}$ in Figure 12, which shows that eq. (13) fits the Bryant and Bisset data much better than the data for the glass-bead composites shown in Figure 10.

Jones and Yiengst[2] made a dilatometric study of vulcanized rubber filled with zinc oxide and barytes. The effect of particle size was

studied by using five zinc oxides having particle diameters between 0.10 and 0.40 μ, and, to a lesser extent, by using barytes having particle sizes between 1 and 12 μ. Jones and Yiengst also studied the effect of cure time of the rubber. These factors affected the volume–elongation curves as might have been expected: i.e., the yield strain was decreased by increasing the cure time and the particle size. The Jones and Yiengst data, however, seem to show that samples prepared with different cure times and with fillers of different particle sizes had the same Poisson's ratio at large extensions, where the dewetting was

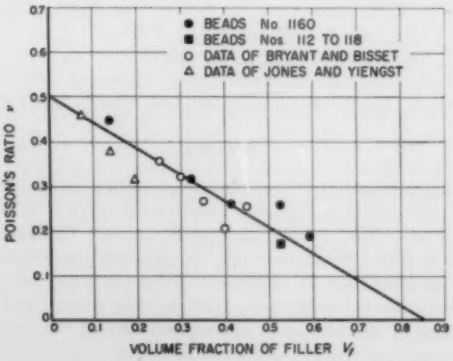

Fig. 13. Variation of Poisson's ratio for several filled systems after dewetting.

essentially complete. If this is correct, Poisson's ratio, after complete dewetting, depends primarily on the volume per cent filler, and not on the particle size of the filler or on the modulus or nature of the elastomer binder.

To test this hypothesis, values of Poisson's ratio for several composites are plotted in Figure 13 against the volume fraction of filler. Included are the average values obtained at 25° C. for the glass-bead composites and the data of Bryant and Bisset[3] given in Figure 11. To obtain Poisson's ratio from some data of Jones and Yiengst,[2] their dilatometric data on vulcanizates containing 0.074, 0.138, and 0.194 volume fraction of 0.40 μ zinc oxide were replotted, and the results are also included in Figure 13. This figure suggests that Poisson's ratio is a linear function of the volume fraction of filler and is independent of the nature of the binder and filler. Since few data are shown for

composites containing filler of different particle sizes, it is premature to speculate on the effect of particle size.

It is a pleasure to acknowledge the assistance of Mr. Dale Jeffries, who constructed the dilatometer and carried out the experimental work.

References

1. Holt, W. L., and A. T. McPherson, *J. Research Natl. Bur. Standards*, **17**, 657 (1936).
2. Jones, H. C., and H. A. Yiengst, *Ind. Eng. Chem.*, **32**, 1354 (1940).
3. Bryant, K. C., and D. C. Bisset, *Proceedings of the Third Rubber Technology Conference (1954)*, T. H. Messenger, ed., Heffer, Cambridge, England, p. 655.
4. Schippel, H. F., *Ind. Eng. Chem.*, **12**, 33 (1920).
5. Green, H., *Ind. Eng. Chem.*, **13**, 1029 (1921).
6. Vogt, W. W., and R. D. Evans, *Ind. Eng. Chem.*, **15**, 1015 (1923).
7. DePew, H. A., and M. K. Easley, *Ind. Eng. Chem.*, **26**, 1187 (1934).

Synopsis

The mechanical properties of five composites containing up to 60% by volume of glass beads (40 to 80 μ in diameter) embedded in a polyvinyl chloride–dioctyl sebacate rubber were studied under large deformations. Elongated ringlike specimens were extended in a dilatometer at 0, 25, and 50°C., and the volume increase was measured as a function of extension. At small extensions, the volume remained constant; above a critical extension or yield point, however, the volume increased because of the formation of vacuoles around the beads. Above the yield point, Poisson's ratio (defined in terms of Hencky strain) was calculated from the rate of volume change with extension and was found to be independent of extension and temperature, but to decrease linearly with the volume fraction of glass. The yield point varied with the temperature and also with the volume fraction of beads, as predicted by a theoretical equation. Some stress-strain data for the composites are presented and discussed in relation to the dilatometric data and the vacuole formation which results from failure of the adhesive bonds between the rubber and the glass beads.

TRANSACTIONS OF THE SOCIETY OF RHEOLOGY III, 137–152 (1959)

A Mechanism for Non-Newtonian Flow in Suspensions of Rigid Spheres

IRVIN M. KRIEGER and THOMAS J. DOUGHERTY,*
Case Institute of Technology, Cleveland, Ohio

Introduction

Many colloidal suspensions and solutions of macromolecules exhibit a viscosity which decreases with increasing rate of shear. This non-Newtonian behavior has been attributed to mechanisms in which the shear stress, transmitted through the continuous medium, orients or distorts the suspended particles in opposition to the randomizing effects of Brownian motion. Variation of viscosity with shear rate is then a result of the lowered resistance to flow offered by the oriented or distorted arrangement. Kirkwood and Plock's[1] explanation of the viscosity of suspensions of rigid ellipsoids and F. Bueche's[2] theory for solutions involve this type of mechanism.

A more general theory of non-Newtonian flow, based on Eyring's theory of rate processes,[3] has been developed by Ree and Eyring.[4] In this theory the viscosity is the sum of contributions of an indefinite number of unspecified "flow units." Since it is not based on any particular model, the Ree-Eyring theory should be applicable to all systems. Unfortunately, the number of parameters required to describe the behavior of a given fluid is not fixed by the theory, nor is it possible to deduce the values of these parameters from other known properties of the system. Reference to a forerunner of the Ree-Eyring theory, in a paper by Tobolsky, Powell, and Eyring,[5], discloses a point of similarity between this theory and the orientation-distortion theories mentioned earlier. Both involve a competition between shearing and thermal forces, and in this competition the size of the suspended particle plays a determining role.

* Firestone Tire and Rubber Fellow. This work forms part of the doctoral dissertation of T. J. Dougherty.

Suspensions of rigid spherical particles are known to exhibit non-Newtonian viscosity, but theories involving orientation or distortion are based on models which are not appropriate to isotropic rigid particles. The Ree-Eyring flow equation has been applied to such a system by Maron and Pierce.[6] Using two flow units, one for the aqueous medium and the second for the spherical polymer particles, these authors were able to fit the viscometric data of Maron and Fok[7] for a synthetic rubber latex. In their attempts to relate the fitted parameters to known properties of the system, however, Maron and Pierce achieved only limited success.

An important clue to the cause of non-Newtonian behavior in rigid sphere suspensions is the observation by Maron and his co-workers[7-10] that the behavior of such systems is Newtonian up to relatively high concentrations; in none of their latex systems did they detect non-Newtonian behavior at concentrations below 20% by volume of suspended polymer. This fact suggests that crowding plays a vital role in the origin of non-Newtonian flow behavior in rigid sphere suspensions. The theory developed in this paper, therefore, takes explicit notice of the interactions between neighboring spherical particles. The resultant flow equation is compared with experimental viscometric data on synthetic latexes and solutions of high polymers.

Derivation of the Flow Equation

Consider a suspension of rigid spheres of radius a in a continuous medium of viscosity η_s. When a shear stress τ is applied, causing the suspension to flow with an overall rate of shear $\dot{\gamma}$, the individual spheres will tend to rotate with an angular velocity $\dot{\gamma}/2$, dragging with them the medium adhering to their surfaces. However, because of concentration fluctuations arising from Brownian movement, there will be at any instant pairs of spheres whose separation is small, i.e., of the order of one diameter. If these nearby spheres were to rotate independently, the shear rate in the medium between the spheres would be inordinately high, as may be seen in Figure 1A. To avoid the consequent high energy dissipation rate, the nearby spheres will tend to rotate as a dumbbell about their center of mass until the shearing motion has caused them to separate. Figure 1B illustrates the hypothetical dumbbell rotation, while Figure 1C is a more realistic picture, intermediate between the other two.

Fig. 1. (A) Schematic diagram of flow pattern if nearby spheres were to rotate independently. (B) Schematic flow pattern if they were to rotate as rigid dumbbell. (C) Diagram of actual flow pattern.

The behavior described above can be treated quantitatively in the following approximate manner. If the separation between two spheres permits them to rotate independently of each other, the spheres will be called singlets and denoted by P_1; if the pair of spheres tends to rotate as a dumbbell, the pair will be called a doublet and denoted by P_2. In the absence of shearing forces, the distribution of singlets and doublets can be represented formally as a chemical equilibrium:

$$2P_1 \underset{k_b}{\overset{k_f}{\rightleftharpoons}} P_2 \tag{1}$$

Here k_f and k_b represent the specific rate constants for the formation and dissociation of doublets, respectively. Imposition of a shearing force introduces a second mechanism for the decomposition of doublets, since they will be separated during the dumbbell rotation.

$$P_2 \xrightarrow{k_s} 2P_1 \tag{2}$$

Here k_s is the specific rate constant for the shear-induced dissociation. Letting n_1 and n_2 be the number of singlet and doublet particles respectively per unit volume, an overall rate equation can be written for the net rate of doublet formation:

$$dn_2/dt = k_f n_1^2 - (k_b + k_s)n_2 \tag{3}$$

The condition for a steady state is $dn_2/dt = 0$, and hence

$$\frac{n_2}{n_1^2} = \frac{k_f}{k_b + k_s} = \frac{k_f}{k_b}\left(1 + \frac{k_s}{k_b}\right)^{-1} \tag{4}$$

Since k_s will be zero in the absence of shear forces, the zero-shear concentrations of singlets and doublets, denoted by $\hat{n}_1$ and $\hat{n}_2$ respectively, will obey the relationship

$$\hat{n}_2/\hat{n}_1^2 = k_f/k_b \tag{5}$$

At this point it is necessary to postulate a relationship between the viscosity of the suspension, $\eta = \tau/\dot{\gamma}$, and the concentrations of singlets and doublets. We assume that

$$\eta/\eta_s = f_1 n_1 + f_2 n_2 = f_1 n + (f_2 + 2f_1) n_2 \tag{6}$$

Here n is the total concentration of spheres,

$$n = n_1 + 2n_2 \tag{7}$$

The factors f_1 and f_2 are assumed to be functions of n, but independent of $\dot{\gamma}$. At zero shear rate n_2 will equal $\hat{n}_2$, and hence the viscosity η_0 in this limit will be

$$\eta_0/\eta_s = f_1 n + (f_2 - 2f_1)\hat{n}_2 \tag{8}$$

At infinite shear rate, all doublets will be dissociated, and hence n_2 will be zero. The viscosity η_∞ at infinite shear rate will then be given by

$$\eta_\infty/\eta_s = f_1 n \tag{9}$$

Equations (6), (8), and (9) may be combined to give

$$\frac{\eta - \eta_\infty}{\eta_0 - \eta_\infty} = \frac{n_2}{\hat{n}_2} \tag{10}$$

and from eqs. (4) and (5),

$$\frac{n_2}{\hat{n}_2} = \frac{n_1^2}{\hat{n}_1^2}\left(1 + \frac{k_s}{k_b}\right)^{-1} \tag{11}$$

We now assume that only a small fraction of the spheres will be paired as doublets, and hence that n_1 and $\hat{n}_1$ are not greatly different from n. With this assumption, eqs. (10) and (11) combine to give

$$\frac{\eta - \eta_\infty}{\eta_0 - \eta_\infty} = \left(1 + \frac{k_s}{k_b}\right)^{-1} \tag{12}$$

To evaluate their ratio, we make use of the fact that k_s and k_b are first-order rate constants for the decomposition of a doublet by the different mechanisms and hence each is reciprocally related to the corresponding mean lifetime. Letting t_b be the mean lifetime of a doublet undergoing thermal dissociation and t_s the mean lifetime of a doublet dissociating solely by shearing forces, we obtain

$$\frac{\eta - \eta_\infty}{\eta_0 - \eta_\infty} = \left(1 + \frac{t_b}{t_s}\right)^{-1} \tag{13}$$

The lifetime of a doublet dissociating under shear is the time required for the dumbbell to rotate to a position such that the two spheres are in different lamina so that they can separate. Taking the angular velocity of the dumbbell as $\dot{\gamma}/2$ and estimating the angle of rotation as $\pi/2$, we obtain

$$t_s = \left|\frac{\alpha_1 \pi/2}{\dot{\gamma}/2}\right| = \alpha_1 \pi/|\dot{\gamma}| \tag{14}$$

(The absolute value is necessary since t_s must be positive, and a factor α_1 is included because of the approximation involved in the value of the angle.) The mean lifetime under thermal decomposition is taken as the time required for the two particles to diffuse apart a distance X,

$$t_b = \overline{X^2}/2D \tag{15}$$

The diffusion constant D is given by the Stokes-Einstein relation

$$D = kT/6\pi a\eta \tag{16}$$

We are assuming here that the diffusion constant of the particle is governed by $\eta = \tau/\dot{\gamma}$, the viscosity of the medium at the prevailing rate of shear. Combining eqs. (15) and (16) we obtain

$$t_b = 3\pi\eta a\overline{X^2}/kT \tag{17}$$

From dimensional considerations it is evident that the magnitude of X, the distance the two particles of a doublet must diffuse apart before they can be considered to be singlets, is proportional to the particle radius a, and hence

$$\overline{X^2} = \alpha_2 a^2 \tag{18}$$

Thus eq. (17) becomes

$$t_b = 3\pi\eta\alpha_2 a^3/kT \tag{19}$$

(Einstein's analysis[11] of the distribution under shear of the velocity of the medium about a spherical particle leads us to believe that α_2 should be close to unity.)

The ratio of mean lifetimes is then

$$t_b/t_s = 3\alpha_2 a^3\eta|\dot{\gamma}|/\alpha_1 kT = 3a^3|\tau|/\alpha kT = |\tau|/\tau_c \tag{20}$$

where $\alpha = \alpha_1/\alpha_2$ and

$$\tau_c = \alpha kT/3a^3 \tag{21}$$

Equation (13) then becomes

$$\frac{\eta - \eta_\infty}{\eta_0 - \eta_\infty} = \left(1 + \frac{|\tau|}{\tau_c}\right)^{-1} \tag{22}$$

This relation between η and τ is our flow equation. Except for the significance attached to τ_c and the use of the absolute magnitude of the shear stress, our flow equation is identical to that proposed on empirical grounds by Williamson[12] and by Peek and MacLean.[13]

Test of the Equation of Flow

The proposed mechanism was tested by fitting the resultant flow eq. (22) to previously published experimental data obtained in this laboratory for two synthetic latex suspensions and a polymer solution. The data of Maron and Fok described the behavior of a butadiene–styrene latex whose average particle diameter was 1390 A. as measured by conductimetric soap titration. Maron and Levy-Pascal's data for a Neoprene latex of 1100 A. diameter were also used for this test, although the presence of an alginate-type creaming agent conferred somewhat anomalous flow behavior on this latex. The polymer solution data of Maron, Nakajima, and Krieger[14] describe the viscosity of a solution of polystyrene of molecular weight 250,000 in *o*-dichlorobenzene. For each of the three sets of measurements, the experimental temperature was 30°C.

The following procedure was used in fitting the flow equation to the experimental data. By inspection of the data, a trial value of τ_c is selected to correspond to a viscosity midway between estimated high

and low-shear limiting values. A graph of the viscosity η vs. $\tau_c/(\tau + \tau_c)$ is prepared; if the selected value of τ_c is correct, the experimental points should lie on a straight line. If the points indicate a curvature, a new value of τ_c is selected and the process repeated until a linear graph is obtained. The intercept of this graph is η_∞ and the slope is $\eta_0 - \eta_\infty$. In this manner, the fitted values of τ_c, η_0, and η_∞ were obtained for each of the three systems at the various concentrations.

For each of the two latex systems studied, essentially the same value of τ_c was found at all concentrations. In other words, τ_c was found to

TABLE I
Values of Parameters of Flow Equations

Volume fraction, v	τ_c, dynes/cm.^{2}	η_∞/η_s	η_0/η_s
	Data of Maron and Fok		
0.2990	46	3.070	3.532
0.3970	"	5.421	7.499
0.4398	"	7.330	12.689
0.4876	"	10.907	24.193
0.5390	"	18.39	88.80
0.5603	"	26.92	167.08
0.5866	"	44.67	448.1
0.6017	"	48.0	1048.0
	Data of Maron and Levy-Pascal		
0.2393	20	2.711	3.151
0.2821	"	3.561	4.599
0.3263	"	4.871	7.168
0.3713	"	7.040	13.690
0.4147	"	11.37	31.39
0.4429	"	15.65	66.95
0.4617	"	30.60	165.72
0.5115	"	86.08	1199.4
	Data of Maron, Nakajima, and Krieger		
0.02986	1000	6.205	8.619
0.04516	1500	9.56	17.54
0.06627	2000	22.03	35.38
0.09625	2000	23.85	85.40
0.12102	4000	57.64	173.53
0.14549	5000	52.30	398.3
0.15948	10000	25.3	921.3
0.17556	10000	151.7	1673.7

be independent of concentration for these systems. For the polymer solutions, however, the fitted τ_c values increased regularly with increasing concentration. Table I lists the values obtained for the parameters τ_c, η_0, and η_∞ for each system and concentration. Due to experimental scatter in the polymer solution data, the accuracy with which the parameters could be determined was considerably lower than for the latexes.

To test the accuracy of the flow equation, the viscosities were calculated at the experimental shear stresses, using the tabulated values of the parameters. Comparison of observed and calculated values is shown in Tables II–IV. For the latex suspensions, agreement between calculated and observed viscosities was within 1% for all except the three highest concentrations; even for these concen-

TABLE II

Comparison of Calculated and Observed Relative Viscosities. Data of Maron and Fok

τ, dynes/cm.^{2}	$\eta_{obs.}$	$\eta_{calc.}$	% error	$\eta_{obs.}$	$\eta_{calc.}$	% error	$\eta_{obs.}$	$\eta_{calc.}$	% error
	$v = 0.2990$			$v = 0.4876$			$v = 0.5866$		
50	3.293	3.291	0.06	17.18	17.28	0.58	404.10	238.16	41.1
100	3.218	3.216	0.06	15.17	15.10	0.46	208.78	171.77	17.7
200	3.157	3.156	0.03	13.44	13.39	0.37	122.21	120.11	1.72
300	3.132	3.131	0.03	12.70	12.68	0.16	96.58	98.28	1.76
500	3.110	3.109	0.03	12.03	12.03	0.00	79.28	78.68	0.76
800	—	—	—	11.66	11.63	0.26	68.01	66.62	2.04
	$v = 0.3970$			$v = 0.5390$			$v = 0.6017$		
50	6.424	6.417	0.11	52.20	52.12	0.15	1089.3	527.1	51.6
100	6.081	6.076	0.08	40.02	40.58	1.40	464.0	363.1	21.8
200	5.802	5.810	0.03	31.55	31.56	0.03	241.8	235.0	2.8
300	5.689	5.697	0.14	27.96	27.75	0.75	176.9	180.9	2.3
500	5.607	5.596	0.20	24.51	24.33	0.73	131.2	132.3	0.84
800	—	—	—	21.98	22.22	1.09	105.3	102.4	2.7
	$v = 0.4398$			$v = 0.5603$					
50	9.879	9.897	0.28	107.07	94.07	12.14			
100	8.993	9.019	0.29	71.18	71.08	0.14			
200	8.363	8.332	0.37	52.20	53.13	1.78			
300	8.082	8.042	0.49	45.39	45.55	0.35			
500	7.790	7.782	0.10	39.15	38.74	1.05			
800	7.597	7.621	0.32	34.80	34.54	0.75			

trated suspensions the agreement is within experimental error except for the low shear stress range. The low-shear, high-concentration points are in the region where triplet and higher multiplet interactions are important, so that the discrepancies in this range are not unexpected. (In fact, these data can be fitted quite well by using smaller values of τ_c, corresponding to an increase in the average dimensions of the interacting particles.) For the polymer solutions, the deviations between observed and calculated values range up to 5%. In view of the larger experimental error in these data, this is considered to be a reasonably good fit.

Since the average radii of the particles is known for the butadiene–styrene latex, it is possible to compute the factor α in eq. (21), namely

$$\alpha = 3a^3\tau_c/kT \tag{23}$$

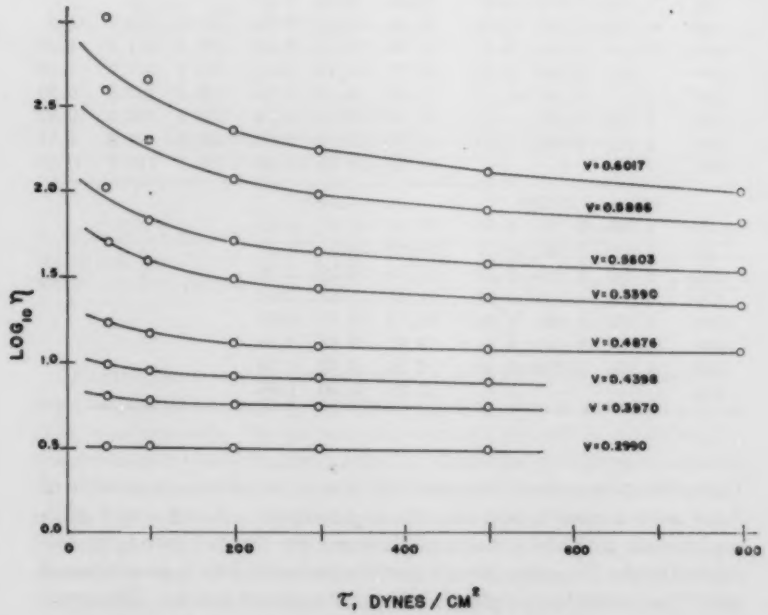

Fig. 2. Graphical comparison of observed (points) and calculated (solid line) viscosities using the experimental data of Maron and Fok.

TABLE III

Comparison of Calculated and Observed Relative Viscosities. Data of Maron and Levy-Pascal

τ dynes/cm.^{2}	$\eta_{obs.}$	$\eta_{calc.}$	% error	$\eta_{obs.}$	$\eta_{calc.}$	% error	$\eta_{obs.}$	$\eta_{calc.}$	% error
	$\nu = 0.2393$			$\nu = 0.3713$			$\nu = 0.4617$		
30	2.888	2.887	0.03	9.712	9.700	0.12	88.85	84.65	4.7
50	2.834	2.837	0.10	8.910	8.940	0.33	69.61	69.20	0.58
100	2.779	2.784	0.18	8.088	8.149	0.75	52.31	53.12	1.54
150	2.759	2.763	0.14	7.799	7.822	0.29	45.89	46.49	1.30
200	2.751	2.751	0.00	7.640	7 644	0.05	42.40	42.88	1.13
300	2.745	2.739	0.22	7.459	7.456	0.04	38.91	39.05	0.35
500	2.744	2.728	0.58	7.311	7.296	0.20	35.79	35.80	0.03
800	—	—	—	—	—	—	33.88	33.90	0.06
	$\nu = 0.2821$			$\nu = 0.4147$			$\nu = 0.5115$		
30	3.984	3.976	0.20	19.34	19.38	0.21	—	—	—
50	3.851	3.858	0.18	17.09	17.09	0.00	481.8	404.2	15.9
100	3.714	3.734	0.53	14.80	14.71	0.61	278.4	271.7	2.41
150	3.667	3.683	0.43	13.81	13.72	0.65	214.1	217.0	1.35
200	3.651	3.655	0.11	13.29	13.19	0.75	186.2	187.3	0.59
300	3.633	3.626	0.19	12.72	12.62	0.78	156.2	155.7	0.32
500	3.621	3.601	0.55	12.22	12.14	0.66	131.0	129.0	1.52
800	—	—	—	11.85	11.86	0.08	113.1	113.2	0.09
	$\nu = 0.3263$			$\nu = 0.4429$					
30	5.793	5.790	0.05	36.47	36.17	0.82			
50	5.539	5.527	0.21	30.29	30.31	0.07			
100	5.247	5.254	0.13	23.70	24.20	2.10			
150	5.139	5.141	0.04	21.37	21.68	1.44			
200	5.083	5.080	0.06	20.12	20.31	0.94			
300	5.023	5.015	0.16	18.97	18.86	0.58			
500	4.951	4.959	0.16	17.95	17.63	1.78			
800	—	—	—	17.08	16.90	1.05			

Using 695 A. for a and 46 dynes/cm.^{2} for τ_e, we obtain an α-value of 1.10; as anticipated, this value is close to unity. Using $\alpha = 1.10$ in conjunction with the τ_e value of 20 dynes/cm.^{2} from Table I, we calculate for the Neoprene latex a particle radius of 920 A. as compared with Maron and Levy-Pascal's measured value of 550 A. The probable source of this discrepancy is the effect of the alginate thickener mentioned earlier.

TABLE IV

Comparison of Calculated and Observed Relative Viscosities. Data of Maron and Nakajima

τ, dynes/cm.^{2}	$\eta_{meas.}$	$\eta_{calc.}$	% error	τ, dynes/cm.^{2}	$\eta_{meas.}$	$\eta_{calc.}$	% error
	$v = 0.04516$				$v = 0.14549$		
99	17.03	17.03	0.00	1291	308.7	322.9	4.60
207	16.55	16.55	0.00	3345	259.0	251.5	2.90
321	16.17	16.11	0.37	4817	223.7	218.6	2.28
435	15.80	15.73	0.44	9841	148.2	155.6	5.00
549	15.32	15.39	0.46	22685	102.5	98.5	3.90
	$v = 0.09625$				$v = 0.17651$		
117	85.71	81.95	4.39	6500	1125	1074	4.67
308	78.81	77.15	2.11	16478	745	726	2.57
2076	54.82	54.01	1.48	22200	641	624	2.68
4120	44.59	43.92	1.50	30150	522	531	1.65
8315	38.93	39.18	0.64	50050	394	405	2.67

TABLE V

Concentration Dependence of Limiting Viscosities

Data of	λ	Low-shear limit η_0/η_s	Low-shear limit p	High-shear limit η_∞/η_s	High-shear limit p
Maron and Fok	1.119	2.76	0.670	2.58	0.782
Maron and Levy-Pascal	1.093	3.44	0.541	2.79	0.591

The increase of τ_c with concentration exhibited by the polymer solutions implies that the polymer molecule, regarded as a spherical particle, progressively shrinks as concentration increases, changing in volume over a 10-fold range. Maron, Nakajima, and Krieger arrived at a similar conclusion from the concentration dependence of η_∞, which they obtained by fitting the experimental data to the Ree-Eyring flow equation. The dimension a computed from the extrapolated zero-concentration value of τ_c is of the order of magnitude of the average end-to-end chain length of a freely-jointed polymer chain of 2300 styrene monomer units, corresponding to the given molecular weight.

TABLE VI
Limiting Viscosities in the Newtonian Range

Volume fraction, v	$(\eta/\eta_s)_{obs.}$	η_∞/η_s	η_0/η_s
	Data of Maron and Fok		
0.0000	1.000	1.000	1.000
0.0306	1.089	1.093	1.139
0.0515	1.164	1.166	1.181
0.1010	1.361	1.369	1.408
0.1795	1.845	1.821	1.933
0.2481	2.491	2.420	2.688
	Data of Maron and Levy-Pascal		
0.0000	1.000	1.000	1.000
0.0091	1.009	1.012	1.035
0.0391	1.106	1.136	1.166
0.0769	1.283	1.288	1.370
0.1160	1.513	1.489	1.642
0.1560	1.775	1.755	2.023
0.1975	2.257	2.118	2.585

Concentration Dependence of Parameters

The parameters of the flow equation which were obtained for the three systems by the fitting procedure described above vary in a regular manner with volume fraction. Because the behavior of τ_c for the polymer solution indicates a variation in the size of the unit of flow, it can not be properly considered as a suspension of rigid spheres. The constancy of τ_c for the two latexes, however, has led us to attempt to apply functional relationships for the concentration dependence of the viscosity of rigid sphere suspensions to the variation of η_0 and η_∞ with volume fraction v.

Those functional relationships which have been proposed and successfully applied over a wide concentration range have two features in common. (*1*) At very low concentrations, they all reduce to the linear form

$$\eta/\eta_s = 1 + [\eta]v \tag{24}$$

where $[\eta]$ is the "intrinsic viscosity;" and (*2*) at some characteristic volume fraction p the viscosity becomes infinite. The quantity p is called the packing fraction, since the approach to infinite viscosity is usually ascribed to the attainment of a close-packed structure. Two well-known equations of this form are those of Eilers[15]

$$\eta/\eta_s = \left[\frac{1 + {}^1/_2[\eta]v}{1 - v/p}\right]^2 \tag{25}$$

and of Mooney[16]

$$\ln(\eta/\eta_s) = [\eta]v/(1 - v/p) \tag{26}$$

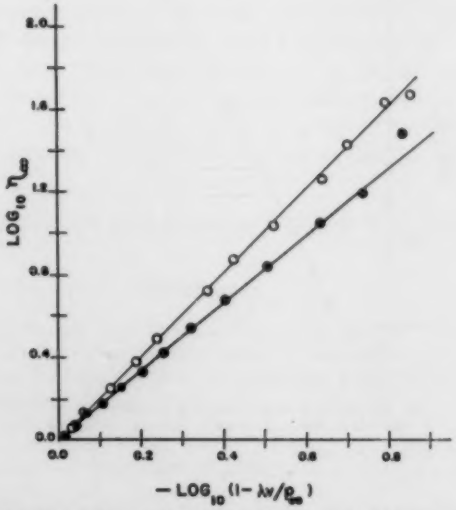

Fig. 3. Graphical test of eq. (29) for high-shear limiting viscosity data. Straight lines are calculated results. Filled circles represent data of Maron and Levy-Pascal; unfilled circles the data of Maron and Fok.

These equations can be fitted to our values of η_0 and η_∞ over most of the concentration range, but an excellent fit over the entire range was obtained using an equation derived by a modification of Mooney's functional analysis:

$$\eta/\eta_s = (1 - v/p)^{-p[\eta]} \tag{27}$$

The derivation of this relationship will be published elsewhere. Because of the adsorbed soap monolayer on the latex particles, the volume fraction of spherical particles is λv rather than v, where λ has been shown to be

$$\lambda = 1 + 6\Delta/D_s \tag{28}$$

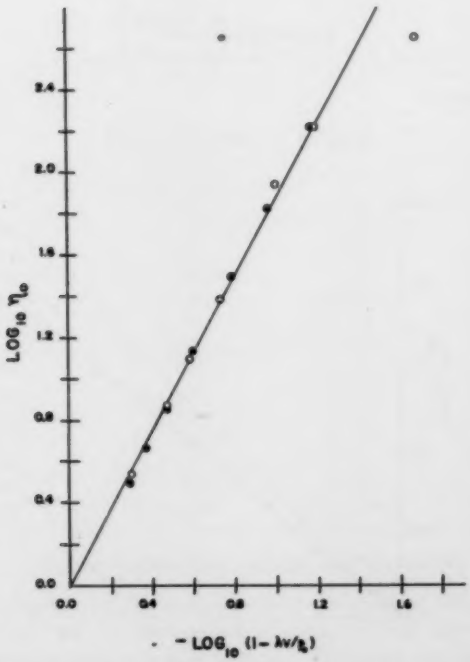

Fig. 4. Graphical test of eq. (29) for low-shear limiting viscosities. Filled circles represent the data of Maron and Levy-Pascal; unfilled circles the data of Maron and Fok.

Here Δ is the thickness of the soap monolayer and D_s the average diameter of the polymer sphere. Equation (27) was modified by substituting λv for v, and written in logarithmic form:

$$\ln (\eta/\eta_s) = - p[\eta] \ln (1 - \lambda v/p) \tag{29}$$

Table V lists the values of λ given by Maron et al., and also the values of $[\eta]$ and p obtained by fitting both high and low-shear limiting viscosities for the two latexes. The goodness of fit can be judged from Figures 3 and 4, which is a graph of eq. (29) together with data from Tables I and II. The values for $[\eta]$ are quite close to Einstein's theoretical prediction of 5/2 except for the low-shear value for the

Neoprene latex, where the presence of the thickening agent is presumably affecting the intrinsic viscosity.

One further point which requires elaboration is the fact that observed flow behavior of the latexes was Newtonian at volume fractions below ca. 0.20, whereas a small but not negligible difference between η_0 and η_∞ is indicated from the fitted equations. This discrepancy as shown in Table VI is a real one; the Newtonian viscosities observed in this concentration range fall between the calculated η_0 and η_∞, and can be represented well by η_∞. A possible explanation is that in this range the counter-ion concentration is not yet large enough to screen the coulombic repulsion between particles, which arises from the adsorbed soap anions, and hence doublet formation is prevented.

The work reported in this paper was supported in part by a National Science Foundation Grant.

References

1. Kirkwood, J. G., and R. J. Plock, *J. Chem. Phys.*, **24**, 665 (1956).
2. Bueche, F., *J. Chem. Phys.* **20**, 1959 (1952); **22**, 603, 1570 (1954).
3. Glasstone, S., K. J. Laidler, and H. Eyring, *The Theory of Rate Processes*, McGraw-Hill, New York, 1947.
4. Ree, T., and H. Eyring, *J. Appl. Phys.*, **26**, 793, 800 (1955).
5. Tobolsky, A. V., R. E. Powell, and H. Eyring, "The Chemistry of Large Molecules" in *Frontiers in Chemistry*, Vol. I, edited by R. E. Burk and O. Grummitt, Interscience, New York, 1943, pp. 125–129.
6. Maron, S. H., and P. E. Pierce, *J. Colloid Sci.*, **11**, 80 (1956).
7. Maron, S. H., and S. M. Fok, *J. Colloid Sci.*, **10**, 482 (1955).
8. Krieger, I. M., and S. H. Maron, *J. Colloid Sci.*, **6**, 528 (1951).
9. Maron, S. H., B. P. Madow, and I. M. Krieger, *J. Colloid Sci.*, **6**, 584 (1951).
10. Maron, S. H., and A. Levy-Pascal, *J. Colloid Sci.*, **10**, 494 (1955).
11. Einstein, A., *Ann. Physik*, **19**, 289 (1906); **34**, 591 (1911).
12. Williamson, R. V., *J. Rheology*, **1**, 283 (1930).
13. Peek, R. L., Jr., and D. A. MacLean, *J. Rheology*, **2**, 370 (1931).
14. Maron, S. H., N. Nakajima, and I. M. Krieger, *J. Polymer Sci.*, **37**, 1 (1959).
15. Eilers, H., *Kolloid-Z.*, **97**, 913 (1941).
16. Mooney, M., *J. Colloid Sci.*, **6**, 162 (1951).

Synopsis

A mechanism is postulated to account for non-Newtonian flow in suspensions of rigid spheres. On the basis of this mechanism, the flow equation $(\eta - \eta_\infty)/(\eta_0 - \eta_\infty) = (1 + |\tau/\tau_c|)^{-1}$ is derived, where η is the viscosity at the shear stress

τ, η_0 and η_∞ are the limiting values of η at zero and infinite shear, respectively, and τ_c is a parameter determined by temperature and particle size. This equation correlates well with published data on latex and polymer systems. For latex suspensions, the parameter τ_c does not depend on concentration and for these systems the dependence of the relative viscosity at a fixed shear stress, η_r, on volume fraction of suspended phase, v, is accurately described by the equation $\ln \eta_r = -p[\eta] \ln (1 - v/p)$, where $[\eta]$ is the intrinsic viscosity and p is the volume fraction at close-packing. In general, the parameters $[\eta]$ and p depend on the shear stress.

TRANSACTIONS OF THE SOCIETY OF RHEOLOGY III, 153–160 (1959)

The Temperature Dependence of Flow Birefringence Parameters

WLADIMIR PHILIPPOFF,* *The Franklin Institute Laboratories for Research and Development, Philadelphia, Pennsylvania*

Introduction

In flow birefringence, one question has not received conclusive treatment. That is: Is the flow birefringence primarily caused by the forces acting in the liquid, or by the orientation of the particles determined by the rate of shear? Up to now, the theories of this effect have been developed for infinite dilution, where the shearing stress and the rate of shear are proportional to each other, so that this decision is difficult to make. In preceding papers,[1–7] we have tried to show that the force equilibrium, in particular the difference in principal stresses, Δp, determines the degree of birefringence, Δn, which means the application of the stress-optical law of solids to streaming liquids. However, there seems to be a way of proving that the stress is primarily responsible for the occurrence of flow birefringence; that is, by the use of measurements at different temperatures. With normal liquids that show flow birefringence, the viscosity can be changed to a considerable degree by varying the temperature. Investigations over a range of rates of shear at different temperatures can therefore be made. Should the rate of shear, D, be the determining quantity, all these measurements should fall on a single straight line, when Δn is plotted versus D. If, however, the shearing stress, τ, or difference of the principal stresses, Δp, is the significant variable for non-Newtonian liquids, plotting birefringence *versus* τ or Δp should give a straight line, indicating a constant stress-optical coefficient, C [expressed in Brewsters (Br.) $= 10^{-13}$ cgs units]. The same reasoning applies to solutions.

* Present address: Esso Research and Engineering Co., Linden, N. J.

The first measurements of the influence of temperature on flow birefringence of solutions were made by Signer and Gross[8] on a 7.8% solution of a low molecular weight polystyrene in tetralin at 10, 20, and 40°C. They found $C = \Delta n/2\tau = 5030$ Br., independent of temperature. Cerf[9] proposed and performed such measurements on solutions in order to decide whether the particles were rigid or soft: plotting Δn against τ would give a straight line only for rigid particles.

Experimental

We have used substances that are somewhat different from the ones usually investigated: (*a*) a normal National Bureau of Standards oil "OB" (polybutene) of about 200 poises viscosity at 25°C., the viscosity of which could be changed by a factor of 100 in a comparatively easily accessible temperature range; (*b*) a medicinal white oil ("paraffin oil") with a viscosity of about 35 cp. at 25°C.; and (*c*) a solution of 3% polyisobutylene of $M \sim 100{,}000$ in the white oil, with a viscosity of 129 cp. at 25°C. at low rates of shear.

The flow birefringence instrument used has not yet been described in detail; it is the same one used in our preceding papers.[1-7] The temperature could be changed between 12°C. (below this temperature dew formation was excessive) and 70°C. The viscosity of the liquids was measured either with a Cannon-Fenske viscometer or with our capillary viscometer. The OB-14 calibration curve of the National Bureau of Standards (viscosity vs. temperature for 20–40°C.) was extended to 10 and 70°C., and the viscosity values used are interpolated from this curve.

Results

In Figure 1, the results of the flow birefringence measurements on the OB oil are shown. The extinction angle, χ, was 45° in all cases, since the OB oil behaved like a normal liquid in this range of rates of shear and shearing stresses. The birefringence was positive.

In Figure 2, results from the measurements on the white oil alone and on the solution of polyisobutylene in this solvent have been plotted together in a composite plot. The viscosities of the white oil and of the solution at the three temperatures are listed in the figure caption. The polyisobutylene solution at the higher rates of shear was non-Newtonian; its flow curve (viscosity vs. shear rate) was measured and the values for the rates of shear used were

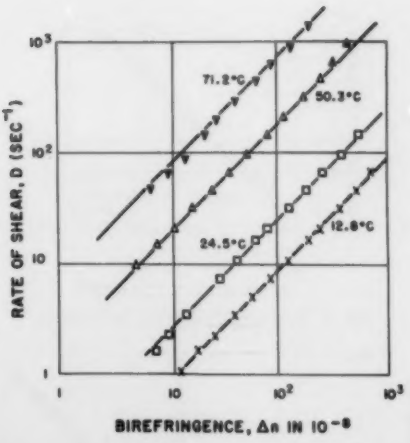

Fig. 1. Flow birefringence of OB-Oil at 17.8, 24.5, 50.3, and 71.2°C. Viscosities: 650, 207, 27.0, and 7.15 poises, respectively.

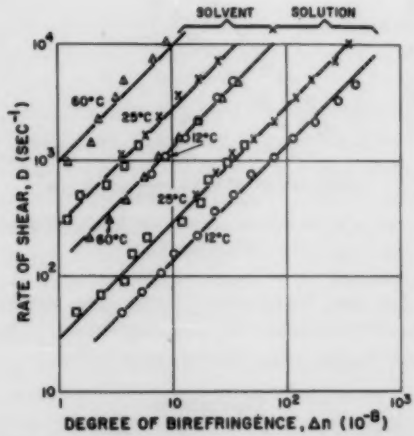

Fig. 2. Flow birefringence of white oil and a 3% polyisobutylene solution in white oil at 12.0, 25.0, and 60°C. Viscosities of the solvent: 0.7507, 0.3545, and 0.0885 poises, respectively. Viscosities of the solution: 2.60, 1.29, and 0.295 poises, respectively.

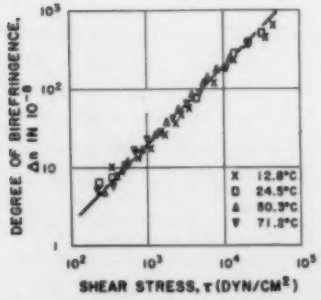

Fig. 3. Plot of Δn vs. τ for the OB-oil.

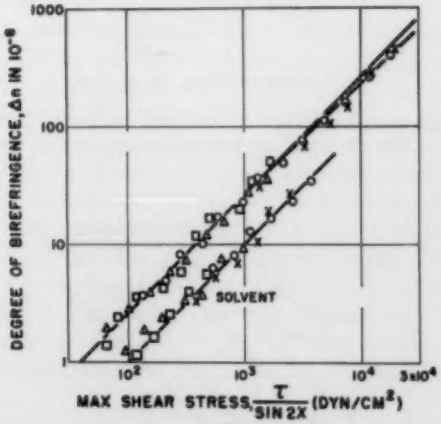

Fig. 4. Plot of Δn vs. τ for the white oil and the 3% polyisobutylene solution in this solvent.

interpolated. In the Newtonian range the measured constant viscosity was used to calculate the shearing stress. The birefringence was positive for both the white oil and the solution.

Discussion

Using the flow birefringence data from Figure 1 and the viscosity values, we have plotted Δn as a function of τ in Figure 3. We see that a complete superposition of all the data is achieved: all the points fall on a single straight line. This proves that for the OB

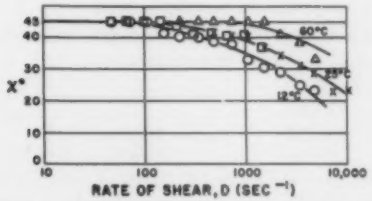

Fig. 5. Extinction angle χ as a function of the rate of shear D for PIB solution in white oil.

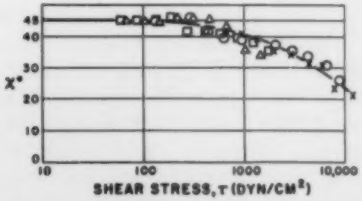

Fig. 6. Extinction angle χ as a function of the shear stress for PIB solution in white oil.

oil, a normal liquid of high viscosity, the birefringence depends specifically on the shearing stress. In the case of Newtonian liquids, $^1/_2\Delta p = \tau$, as $\sin 2\chi = 1$.

The same procedure was followed for the white oil, using the viscosity and birefringence data from Figure 2. The result is seen in Figure 4 (bottom curve). Data on the polyisobutylene solution were also taken from Figure 2: $^1/_2\Delta p = \tau/\sin 2\chi$ was calculated and plotted in Figure 4 (top curve).

In Figure 5, the extinction angle for the polyisobutylene solution as a function of rate of shear is shown. In Figure 6, the same data are plotted as a function of shearing stress; in this case all the points lie on one single curve.

We therefore feel that we have given conclusive proof that the two birefringence parameters—degree of birefringence, Δn, and extinction angle, χ—are exclusively determined by the shearing stress or the difference in principal stresses, and depend on the rate of shear only through the (possibly non-Newtonian) viscosity.

The values of the stress-optical coefficient, C, for the four series of experiments on the PIB solution are listed in Table I.

TABLE I
Stress-Optical Coefficients C of PIB Solution in White Oil at Different Temperatures

Temp., °C.	Cylinder	C, Br	Error, Br
12	II	1435	±73
25	II	1400	±75
25	III	1356	±41
60	III	1425	±56
Mean		1404	±72 (5.5%)

In Table II the stress-optical coefficients for the different polyisobutylenes and solvents used are listed. There seems to be a systematic decrease in C with decreasing molecular weight, probably due to the fact that short molecules do not follow the usual coil statistics. The OB oil has a value of C roughly 30% lower than the rubbery polyisobutylene (B100).

TABLE II
Stress-Optical Coefficients and Refractive Indices

Material	n_{25}	C, Br.	Remarks
Polyisobutylene			
B100	1.508	+1500	100%
B100	1.508	+1500	0.1–9% decalin
LM/MS	1.507	+1300	100%
Used	1.473	+1404	3% in white oil
OB oil	1.492	+975	100%
Decalin	1.474	+190	—
White oil	1.473	+550	—

The case of the polyisobutylene solution just described is remarkable in the fact that the white oil solvent has a value of $C = 550$ Br.—i.e., about 35% as great as that for the solute. Notwithstanding this large value, the experimental value of C for the solution is extremely close to that of a 100% polyisobutylene (Vistanex LM-MS) determined previously.[5] It is difficult to understand why the solvent seems to make no contribution to the birefringence of the solution. On the other hand, the index of refraction of decalin[7] was practically identical to that of the white oil. This would suggest the possibility of the C's being equal also. In Table I, the C's at

different temperatures were listed together with the root-mean-square errors. Within the mean experimental error of $5^1/_2\%$, we could not detect any effect of temperature between 12 and 60°C. in a more than 100-fold range of Δp and Δn. The change in absolute temperature should have resulted in a 17% change which is about three times the experimental error. Why this temperature independence should exist is not quite clear. Possibly the index of refraction changes with the change in density and diminishes the influence of the absolute temperature.

From these measurements, it is also seen that the value of C for the white oil, a low molecular weight liquid, is of the same order of magnitude as the ones for the polyisobutylene. For that matter, in a previous publication[7] it was shown that another low molecular weight liquid, benzyl benzoate, has a value of about 2730 Br., which is much higher than that of the polyisobutylene, and cinnamic aldehyde has a value of 4670 Br.

The data have also been plotted according to a suggestion of Peterlin;[10] here the quantity plotted on the abscissa is the increase of shearing stress by the solute. Practically, we subtracted ($\eta_{solvent} \times D$) from τ values. The plot gave a completely straight line up to a value of this function of 3000 dynes/cm.^{2}. However, above this value the birefringence rose sharply with a deviation from the straight line value of up to 40%. This top region for the function is the one where the non-Newtonian behavior starts and the influence of χ on Δp becomes important. We therefore think that the former relation, shown in Figure 4, has the more general significance.

According to the criterion of Cerf,[9] if the plot of Δn vs. shearing stress gives a single common curve, the particles should be rigid. However, this is probably not the case for the polyisobutylene investigated. It is therefore important to get more data in order to investigate this point in greater detail. Also, a continuation of these measurements into the range of higher dilutions of the polyisobutylene would be important in order to decide whether the C value of 1400 Br. remains constant as concentration changes.

Plotting values of the recoverable shear, s, versus shearing stress for the PIB solution, we could approximate the curve obtained by a straight line in the region of low shearing stress. From the slope of this line, a shear modulus, $G = 3500$ dyne/cm.^{2} was found. As the concentration of the polyisobutylene was 3% by weight and the

density of the solution 0.8664 g./cc., we can calculate the molecular weight of the polymer, employing a formula used previously:[1] $M = RTc/2G$, where c is the concentration of the polymer in g./cc. Using the G value mentioned, the molecular weight value obtained is $M = 92{,}000$. This seems to be of the right order of magnitude, since the polymer Vistanex LM-S investigated by Leaderman[11] had a molecular weight of 85,400. The value of M for the LM-MS polymer measured at 100% concentration and calculated in the same way as above is 203,000. These values show that the proposed formula is apparently useful for determining weight-average molecular weights from viscosity and birefringence data.

The measurements on the OB oil were performed by Mr. John G. Brodnyan. Those on the white oil and polyisobutylene solution were by Gwynn K. McConnell, to whom thanks are due.

The white oil and polyisobutylene solution were supplied by the Esso Research and Engineering Company, Linden, New Jersey, who also sponsored the work, and whose help is gratefully acknowledged.

References

1. Philippoff, W., *J. Appl. Phys.*, **27**, 984 (1956).
2. Philippoff, W., *Nature*, **178**, 811 (1956).
3. Philippoff, W., *Trans. Soc. Rheol.*, **1**, 95 (1957).
4. Brodnyan, J. G., F. H. Gaskins, and W. Philippoff, *Trans. Soc. Rheol.*, **1**, 109 (1957).
5. Philippoff, W., F. H. Gaskins, and J. G. Brodnyan, *J. Appl. Phys.*, **28**, 10 (1957).
6. Brodnyan, J. G., F. H. Gaskins, W. Philippoff, and E. G. Lendrat, *Trans. Soc. Rheol.*, **2**, 285 (1958).
7. Philippoff, W., "Stress-Optical Analysis of Fluids," in *Acta Rheol.*, in press.
8. Signer, R., and H. Gross, *J. Phys. Chem.*, **A165**, 161 (1933).
9. Cerf, R., Thesis, Strasbourg (1951); *J. Polymer Sci.*, **23**, 103, 125 (1957). H. Schwander and R. Cerf, *Helv. Chim. Acta*, **34**, 436 (1951).
10. Peterlin, A., and R. Signer, *Helv. Chim. Acta*, **36**, 1572 (1953).
11. Leaderman, H., R. G. Smith, and R. W. Jones, *J. Polymer Sci.*, **14**, 47 (1954).

Synopsis

Measurements of flow birefringence on two hydrocarbon oils and a solution of polyisobutylene in white oil were made at different temperatures. Plotting the values as a function of Δp (the difference of principal stresses) gives a single curve independent of the temperature. This indicates that the birefringence is primarily caused by the shearing stresses.

TRANSACTIONS OF THE SOCIETY OF RHEOLOGY III, 161–180 (1959)

Theory and Analysis of Peel Adhesion: Mechanisms and Mechanics

D. H. KAELBLE, *Central Research Department, Minnesota Mining and Manufacturing Co., St. Paul, Minnesota*

I. Introduction

Unbonding in peel might be aptly termed the "zipper" mechanism for bond failure. A bond involving a flexible member may display high strength in shear. As the peel angle increases from zero, the force required to initiate and propagate a failure interface decreases by orders of magnitude due to a mechanism familiarly termed "peel" or "stripback."

Bond analysis of overlap shear by Goland and Reissner[1] identifies two sets of bond forces: "tearing" forces, which are normal to the bond, and "shear" forces, coplanar with the bond. Hata and coworkers[2,3] recognize and treat the moment arm of the applied force as influenced by adherend flexibility and angle of peel. An internal bond stress distribution in peel, for a peel angle of 90°, is calculated by Spies,[4] who also provides an explicit solution for peel force assuming cohesive failure of a Hookean interlayer. Bikerman[5] has more recently treated peel phenomena at a peel angle of 90° with explicit solutions for both Newtonian interlayer flow and cohesive failure of a Hookean interlayer.

An objective of this discussion is to provide: (*a*) a definition of peel which applies where either one or both of the adherends are flexible, and (*b*) a definition general with respect to angle of peel, and modes or mechanisms of bond failure.

II. Theory

A. Definition of "Simple Stripback"

The descriptive assumptions for an idealized type of peel termed "simple stripback" are listed:

1. A steady-state unbonding process.
2. Properties of the flexible member:
   a. of slender rectangular cross section
   b. elastically (Hookean) deformed
   c. bonded and unbonded portions of semi-infinite length.
3. Properties of the forces:
   a. applied force—acts in tension along the central plane of the flexible member.
   b. shearing forces—distributed over the bonded interface of the flexible member.
   c. cleavage forces—a highly localized parallel array, perpendicular to the bond plane.
   d. all forces uniformly distributed across the bond width.

The first assumption defines the unbonding as progressing at some constant velocity, other than zero, and is described by a balance of applied and reactive forces and moments of force. The second assumption describes a thin ribbon adherend, elastically deformed in tension and flexure, whose deformation is uncomplicated by end effects. The properties of the forces as indicated in the third assumption will be subsequently amplified upon.

B. Deformation Curve of the Flexible Member

Preliminary to attacking the broad definition of peel, let us examine the characteristics of the elastic bending curve of the flexible member under tension. This deformation curve controls two important factors in peel: (*a*) the effective moment arm of the applied force, and (*b*) the curvature at the bond boundary and the resulting stress distributions. The following discussion represents a special case of buckling of centrally compressed bars as presented by Timoshenko.[6] For simplicity it is assumed that the bonded portions of the flexible member satisfy the conditions of a built-in end and that weight and centrifugal effects may be neglected.

Figure 1 presents a schematic profile of this deformation curve. The exact differential expression for elastic bending is:

$$EI(d\theta/ds) = pm' \tag{1}$$

By differentiating eq. (1), introducing the relation $dm' = ds \sin \theta$, and multiplying by $d\theta/ds$ we obtain:

$$EI(d\theta/ds)\, d(d\theta/ds) = P \sin\theta\, d\theta$$

or

$$EI \int_0^\omega (d\theta/ds)\, d(d\theta/ds) = P \int_0^\omega \sin\theta\, d\theta$$

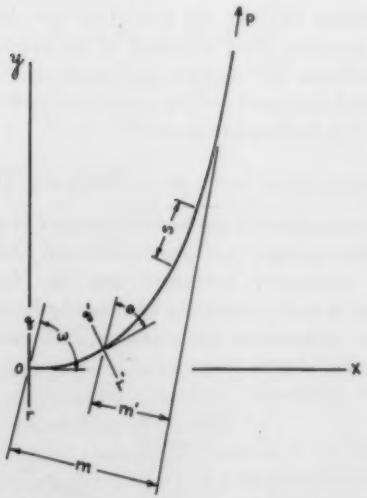

Fig. 1. Deformation curve of the flexible member.

By integrating and taking into account boundary conditions, namely that curvature and angular deflection are zero when $m' = 0$, we obtain:

$$\frac{EI}{2}\left(\frac{d\omega}{ds}\right)^2 = P(1 - \cos\omega) \tag{2}$$

which represents an independent differential expression for the deformation curve. By writing eq. (1) for the case where $m' = m$ and $\theta = \omega$, substituting into eq. (2), and rearranging terms, the following relation results:

$$m = \left[\frac{2EI\ (1 - \cos\omega)}{P}\right]^{1/2} \tag{3}$$

Rewriting eq. (2) we obtain:

$$d\omega/ds = \left[\frac{2P\,(1 - \cos\omega)}{EI}\right]^{1/2} \tag{4}$$

where eq. (4) expresses $(d\omega/ds)$, the boundary curvature, and eq. (3) expresses m, the moment arm, in terms of its applied force P, the flexible member stiffness EI, and the peel angle ω. These equations differ from the usual circular bending approximations by the appearance of the factor 2 in both expressions.

C. The Steady State in Terms of Forces and Moments

A schematic cross-section of the bond boundary is shown in Figure 2. Two coordinate systems are presented with the (x_0,y_0) system representing the stationary substrate and the (x,y) coordinates defining the center of action and the translating force system. The line of action of P, defined by its ω and m, lies outside the flexible member in the section of this view.

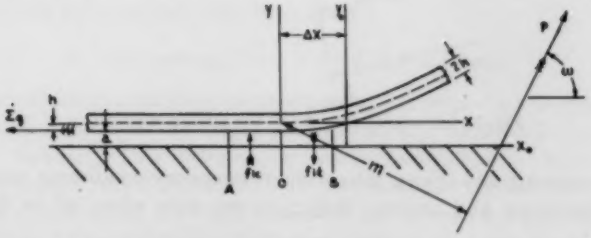

Fig. 2. External forces acting on the flexible member (schematic).

As indicated in the assumptions, two systems of bond forces or potential mechanisms of failure in peel are identified. These are cleavage and shear. A rigorous definition of these stress distribution functions is not attempted here since this would involve further restrictive assumptions regarding the bond interlayer and failure interface. Evaluation of the requirements for steady-state equilibrium produce the following relations:

for the forces

$$P = (P_c + P_s)^{1/2} \tag{5}$$

$$P_c = P \sin \omega = \Sigma f_t - \Sigma f_c \tag{5a}$$

$$P_s = P \cos \omega = \Sigma q \tag{5b}$$

for the moments of force

$$M = Pm = M_c + M_s \tag{6}$$

$$M_c = Pm_c = \Sigma f_t x_t \tag{6a}$$

$$M_s = Pm_s = h\Sigma q \tag{6b}$$

and for the moment arms

$$m = \left[\frac{2EI\ (1 - \cos \omega)}{P}\right]^{1/3} \tag{7}$$

$$m_c = m - h \tag{7a}$$

$$m_s = h \tag{7b}$$

These reactive forces and moments are simply defined as total summations of their positional increments. However, without sacrificing generality some description is possible.

The cleavage forces f are highly localized at the bond boundary where the flexible member undergoes a sudden change from maximum bending to zero curvature. At high stripping angles regions AO and OB are, respectively, zones of tension and compression. The work of Spies[4] adequately justifies the implied assumption that the cleavage forces become negligible after the initial region of boundary tension and interior compression. The general form for the cleavage stress distribution function resembles that of a highly damped harmonic decay curve.

The shear stresses may be uniformly distributed throughout the bond for inextensible flexible members. An assumption of finite extensibility results is some form of an exponential decay function with maximum stress at the boundary region. Except at very low angles of peel it may be shown, after the manner of Spies, that the maximum shear stress is negligible with respect to the maximum tensional cleavage stress.

In "simple stripback" as defined here, ω may vary from 0 to 180°. The reactive bond forces depend upon the magnitudes of both the sin ω and cos ω components of the applied force. At a peel angle of 90°, neglecting bending strains, only cleavage forces exist. At some

low angle of peel the summed cleavage forces are negligible compared to shear forces. In addition, due to the offset distance h of P and shear forces Σq, at some low angle prescribed by eq. (7) and eq. (7a) the cleavage forces become compressional in region OB and tensional in regior OA.

This discussion is confined to those conditions of applied force and peel angle where the flexible member half-thickness h is negligible compared to the magnitude of m. Under these conditions the cleavage failure mechanism predominates and the following relations defining this mechanism apply:

by restatement of eq. (5a)

$$P = (\Sigma f_t - \Sigma f_c)/\sin \omega \tag{8}$$

by substitution of eq. (6a) and eq. (7) where $m_c = m$:

$$P = (\Sigma f_t x_t)^2/[2EI(1 - \cos \omega)] \tag{9}$$

Equation (8) states that a direct proportionality exists between the net summation $(\Sigma f_t - \Sigma f_c)$ of bond cleavage forces and P. Equation (9) expresses a second-power relation between P and the total summation of cleavage moments of force $(\Sigma f_t x_t)$.

The sensitivity of the peel force to bond strength variables is readily understood in terms of eq. (9) due to the exponential relation between $\Sigma f_t x_t$ and P. The distribution of cleavage bond forces is shown to be a function of peel angle by eq. (8) since at $\omega = 90°$, $\Sigma f_t - \Sigma f_c = P$ and at $\omega = 180°$, $\Sigma f_t - \Sigma f_c = 0$.

D. Peel of Two Flexible Members by Cleavage

The treatment of the mechanics of peel tests may be extended to include the system involving two flexible members joined by an adhesive bond or interlayer. The conditions relating to the "simple stripback" of a flexible member from a rigid substrate apply. In addition, it is assumed that the moment arm of forces P_A and P_B are large compared to the combined thickness of the flexible members and the bonding interlayer. The geometry of this two component system is presented schematically in Figure 3.

From the geometry and conditions of steady-state equilibrium it may be observed that

(*a*) for the system:

$$\alpha + \beta = \pi \tag{10}$$

$$P_A = -P_B \tag{11}$$

$$(\Sigma f_i x_i)_A = -(\Sigma f_i x_i)_B \tag{12}$$

(*b*) for the individual members A and B:

$$(pm)_A = (\Sigma f_i x_i)_A \tag{13}$$

$$(pm)_B = (\Sigma f_i x_i)_B \tag{14}$$

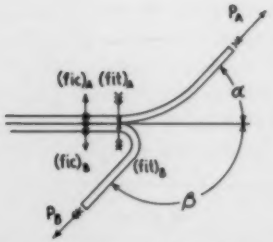

Fig. 3. Peel of two bonded flexible members.

From eqs. (10) through (14) it may be seen that:

$$m_A = m_B = m \tag{15}$$

From the deformation curve of an elastic member bent in tension:

$$m = \left(\frac{2EI\,(1-\cos\alpha)}{P}\right)_A^{1/2} = -\left(\frac{2EI\,(1-\cos\beta)}{P}\right)_B^{1/2} \tag{16}$$

By the introduction of eq. (11) and accounting for the fact that $\cos\beta = -\cos\alpha$, eq. (16) may be written as:

$$(EI)_B/(EI)_A = (1-\cos\alpha)/(1+\cos\alpha) = (\tan\alpha/2)^2 \tag{17}$$

If I_B is known, then E_B may be calculated by rewriting eq. (17) as:

$$E_B = [(EI)_A/I_B]\,(\tan\alpha/2)^2 \tag{18}$$

If one of the members has known values of E_A and I_A, and if P_A and α are measured, then the summation of moments in the bond may be calculated by the following expression:

$$(\Sigma f_i x_i)_B = -[2(EIP)_A (1 - \cos \alpha)]^{1/2} \tag{19}$$

Equations (18) and (19) suggest that any tape construction may be bonded to an ideally elastic substrate, and both the summation of tensional and compressional moments of force in the bond ($\Sigma f_i x_i$) and the net effective modulus of elasticity of the tape in flexure may be measured simultaneously.

E. Work of Peel

Utilizing the theory of peel, the bond strength in peel may be expressed in energy or work terms after the fashion of Rivlin.[7] The

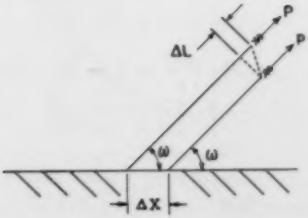

Fig. 4. Work of peel.

effective peel work may be defined as the product of P and a displacement ΔL in the direction of this force, as indicated by the following expression:

$$W = P\Delta L \tag{20}$$

A schematic sketch describing this relation is shown in Figure 4. For "simple stripback," where the shape of the deformation curve is unchanged, the geometry indicates:

$$L = (1 - \cos \omega)\Delta X \tag{21}$$

where ΔX is the equilibrium displacement of the bond forces. By substitution of eq. (21) into eq. (20):

$$W = P(1 - \cos \omega)\Delta X \tag{22}$$

On comparing eqs. (22) and (9) it may be seen that the common term $(1 - \cos \omega)$ occurs. In eq. (22) this term is related to the degree of translation of bond forces relative to that of the applied force; in eq.

(9) it relates the magnitude of P to m. By combining eqs. (22) and (9) we obtain:

$$W = (\Sigma f_i x_i)^2 \Delta X / 2EI \tag{23}$$

Equation (23) expresses the "effective work of peel" in terms of the summation of moments $\Sigma f_i x_i$ independent of the geometry of the test (i.e., the stripping angle). If $\Sigma(f_i x_i)$ is independent of stripping angle, the work will be independent of stripping angle.

III. Experimental

Experiments designed to provide support for the theory were conducted on bonds containing a pressure-sensitive adhesive interlayer. The particular advantage of this system is due to the fact that an equilibrium bond is easily established and under constant conditions of rate and temperature the peel force is essentially invariant, thus fulfilling the condition of steady-state unbonding.[8] In addition, since

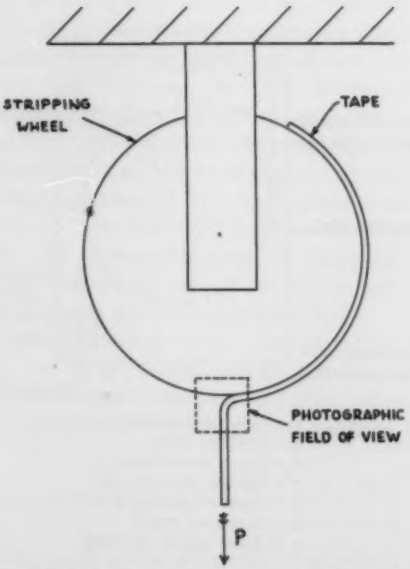

Fig. 5. Photographic study of tape unwind (90° angle of peel).

the force of peel, for pressure-sensitive adhesive bonds, changes markedly with both rate and temperature, the apparent bond strength may be systematically varied by controlling these physical conditions of test.[9,10]

Unless otherwise noted, the rigid adherend consists of a rigidly clamped cellophane surface. Bonds were established by multiple passes of a mechanically driven $^1/_2$" diameter steel roller loaded to 3.0 lb. Tests were conducted at 25 ± 1°C. and 50 ± 5% relative humidity. The combined reproducibility of the bonding process and peel test was about ±4%.

A. Photographic Study of Roll Unwind

The special apparatus developed by Stedry[11] produced data applied to the test of eq. (9). Figure 5 provides a schematic view of the experimental setup. Highspeed motion picture films were taken of the stationary stripping point for various rates of peel. The force P and the deformation curve of the flexible member were then measured.

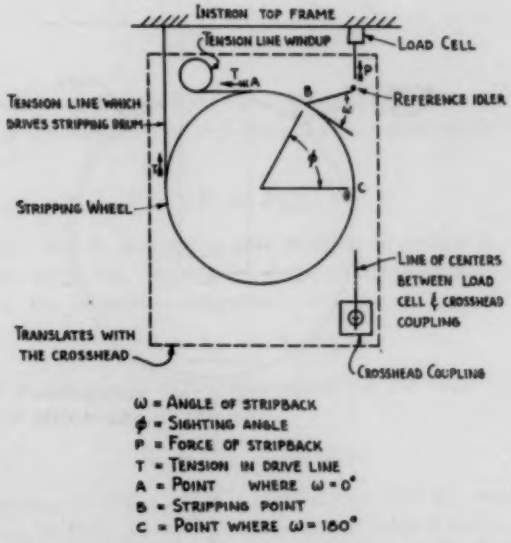

Fig. 6. Schematic sketch of stripback testing device.

B. All-Angle Tape Stripback Testing

A special apparatus was designed to obtain precise peel force measurements over wide ranges of controlled rate and angle of peel. This tester was designed as an accessory to the Instron Tensile Tester[13] which provides a wide range of stripback rates (0.02 to 20 in./min.) and an extremely sensitive load sensing and recording system. Supplementary equipment included a temperature control oven permitting tape bonding and stripback testing over a temperature range from −50 to 200°C. A single test strip of 12″ length provided data for rates of 0.02, 0.2, and 2.0 in./min. over the full range of angles. An additional 12″ strip supplied the 20 in./min. results as well as additional rechecks of the data obtained for the slower rates. A tape can be tested in this manner in 1 or 2 hours, depending on the number of points measured.

The principle of the stripback operation is illustrated diagrammatically in Figure 6. After the tape has been bonded to the surface of the stripping wheel and the angle of stripback ω selected, the tension line (one end of which is attached to the fixed top frame of the Instron) drives the stripping wheel at a perimeter velocity just equal to that of the moving crosshead. The bonded test tape advances to the stripping point B at the same rate that the unbonded tape departs, thereby establishing a condition of transient equilibrium which maintains the sighting angle ϕ and the stripping angle ω constant. As long as the stripped tape and the tension line connecting the translating and stationary portions of the apparatus are parallel and do not change length, this condition is maintained independent of the rate of stripback. To change the angle of stripping, the operator changes the lengths of either the tape or the tension line, and B moves to a new equilibrium position between points A and C.

The reference idler is located along a line of centers between the load cell and the crosshead mount and at the intersection of two perpendicular planes tangent to the stripping wheel at points A and C. An inspection of the geometry of this system indicates the following equation:

$$\omega \text{ (degrees)} = 90 - \phi + \tan^{-1} \frac{1 - \sin \phi}{1 - \cos \phi}$$

relating the sighting angle ϕ and the angle of stripback ω. Utilizing a specially designed protractor sighting device provided with parallax

correction, the sighting angle may be determined within $\pm 0.2°$ and the stripping angle from a plot of ϕ vs. ω.

C. Measurement of Young's Modulus

Young's modulus values for the flexible members were obtained from tensile stress-strain curves measured on the Instron Tensile Tester.

IV. Results and Discussion

A. A Test of Theory

A good test of the basic assumptions involved in the theory of tensile peel of a flexible from a rigid member is gained by applying eq. (3) to real systems. The data required for this test were provided by an earlier photographic study of the geometry of peel-back of cellophane tape conducted by Stedry.[11] Table I presents information concerning the test conditions, nature of the bond, and measured values of P and flexible member m. m is assumed equal to the measured average radius of curvature of the delaminated backing.

TABLE I
Stripping Force and Backing Moment Arm for 90° Cellophane Tape Roll Unwind

Temp., °F.	R. H. %	Adhesive	Rate, cm./min.	p, lb.	$m \times 10^3$, in.	$Pm \times 10^3$, lb. in.	$Pm^2 \times 10^5$ lb. in.^{2}	$E \times 10^{-5}$, lb./in.^{2}
70–80	34–41	Rubber-resin blend	1	0.13	32	4.16	13.3	4.58
			10	0.53	16	8.50	13.6	4.70
			100	1.28	12	15.4	18.5	6.40
			1000	1.98	9	17.8	16.0	5.53
74–76	24–26	Acrylate copolymer	1	0.53	22.8	12.1	27.6	9.53
			10	0.75	19.7	14.8	29.2	10.1
			100	1.03	15.4	15.9	24.5	8.45
			1000	1.45	10.1	14.7	14.9	5.16
73–74	11–16	Acrylate copolymer	1	0.84	17.6	14.8	26.0	8.96
			10	1.15	14.6	16.8	24.5	8.45
			1000	1.50	11.3	17.0	19.2	6.63

Equation (3) may be rewritten in the following forms:

$$pm^2 = 2EI(1 - \cos \omega) \tag{24}$$

$$E = pm^2/[2I(1 - \cos \omega)] \quad (25)$$

Equation (24) predicts the quantity (pm^2) to be a constant characteristic of the backing, for a fixed angle ω. The calculated values of (pm^2) tabulated in Table I for each set of stripping data substantially confirm this predicted constancy over a wide range of stripping rates and forces. The moment of inertia I of the flexible member about its neutral axis may be calculated by applying the following expression:

$$I = b(2h)^3/12 = 1.45 \times 10^{-10} \text{ in.}^4$$

where for the cellophane tape, $b = 0.05''$ and $2h = 0.0015''$. The values of Young's modulus of elasticity E based on stripping measurements calculated from eq. (25) are tabulated in Table I. The tangent modulus values reported in Table II, resulting from room temperature (25°C.) measurements at low extensions (1.25% or less), are in reasonable qualitative agreement with those calculated from stripping data.

TABLE II
Young's Modulus of Cello #600 Put 78 Tape Backings

Test Temp., °C.:	75	25	−18
R. H., %:	—	50	—
% Elongation	$E \times 10^{-5}$, lb/in.^{2}	$E \times 10^{-5}$, lb/in.^{2}	$E \times 10^{-5}$, lb/in.^{2}
0.25	6.70	8.53	15.1
0.75	5.20	6.71	11.9
1.25	3.80	3.65	8.20
1.75	2.50	1.85	4.15
2.25	1.95	1.31	2.24
2.75	1.43	0.99	1.41
3.26	1.14	1.33	1.43
3.75	—	0.95	1.15
4.25	—	0.90	0.64

B. The Force-Angle Function

If the summation of moments $\Sigma f_i x_i$ of tensional and compressional forces in the bond are independent of the stripping angle and cleavage is the controlling failure mechanism, then for steady-state stripping, from eq. (9), P should vary inversely as $(1 - \cos \omega)$.

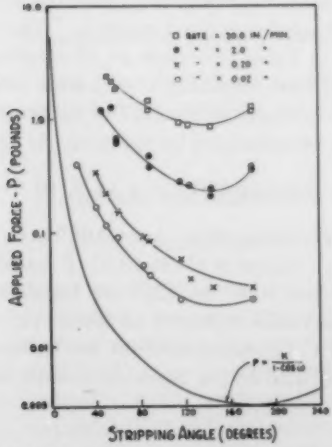

Fig. 7. Peel force P vs. angle ω for polyester tape.

Several types of peel test results confirm this P–ω relation. Figures 7, 8, and 9 present steady-state peel force data as a function of stripping angle for three pressure-sensitive tape bonds. The only property

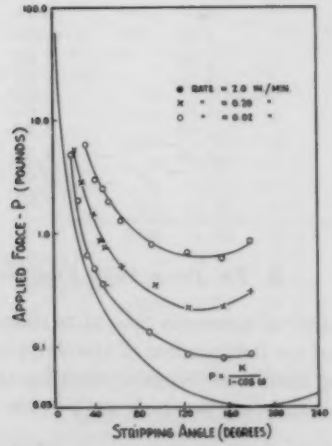

Fig. 8. Peel force P vs. angle ω for cellophane tape.

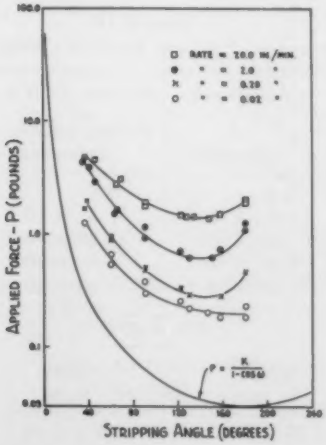

Fig. 9. Peel force P vs. angle ω for spring steel tape.

varied for the three bonds is the composition and flexibility of the flexible member, as described in Table III. These data are typical of pressure-sensitive type bonds where the distribution of forces in the bond is strongly influenced by rate effects. Plotting stripping force P on a logarithmic ordinate scale facilitates comparison of force-angle plots at different rates. Changing the stripping rate and the resultant $\Sigma f_i x_i$ values should merely translate the force-angle curve along the log P ordinate without changing the shape of the function, if the inverse relation between stripping force P and $(1 - \cos \omega)$ applies. A change in the shape of this force-angle plot, at constant rate, indicates the deviation of experimental data from theory.

To illustrate the effect of stripping rate upon the shape of the force-angle plots, eq. (9) is represented graphically in Figures 7 through 9, where

$$\Sigma f_i x_i / 2EI = K$$

At low stripping rates, and accompanying lower stripping forces, experimental data confirm extremely well the theoretical inverse P vs. $(1 - \cos \omega)$ relationship over a wide range of angles. At higher stripping rates the deviation becomes more marked. It may also be

TABLE III
Comparative Properties of Tape Bonds at a Stripping Angle of 90°
(Adherend: cellophane. Adhesive interlayer: rubber-resin; thickness, 0.001 in.)

	Flexible member type		
	Polyester	Cellophane	Steel
b, in.	0.5	0.5	0.5
$2h$, in.	1.0×10^{-3}	1.5×10^{-3}	1.0×10^{-3}
I, in.^{4}	4.16×10^{-11}	1.45×10^{-10}	4.16×10^{-11}
E, lb./in.^{2}	5.0×10^{6}	6.8×10^{6}	1.0×10^{7}
EI, lb. in.^{2}	2.08×10^{-4}	9.85×10^{-5}	4.16×10^{-4}

	Peel Properties					
Rate, in./min.	P, lb.	$\Sigma f_i x_i$, lb. in.	P, lb.	$\Sigma f_i x_i$, lb. in.	P, lb.	$\Sigma f_i x_i$, lb. in.
0.02	0.044	1.35×10^{-3}	0.13	5.1×10^{-3}	0.32	16.3×10^{-3}
0.20	0.079	1.80×10^{-3}	0.31	7.8×10^{-3}	0.50	20.8×10^{-3}
2.00	0.39	4.00×10^{-3}	0.81	12.6×10^{-3}	1.00	28.8×10^{-3}
20.00	1.22	7.10×10^{-3}	—	—	1.90	39.8×10^{-3}

noted that the deviation is uniformly more marked as the stripping angle is increased for all rates. A qualitative explanation of these deviations is available when the dual effect of tensile and flexural strains upon the Young's modulus of the backing in the region of the stripping is considered. On the convex side of the flexed backing the tensile and flexural strains are additive, and at higher stripping forces non-Hookean, with an accompanying lower Young's modulus. As the stripping angle increases, the backing length under high flexural strain increases. Both these effects tend to cause non-elastic buckling of the backing, thus decreasing the backing m, and requiring a corresponding increase in the stripping force P to maintain the conditions of static equilibrium required by eqs. (6) and (6a). The non-Hookean type flexural deformation of the convex side of the flexible member is not fully recoverable, and produces set or curl which increases with rate and angle of delamination. It may be noted that the force-angle functions for the more elastic spring-steel tape (see Fig. 9) more closely fit the theoretical curve at higher levels of P, in agreement with the above argument.

Hata has given particular attention to the relation of stripping angle to stripping load for thin films of benzoyl cellulose, celluloid,

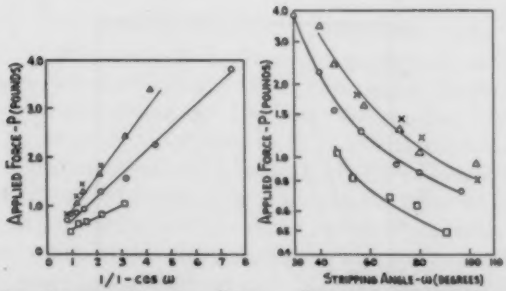

DRYING CONDITIONS	PLASTICIZER	SYMBOL	SLOPE - C	INTERCEPT - Pk
1 MONTH - SPRING	NONE	-○-	.467	.294
1 MONTH - SUMMER	NONE	-△-	.727	.226
1 YEAR	10% TCP	-×-	.727	.226
1 YEAR	40% TCP	-□-	.277	.225

Fig. 10. Peel force P vs. angle ω for benzyl cellulose from Dural (fixed angle method).

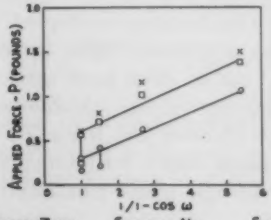

PAPER TYPE	SAMPLE NO.	SYMBOL
UNCOATED BOOK	28	-×-
COATED BOOK	5376	-○-
OFFSET	100	-□-

Fig. 11. Peel force P vs. angle ω for paper bond strength (Bekk Surface Tensile Tester Method).

and polyvinyl butyral bonded directly to metal or glass by solvent activation or combined heat and pressure.[2,3] Results of this study indicate good agreement between experimental results and the predicted linear inverse relation between stripping force P and $(1 - \cos \omega)$ for bonds involving no adhesive interlayer. Plots of these data for the tensile peel of benzyl cellulose from Dural are presented in Figure 10.

The Bekk Surface Tensile Tester measures the force necessary to tear the surface layer of a strip of paper which has been bonded to a

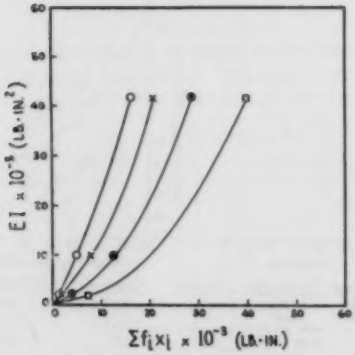

Fig. 12. Effect of the physical properties of the flexible member.

flat metal bar. The effect of angle of force application upon tearing force has been studied by the Institute of Paper Chemistry.[12] Over a range of angles from 36 to 90° the linear inverse relation between tearing force and $(1 - \cos \omega)$ show good agreement with reported experimental data for this type of peel, which involves internal failure of the flexible member. Plots of peel force (P) versus $[1/(1 - \cos \omega)]$, in Figure 11, give linear curves for internal peel delamination of three types of paper over the above-mentioned range of stripping angles.

Thus, this definition of peel would appear to provide a satisfactory explanation of the dependence of stripping force on angle for (*a*) p.s. bonds, (*b*) bonds having no highly elastic interlayer, and (*c*) delamination involving cohesive failure. It is interesting to note that while the peel force, in general, increases with decreasing angle of peel, the work of peel as defined by eqs. (22) or (23) remains constant or decreases with peel angle.

C. Influence of the Flexible Member

Additional information concerning the distribution of force in the bond is supplied by peel tests of a pressure-sensitive bond in which only the thickness and Young's modulus of the flexible member are varied to produce corresponding variations in EI. Descriptions of the bonds and values of P at rates of 0.02, 0.20, 2.00, and 20.0 in./min. ($\omega = 90°$) are summarized in Table III. The apparent summation

of moments of the adhesive bond $\Sigma f_i x_i$ is calculated by eq. (9). The dependence of $\Sigma f_i x_i$ upon EI is illustrated graphically in Figure 12. At the lowest rate of stripping, 0.02 in./min., where the flexible member undergoes predominantly Hookean deformation, $\Sigma f_i x_i$ would appear to be directly proportional to EI. At high rates of stripping, due to the buckling effect of the backing, eq. (9) no longer accurately applies and calculated values of $\Sigma f_i x_i$ are smaller than the true value, producing the upward curvature in the curves represented in Figure 12. These results might indicate that for simple stripback, at constant rate, $(d\omega/ds)$ is a constant and $\Sigma f_i x_i$ is influenced only by the magnitude of EI. The Bikerman[5] equation for 90° peel involving a Newtonian adhesive interlayer may be written:

$$P = \left(12 \frac{K}{t_m} \frac{\eta b}{a}\right)^{1/2} (EI)^{1/2} \tag{26}$$

and for cohesive failure of a Hookean interlayer:

$$P = \frac{0.71 b^{3/4} \sigma_0}{a^{1/4} Y^{1/4}} (EI)^{1/4} \tag{27}$$

where b is the bond width, a the interlayer thickness, K/t_m a peel-rate factor, η the interlayer Newtonian viscosity, σ_0 the adhesive stress at failure, and Y the interlayer Young's modulus. For 90° peel, eq. (9) becomes

$$P = (\Sigma f_i x_i)^2 / 2EI \tag{28}$$

Combining eq. (28) with eq. (26), we find, other factors being held constant, that $\Sigma f_i x_i$ is proportional to $(EI)^{3/4}$ for a Newtonian interlayer. A similar combination of eq. (28) and eq. (27) predicts that $\Sigma f_i x_i$ is proportional to $(EI)^{5/8}$ for cohesive failure of a Hookean interlayer.

Conclusions

In conclusion, it is suggested that this definition of peel may have the following applications:

1. Provide a basis for a more general theoretical analysis of peel adhesion, involving explicitly-defined interlayer rheology and mechanism of failure.

2. Assist in the better understanding of present diverse methods of bond-strength testing of adhesive joints involving flexible members.

References

1. Goland, M., and E. Reissner, *J. Appl. Mechanics*, **11**, A-17 (1944).
2. Hata, T., *Chem. High Polymers (Japan)*, **4**, 67 (1947).
3. Hata, T., and I. Uematsu, *Chem. High Polymers (Japan)*, **4**, 77 (1947).
4. Spies, G. J., *Aircraft Eng.*, **25**, 64 (1953).
5. Bikerman, J. J., *J. Appl. Phys.*, **28**, 1484 (1957).
6. Timoshenko, S., *Theory of Elastic Stability*, McGraw-Hill, New York, 1936.
7. Rivlin, R. S., *Paint Technol.*, **9**, 215 (1944).
8. Bright, W. M., Case Institute Symposium on Adhesion, Cleveland, April, 1952.
9. Busse, W. F., J. M. Lambert, and R. B. Verdery, *J. Appl. Phys.*, **17**, 376 (1946).
10. Hendricks, J. O., G. F. Lindner, and F. J. Wehmer, *Rubber Age*, **32**, 327 (1952).
11. Stedry, P. J., unpublished experiments.
12. Institute of Paper Chemistry Report No. 31, to The American Paper and Pulp Association, February, 1941.
13. Instron Engineering Corporation, Canton, Mass.

Synopsis

An idealized type of tensile peel is defined which substantially represents real systems in the range of low peel forces. The theory applies to the steady-state unbonding of (*a*) a flexible and a rigid member and (*b*) two flexible members. Failure interface propagation is discussed in terms of two stress mechanisms. The first is boundary cleavage, which involves compression-tension bond stress, and the second boundary shear, involving bond stress in simple shear. The theory is general with respect to the stripping angle, and a definition of work of peel is developed which is independent of this variable. Experimental confirmation of the theory is provided by photographic studies of the peel process. A new experimental device is described which permits precise measurement of peel force over a wide range of controlled angles of peel, rate and temperature. Bonds involving both soft viscoelastic interlayers and no interlayer are evaluated and discussed in terms of the theory.

TRANSACTIONS OF THE SOCIETY OF RHEOLOGY III, 181-203 (1959)

The Behavior of Jets of Viscoelastic Fluids

FREDERICK H. GASKINS* and WLADIMIR PHILIPPOFF†, *Laboratories for Research and Development, The Franklin Institute, Philadelphia, Pennsylvania*

Introduction

Many investigations have been conducted into the behavior of liquid jets.[1-3] These have dealt principally with free-flying jets of simple viscous liquids, for which the primary parameters have been described; they are the viscosity, density, and surface tension. When polymer solutions or other viscoelastic liquids are being dealt with, the existing theoretical treatments have proven to be inadequate to account for the observed behavior. The investigations[4,5] that have been conducted with polymer solutions have generally emphasized the importance of viscosity, but have made little reference to the effect of the elasticity necessarily introduced.

As part of a general experimental program into the factors contributing to the stability of liquid jets, we have had to deal with viscoelastic behavior.

This paper presents experiments that were made with viscous and viscoelastic liquids in jets in which the marked qualitative difference in velocity behavior is readily observable. The experimental conditions under which these tests were made are described, particularly because the constant-volume driven gun developed for this application is uniquely advantageous to define accurately the initial velocity imparted to extrude the test fluid.

The Hagenbach treatment[6] of the behavior of jets of simple viscous liquids expelled after Newtonian flow through a capillary (nozzle) has been modified and extended to be applicable when non-Newtonian flow is present. Further, a treatment is derived for the behavior of

* Present address: Aeroprojects Inc., West Chester, Pa.
† Present address: Esso Research & Engineering Co., Linden, N. J.

viscoelastic liquids which is analogous to the Hagenbach treatment for viscous liquids. This novel treatment leads to an evaluation of the elastic energy present in the jet by analysis of the kinetic energy balance occurring in terms of the velocity relationships.

2. Experimental Conditions

2.1. Instrumentation

The fluid jets are extruded at a known velocity by expelling a volume of the test fluid through a cylindrical nozzle at a predetermined rate. The instrument devised for this purpose is based on a design by Gill and Gavis,[7] which has been modified to give a constant efflux volume; it is shown in Figure 1. It consists of a cylinder and a

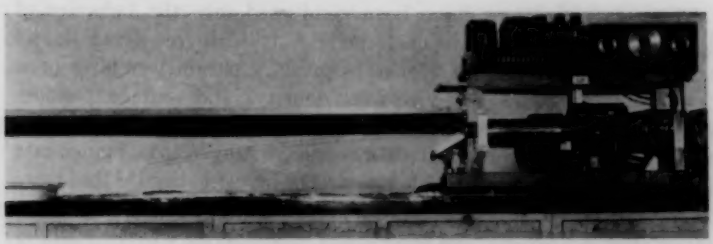

Fig. 1. Jet extrusion instrument.

piston which are rigidly mounted on a massive framework. The piston, which transmits the expulsion force to the fluid, is actuated by a so-called bridge-jack which is driven by a reversible motor through a series of reduction gears of adjustable ratio. A "delayed reversal" switch has been incorporated to allow the automatic reversing of the direction of piston travel. This prevents the piston from overrunning and breaking the front endplate.

The pressure exerted inside the cylinder can be determined by a gage which is mounted on the front endplate of the instrument.

Cylindrical nozzles of various diameters are used with this instrument in order that a wide range in velocities may be available. Table I shows the dimensions of the nozzles and the theoretical velocity range that can be impressed. The rates of shear listed are those occurring within the nozzles. It can be seen that the theoretical veloc-

TABLE I
Dimensions and Operating Ranges for Jet Extrusion Nozzles[a]

Nozzle no.	Length l, cm.	Diameter d, cm.	Theoretical impressed velocity, v_0, cm./sec.		Rate of shear, D, sec.$^{-1}$	
			Minimum	Maximum	Minimum	Maximum
1	5.97	0.1819	1.29×10^1	3.26×10^3	5.68×10^2	1.43×10^5
2	5.74	0.0391	2.80×10^2	7.07×10^4	5.74×10^4	1.45×10^7
3	5.98	0.152	1.84×10^1	4.65×10^3	9.68×10^3	2.45×10^5
4	2.49	0.1827	1.28×10^1	3.24×10^3	5.61×10^2	1.42×10^5
5	2.54	0.0473	1.92×10^2	4.85×10^4	3.24×10^4	8.19×10^6
6	2.48	0.1210	2.92×10^1	7.37×10^3	1.93×10^3	4.87×10^5
7	2.53	0.0193	1.15×10^3	2.91×10^5	4.77×10^5	1.21×10^8
8	2.53	0.0612	1.15×10^3	2.89×10^4	1.51×10^4	3.79×10^6

[a] Minimums based on gear ratio, $n = 0.0629$. Maximums based on gear ratio, $n = 15.89$.

ity range is 12.8 to 291,000 cm./sec. The practical upper limit is dictated by the mechanical setup, and would certainly fall far below the theoretical value stated. Nevertheless, an extensive range in operating conditions is available.

The jets are extruded horizontally, the trajectory being measured directly and/or photographed over the entire path of flight or any segment thereof. The photography is carried out with a Graflex camera and either a Strobolume flash unit of 9 μsec. duration or a modified flash unit of 2 μsec. duration.

2.2. Experimental Parameters

By having the cylindrical capillary nozzles in series with the main cylinder, the conditions under which the flow occurs can be exactly pre-determined. The primary flow parameters are the impressed or "continuity" velocity,

$$v_0 = Q/A_2 = (A_1/A_2)(dL/dt) \qquad \text{in cm./sec.} \tag{2.1}$$

where, v_0 is the initial mean relative velocity of jet to air, in cm./sec.; Q is the volumetric rate of extrusion, in cm.^{3}/sec.; A_1 and A_2 are the cross-section areas of the main cylinder and the nozzle, respectively, in cm.^{2}; (dL/dt) is the rate of piston travel, in cm./sec.; and the velocity in flight evaluated using the ballistics equation which assumes a parabolic trajectory,

$$v_F = x\sqrt{g/2y}, \qquad \text{in cm./sec.} \tag{2.2}$$

where, v_F is the horizontal component of the flight velocity of the jet relative to the air, integrated over the range, in cm./sec.; x is the horizontal distance traversed (range), in cm.; y is the distance of fall, in cm.; g is the gravitational acceleration constant (980.7 cm./sec.^{2})

In addition, two rheological parameters can be readily determined. One is the rate of shear occurring in the nozzle,

$$D = 4Q/\pi r^3 = (4/r)v_0, \qquad \text{in sec.}^{-1} \tag{2.3}$$

where r is the radius of the nozzle, in cm., and v_0 is the "continuity velocity." The other is the shearing stress,

$$\tau = rP/2L, \qquad \text{in dyne/cm.}^2 \tag{2.4}$$

where P is the pressure drop across the nozzle (gage reading), in dyne/cm.^{2}, and L is the length of the capillary nozzle, in cm.

Note: The value of τ calculated by eq. (2.4) has to be corrected for kinetic energy, etc., to obtain the "true" shear stress developed within the nozzle; by the same token, the rate of shear according to eq. (2.3) must be corrected by $(n + 3)/4$ when non-Newtonian flow occurs, if $n = d \log D/d \log \tau$ is significantly larger than unity. These evaluations are discussed in detail in reference 8.

2.3 Test Fluids

Dibutyl phthalate (DPB), water, and an unmodified lubricating oil were the pure (viscous) liquids used during this investigation. The polymers, all dissolved in DBP at various concentrations, were:

Polyisobutyl methacrylate (PIBMA) supplied by the Chemical Warfare Labs., U. S. Army Chemical Center.

Cellulose acetate–butyrate copolymer (CAB), commercial grade (EAB-381-20).

Cellulose nitrate (NC, no. 1) commercial grade (RS$^1/_4$ sec.).

Cellulose nitrate (NC, no. 2) dynamite grade.

The physical properties of the solutions were measured. For 0.5%-by-weight solutions and for DBP the densities were between 1.04 and 1.05 g./cm.^{3}, the surface tensions were approximately 33 dyn./cm., and the relative viscosities were 1.2 to 2.4 based on a viscosity of 0.1598 poise for DBP at 25°C.

TABLE II
Rheological Properties of Test Solutions

Rate of shear, D, sec.$^{-1}$	Shear stress, τ, dyne/cm.^{2}	Viscosity, η, poise	Recoverable shear, s	Shear modulus, G, dyne/cm.^{2}	Normal stress, P_{11}, dyne/cm.^{2}	Relaxation time, T_R, msec.	Velocity in jet extrusion, v_0, cm./sec.
0.5% Polyisobutyl Methacrylate in Dibutyl Phthalate							
25,000	6,690	0.268	36	136	24,000	1.44	571
100,000	24,600	0.246	50	493	123,000	0.50	2280
250,000	57,600	0.230	54	1,070	311,000	0.216	5710
0.5% Cellulose Acetate–Butyrate in Dibutyl Phthalate							
25,000	6,830	0.273	~0				571
100,000	20,900	0.279	6	3,480	125,000	0.060	2280
250,000	44,700	0.179	19	2,300	868,000	0.076	5710
1.0% Cellulose Nitrate in Dibutyl Phthalate (commercial grade)							
25,000	6,690	0.268	~0				571
100,000	24,600	0.246	~0				2280
250,000	58,400	0.234	1	58,400	58,400	0.0040	5710

The rheological properties of some of the solutions were determined in a high pressure capillary viscometer using the "capillary length effect."[8] The results are shown in Table II.

3. Experimental Results

Preliminary tests with viscoelastic solutions showed that the flight velocities were often smaller by a considerable amount than those impressed at the nozzle. This deviation from the theoretical expectation, which, in a first approximation, would be expected to hold, resulted in a careful analysis of the experimental setup. By having the values of v_0 calculated from the piston travel rate [the second part of eq. (2.1)], direct measurements were made of the efflux volume against time. This provided a check on the first part of eq. (2.1), and gave results which were precise to better than 1%. Therefore, the instrumentation was performing properly.

The test fluids were then examined systematically in order to define better the relationship between the flight velocity, v_F, and the "continuity velocity," v_0. The materials were investigated at a series of velocities in the range of 100 to 1500 cm./sec. using one or more cylindrical nozzles with results as follows.

3.1. Viscous Liquids

The water was expelled at 766 cm./sec. from a nozzle with a diameter of 0.1827 cm. It was found that the water sprays apart immediately upon emergence from the nozzle so that no evaluation of v_F could be made within the velocity range cited.

The lubricating oil (η = 19.2 cps. at 37.5°C.) at the same v_0 gave a v_F of 1050 cm./sec.; the ratio v_0/v_F was 0.730. The values of v_F in this case are unreliable because the jets formed sprays which cannot be evaluated accurately in this way.

The dibutyl phthalate was measured in five capillary nozzles (nos. 1, 4, 5, 6, and 8) with a four-to-one difference between the largest and smallest diameters. The results as shown in Figure 2 are that all of the data fit a straight line with a mean slope of 0.801 within experimental error. These data were evaluated by the method of least squares to get an accurate result. The divergence above 10 m./sec. is due to the jet's disintegrating into a spray; below this level, uniform jets with a parabolic trajectory were obtained. It should be

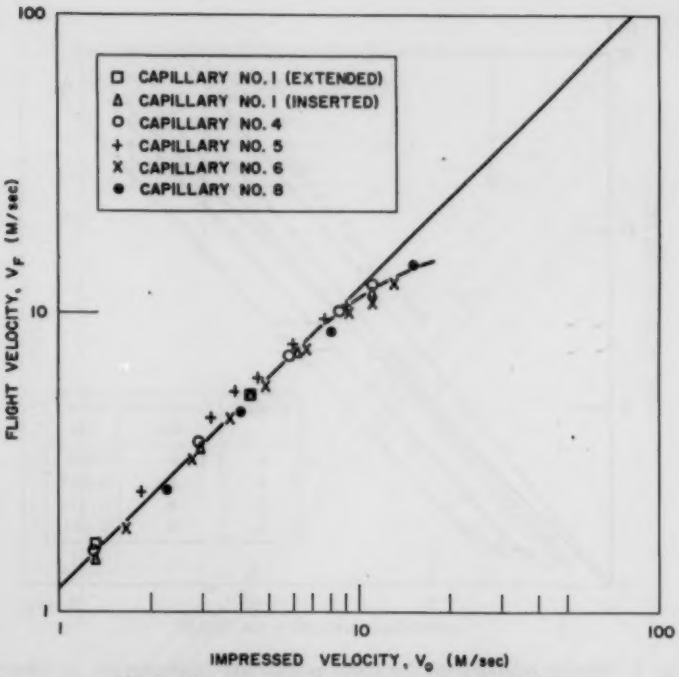

Fig. 2. Velocity relationships for dibutyl phthalate.

noted that one of the runs was made with a nozzle of 5 cm. length inserted into the cylinder. This test of the "Borda effect," to be discussed, is indistinguishable from the other runs with the same cylindrical nozzles in the normal or extended position.

3.2. Viscoelastic Liquids

(a) **Polyisobutyl Methacrylate in Dibutyl Phthalate.** The PIBMA in DPB was investigated at 0.5 and 0.25% concentrations (by weight of solution), the results for the two concentrations being qualitatively the same. For the 0.5% solution four capillaries were used (nos. 4, 5, 6, and 8). The results in Figure 3 show a marked difference from the results obtained for viscous liquids. None of the curves, for the nozzles used, fit either the theoretical ratio of $(v_0/v_F) = 0.801$ or the

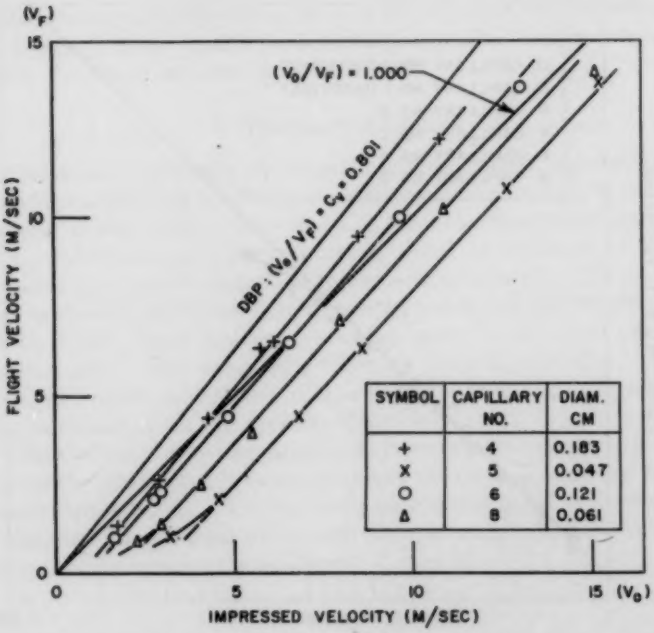

Fig. 3. Velocity relationships for 0.5% polyisobutyl methacrylate in dibutyl phthalate.

1:1 relationship. Rather there is a significant decrease in v_F for a given v_0. Also, the magnitude of the difference increases with decreasing size of radius. (*Note:* The smaller the radius, the higher the rate of shear range involved; therefore, while the curves are correlatable on the basis of equivalent jet velocities, they represent different initial flow conditions within the nozzles.)

An interesting point to be observed is that the curves are generally linear and are displaced parallel to the theoretical curve, which represents the DBP data.

(b) Cellulose Derivatives in Dibutyl Phthalate. The cellulose-derivative solutions were investigated in nozzle no. 4 (d = 0.1827 cm). The results for 0.5% cellulose acetate–butyrate, 0.5, 1.0, and 2.0% cellulose nitrate (commercial grade) and 0.5% cellulose nitrate

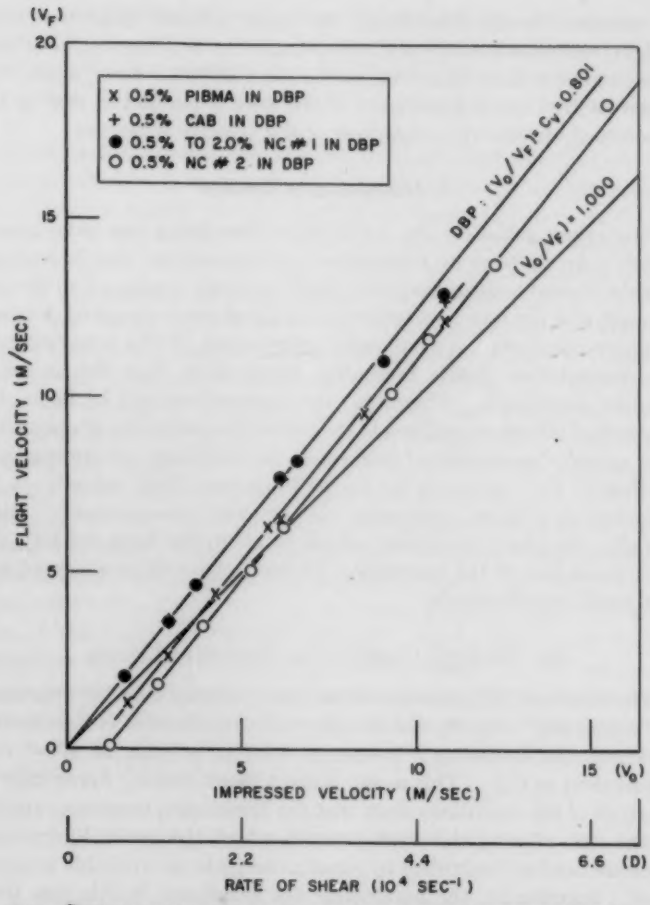

Fig. 4. Velocity relationships for various polymers in dibutyl phthalate.

(dynamite grade) in DBP are shown in Figure 4, together with the data for 0.5% PIBMA in DBP using the above-mentioned nozzle.

As seen in this figure, the solutions of the two commercial grade polymers, CAB and NC #1, gave results which coincide entirely with the results for DBP up to the velocity at which disintegration of the

jet occurs. On the other hand, the highly nitrated (high molecular weight) cellulose in solution shows a drop in v_F as a function of v_0 that is even greater than that obtained for the PIBMA. Here, again, it is apparent that the displacement of the lines is parallel to that of the theoretical, despite the magnitude of the velocity difference.

4. Discussion of Results

The investigation of the velocities of free-flying jets gave results which were contrary to expectation on two counts: the Newtonian liquids showed a 20% increase in flight velocity compared to the impressed, and the non-Newtonian materials showed a marked decrease in many instances. A systematic examination of this behavior gave the quantitative results presented, which show that this is not a random occurrence. Therefore, the explanation had to lie in the theoretical treatment applied to the particular conditions of operation. The primary parameter of interest is the discharge (or contraction) coefficient, $C_v = v_0/v_F$, so far as the theoretical flight velocity to be expected at a given continuity velocity level is concerned. Additionally, the exact conditions, which result in the large velocity differences shown by the viscoelastic solutions, have to be analyzed and evaluated quantitatively.

4.1 Discharge Coefficient for Newtonian Liquids

The observed 20% increase of the flight velocity over the impressed or "continuity" velocity did not agree with the theories of viscometry, which in the Boussinesq[9] treatment lead to a value of $m = 1.12$ (equivalent to C_v). This would mean a flight velocity lower than v_0. Analysis of the conditions show that the Boussinesq treatment applies in the case of a regular viscometer in which the active hydrostatic pressure head is diminished by kinetic energy to an available pressure head. Specifically, the parameters are calculated in this case from the total pressure utilized, knowing *a priori* that there are losses other than that to viscous flow.

The calculations of Hagenbach[6] in his original publication, in which he treated the boundary conditions of our problem directly, lead to a discharge coefficient of ~0.8. Hagenbach's reasoning assumed an exit velocity that would not be changed by the kinetic energy in the liquid, even though the kinetic energy is very high. This is the case in

our jet extrusion instrument, where the speed of the motor is not influenced by the pressure in the liquid; also, the parameters are evaluated from the change in kinetic energy at the nozzle exit and in flight. Therefore, Hagenbach's theory is the pertinent one for these conditions.

Examination was also made of the classical statement that the discharge coefficient is caused by the liquid entering a capillary tube, with the flow outside of the capillary leading to the so-called "vena contracta." We checked the results of this theory, as reported by Birkhoff and Zarantonello,[10] by reversing the cylindrical nozzle so that it was inserted into the cylinder with a 360° influx. This is called the "Borda tube effect." The data reported in the reference gave a change in C_v from 0.611 for the extended capillary to 0.500 for the inserted, presumably using water as the test medium. Our results show no detectable difference in the velocities whatsoever using capillaries of $d = 0.182$ cm., with one $L = 5.97$ cm. extended and inserted, and another $L = 2.40$ cm. extended. These results show that the Borda tube effect may be damped out by the viscous dibutyl phthalate, whereas the effect is reputedly quite noticeable in the experiments described. Also, the results with three geometrical configurations establish that laminar flow is present, and no turbulence occurs within the tube. These aspects have been substantiated by evaluation of the Reynolds numbers involved which shows that critical values are not attained within this velocity range (to 1500 cm./sec.).

The treatment of Hagenbach is repeated in the Appendix; however, it is given in a different way from the original in order that the resulting equations can be extended to the case of non-Newtonian flow. The result of the evaluation is that

$$C_v = v_0/v_F = 1/\sqrt[3]{2} = 1/1.2599 = 0.7937 \tag{4.1}$$

This theoretical value is equal, within experimental error, to the value of 0.801 determined experimentally. This means that for a viscous, Newtonian liquid, the diameter of the jet decreases by $\sqrt{C_v} = 0.890$ or by 12% as compared to the diameter of the capillary tube. Also, the flight velocity to impressed velocity relationship is

$$v_F = v_0/C_v = \sqrt[3]{2}v_0 = 1.260v_0 \tag{4.2}$$

4.2 Discharge Coefficient for Non-Newtonian Liquids

The Hagenbach derivation in Appendix I is applicable to the behavior of Newtonian (viscous) liquids. For viscoelastic polymer solutions, the flow behavior is generally non-Newtonian. Therefore, the discharge coefficient must include the "Power Law," which is likewise included in the evaluation of velocity gradient for the capillary

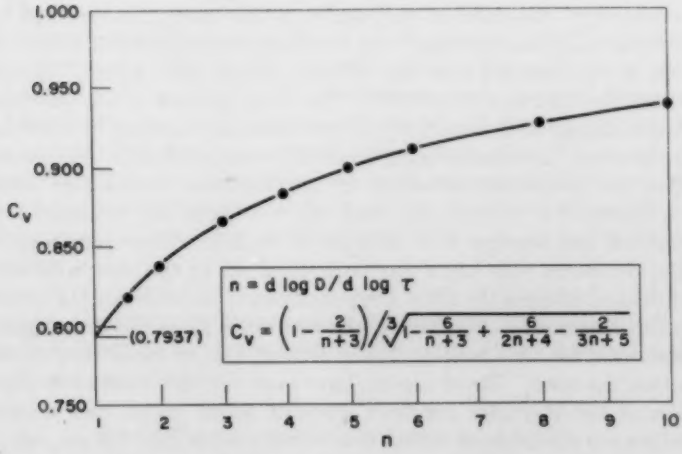

Fig. 5. Evaluation of discharge coefficient as a function of the "viscous" slope.

viscometer flow of these materials. The Hagenbach treatment has been extended to include the "Power Law," but not possible elastic effects, i.e.,

$$\partial v/\partial r = K\tau^n \tag{4.3}$$

This derivation, which is presented in Appendix II, leads to

$$C_v = \frac{1 - \dfrac{2}{n+3}}{\sqrt[3]{1 - \dfrac{6}{n+3} + \dfrac{6}{2n+4} - \dfrac{2}{3n+5}}} \tag{4.4}$$

where

$$n = \partial \log D / \partial \log \tau \tag{4.5}$$

is the "viscous slope," i.e., the slope of the D or $(\partial v/\partial r)$ vs. τ curve in double-logarithmic plot ("flow curve").

The C_v, so evaluated, is the discharge coefficient which correlates the continuity velocity impressed on the viscoelastic fluid with the *theoretical* velocity of the jet in flight assuming non-Newtonian viscous flow of the fluid through the nozzle. The numerical evaluation of eq. (4.4) has been carried out, the results being presented in graphical form in Figure 5 for n between 1 and 10. It should be noted that this correction for the behavior of non-Newtonian fluids in free-flying jets is equivalent to the standard correction for the parabolic distribution of velocity across the radius in capillary viscometry (cf. ref. 8). For $n \to \infty$, a constant velocity over the entire cross section results and $C_v = 1$. Non-Newtonian flow, alone, therefore, can change C_v only from 0.7937 to 1.0000.

4.3 Elastic Energy in Jets of Viscoelastic Fluids

The significant decrease in flight velocity as compared to the impressed velocity, for viscoelastic fluids, could not be accounted for by the existing theories, which deal only with viscous behavior. Nor does taking into account the non-Newtonian flow of these solutions explain the large difference. As seen in Figure 5, C_v varies between 0.79 and 0.94 under ordinary conditions; this means that the theoretical flight velocity for any material after undergoing Newtonian or non-Newtonian viscous flow should be from 6% to 26% *higher* than the impressed velocity. Therefore, the elastic energy developed in viscoelastic materials under flow conditions has to be considered. In reference 8 it was stated that "the elastic energy, imparted to the liquid at the entrance of the capillary, is carried out of the capillary by the flowing liquid and dissipated outside the capillary much in the same way as the kinetic energy." Equations were derived therein for evaluating the elastic energy as recoverable shear, s, or normal stress, P_{11}, from the pressure vs. L/R relationships obtained during the flow through the tube. Under the present experimental conditions, we have a direct manifestation of the elastic energy from the effects obtained outside of the tube; these effects are that the jet diameter increases and the flight velocity decreases.

Nevertheless, the continuity equations are satisfied in that volume-time constancy is obtained.

The total energy transported out of the capillary tube is recovered as both kinetic energy and potential (or elastic) energy. Knowing the kinetic energy imparted to the fluid (from the theoretical flight velocity, $v_I = v_0/C_v$) and the kinetic energy utilized to propel the fluid through space (from the actual flight velocity, v_F), we can evaluate the elastic energy as the difference in these kinetic energies. In order to do this, one has to evaluate an "elastic discharge coefficient" to take into account any nonlinearity in the shear stress, τ, vs. recoverable shear, s, behavior, since the shear modulus, $G = \tau/s$, is generally not a constant.

The derivation of the elastic parameters is given in Appendix III, but can be summarized as follows:

The elastic discharge coefficient is calculated from the slope of the shear stress-recoverable shear curve, assuming the same velocity distribution over the cross section as is usual in the treatment of non-Newtonian flow, as:

$$C_e = (n' + 1)(n' + 3)/2 \tag{4.6}$$

where

$$n' = \partial \log \tau / \partial \log s \tag{4.7}$$

is the elastic slope, i.e., the slope of the τ vs. s curve in double-logarithmic plot.

The numerical evaluation of C_e shows that as n' varies from 0 to 1, C_e takes on values from 1.5 to 4.0; it is thus possible for four-fold differences in velocities to occur that account for the observations noted.

Having the elastic discharge coefficient, the elastic energy can be evaluated as normal stress,

$$P_{11} = C_e C_v (v_T^2 - v_F^2)\rho \tag{4.8}$$

where, P_{11} is the normal stress at the wall, in dyne/cm.^{2}; C_v is the fluid density, in g./cm.^{3}; v_T is the theoretical flight velocity $= v_0/C_v$, in cm./sec.; and v_F is the actual flight velocity, in cm./sec.

This eq. (4.8) probably does not represent the final formulation. For example, one factor that should be included is the stated effect of the elasticity on the flow pattern in the nozzle; in other words, the

change in shear stress and rate of shear distribution across the radius under the influence of normal stress must be calculated.

The elastic energy in viscoelastic fluid jets has not yet been quantitatively evaluated by the method described; additional data from the capillary viscometer and from flow birefringence in the same range of D are required before experimental proof of the relationships can be offered.

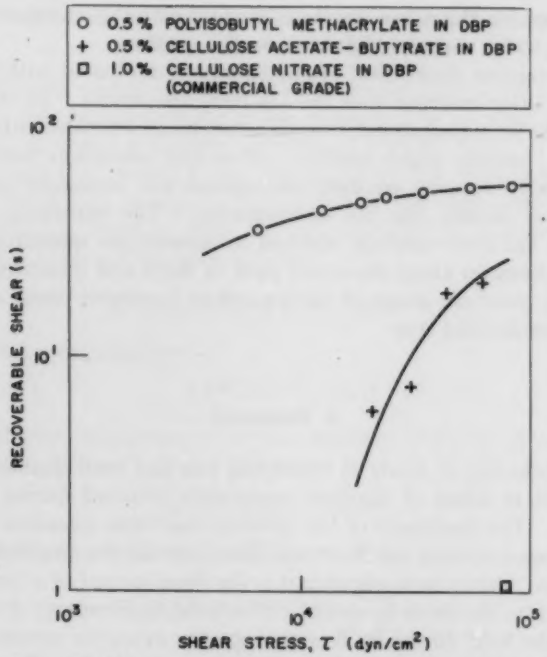

Fig. 6. Recoverable shear vs. shear stress for three different polymers in dibutyl phthalate (at 25°C.).

Some data were obtained in the capillary viscometer using the "capillary length effect" technique (see ref. 8). These results, which are given in Figure 6 as a plot of log s vs. log τ, show the comparative elastic nature of three of the solutions. The commercial grade nitrocellulose solution shows an s of unity (100% shear) this being attained

at a rate of shear ($>10^5$ sec.$^{-1}$) which is beyond that used in the jet extrusion experiments. In the range of the jet operation (up to 50,000 sec.$^{-1}$), no elastic effects were detectable in the capillary, and, as was shown in Figure 4, no velocity decrease was observed. The PIBMA solution shows a large s even in the range of jet operation, and this result correlates qualitatively with the large difference in the v_F vs. v_0 curve. The CAB solution has a large s at high rates of shear, but the values are too small to be measurable in the range of D below 50,000 sec.$^{-1}$; this again correlates directly with the jet velocity comparison, which shows no difference for this solution.

Examination shows that elastic energy is dissipated within milliseconds after emergence of the jet from the nozzle. In the cases where the jet was analyzed, the relaxation times were always below 30 millisec., usually much smaller. After this relaxation period, the jet velocity remains constant throughout the remainder of flight (unless of course, the jet disintegrates). The constancy of the velocity has been carefully checked by microscopic measurement of the jet diameter along the entire path of flight and measurement of the true parabolic shape of the trajectory in several cases, and the stated results held true.

5. Summary

The behavior of fluids in free-flying jets has been quantitatively described in terms of the flow parameters involved during jet extrusion. The treatment of this problem has been extended to take into account not only the Newtonian flow, but also the non-Newtonian response. Particularly significant is the development of a treatment analogous to the above by means of which the elastic energy developed within the fluid during its flow through the extrusion nozzle can be evaluated solely in terms of the kinetic energy relationships outside of the nozzle. It must be restated that this equation for evaluating elastic energy as normal stress probably does not represent the final formulation; additional experimental confirmation has to be obtained. Nevertheless, this is a new method for measuring elastic energy, and one which appears to have advantages for the investigation of viscoelastic materials due to the simplicity of the experimental technique involved.

This work was performed under contract with the U. S. Army Chemical Warfare Laboratories, Army Chemical Center, Edgewood, Md., whose support is gratefully acknowledged by the authors.

Appreciation is also expressed to Mr. Alan J. Dietrich, who performed the jet extrusion measurements, and to Mrs. Margaret T. Meyer, who carried out the capillary investigation and the microscopic analysis of the jets.

APPENDIX I

Modification of Hagenbach Derivation of the Discharge Coefficient for Newtonian Liquids

The kinetic energy of the mass of emerging liquid with a certain velocity distribution over the radius is equated to the kinetic energy in flight, assuming a uniform velocity, v_0, over the area. The mass of the liquid is given as the area multiplied by the velocity and density. The kinetic energy is determined by the mass multiplied by $^1/_2v^2$. For the capillary tube, the velocity must be integrated over the radius to obtain the basic equation:

$$\int_0^R {}^1/_2 \cdot 2\pi\rho r dr \cdot v \cdot v^2 = {}^1/_2\pi R^2 \cdot \rho v_F^3 \tag{A-1}$$

This can be simplified to:

$$2\int_0^R v^2 r dr = R^2 v_F^3 \tag{A-2}$$

The velocity distribution over the capillary radius is obtained by integrating Newton's Law. The result is:

$$v = v_{max}[1 - (r/R)^2] \tag{A-3}$$

Introducing eq. (A-3) into eq. (A-2), we obtain:

$$2v_{max}^3 \int_0^R [1 - (r/R)^2]^3 \frac{r}{R} \cdot \frac{dr}{R} = v_F^3 \tag{A-4}$$

Let $y = 1 - (r/R)^2$, then $dy = -2(r/R)d(r/R)$
and

$$-v_{max}^3 \int_1^0 y^3 dy = -v_{max}^3 \cdot y^4/4 \Big|_1^0 = {}^1/_4 v_{max}^3 = v_F^3$$

$$v_{max} = \sqrt[3]{4} \cdot v_F \tag{A-5}$$

We now apply the continuity equation:

$$Q = \pi R^2 \cdot v_0$$

where Q is the efflux volume, in cm.^{3}/sec. and

$$Q = 2\pi \int_0^R vrdr = 2\pi v_{max} \int_0^R [1 - (r/R)^2]rdr$$

$$= 2\pi v_{max} {}^1/_4 y^2 \Big|_1^0 = (\pi/2)R^2 v_{max}$$

Equating the two expressions for Q:

$$Q = \pi R^2 \cdot v_0 = (\pi/2)R^2 v_{max}$$

$$v_0 = {}^1/_2 v_{max}$$

Introducing eq. (A-5) we obtain:

$$v_0 = {}^1/_2 \sqrt[3]{4} \cdot v_F$$

or, for the velocity of the jet in flight:

$$v_F = (2/\sqrt[3]{4}) \cdot v_0 = \sqrt[3]{2} \cdot v_0 \qquad \text{(A-6)}$$

The discharge coefficient C_v for Newtonian flow is

$$C_v = v_0/v_F = 1/\sqrt[3]{2} = 1/1.2599 = 0.7937 \qquad \text{(A-7)}$$

APPENDIX II

Extension of the Hagenbach Treatment to Non-Newtonian Liquids

The first expression to be considered is the relationship between the velocity integrated over the radius, r, and the assumed uniform velocity, v_0, to the velocity gradient:

$$v - v_0 = \int_0^r \left(\frac{dv}{dr}\right) dr \qquad \text{(A-8)}$$

The velocity gradient can be expressed in terms of the shear stress by introducing the "Power Law" (see ref. 8):

$$\left(\frac{dv}{dr}\right) = K\tau^n = K\left(\frac{rP}{2L}\right)^n = K\tau_R{}^n \left(\frac{r}{R}\right)^n \qquad \text{(A-9)}$$

Incorporating eq. (A-9) into eq. (A-8), we obtain:

$$v - v_0 = R \int_0^r K\tau_R{}^n \left(\frac{r}{R}\right)^n \frac{dr}{R}$$

Let $x = r/R$. Then:

$$v - v_0 = K\tau_R{}^n \cdot R \int_0^1 x^n dx = K\tau_R{}^n R \left(\frac{x^{n+1}}{n+1}\right)$$

For $x = 0, v = v_0$; for $x = 1, v = 0$ and $-v_0 = \dfrac{K\tau_R{}^n R}{n+1}$

Therefore:

$$v - v_0 = -v_0 x^{n+1}$$

or:

$$v = v_0 (1 - x^{n+1}) \tag{A-10}$$

Introducing eq. (A-10) into the Newton's law integration (A-4) results in:

$$2 v_{max}{}^3 \int_0^1 (1 - x^{n+1})^3 \, x dx \tag{A-11}$$

The expansion is:

$$2 v_{max}{}^3 \int_0^1 (1 - 3x^{n+1} + 3x^{2n+2} - x^{3n+3}) \, x dx$$

$$= 2 v_{max}{}^3 \left[\frac{1}{2} - \frac{3}{n+3} + \frac{3}{2n+4} - \frac{1}{3n+5}\right] = v_F{}^3$$

$$v_{max} = v_F \sqrt[3]{\frac{1}{1 - \dfrac{6}{n+3} + \dfrac{6}{2n+4} - \dfrac{2}{3n+5}}} \tag{A-12}$$

For

$$n \to 1, \quad \sqrt[3]{\ } \to \sqrt[3]{4}$$
$$n \to \infty, \quad \sqrt[3]{\ } \to 1$$

Applying the continuity equation, including the expression for v (in eq. A-10) gives:

$$Q = 2\pi \int_0^R v r dr = 2\pi R^2 \int_0^R v_0 (1 - x^{n+1}) \, x dx$$

and

$$Q = 2\pi R^2 v_{max} \int_0^1 (x - x^{n+2}) \, dx = 2\pi R^2 v_{max} \left[\frac{1}{2} - \frac{1}{n+3}\right] \tag{A-13}$$

For $n \rightarrow 1$, $[\ \ ] \rightarrow 1/4$. Therefore:

$$\pi R^2 v_0 = 2\pi R^2 v_{max}\left[\frac{1}{2} - \frac{1}{n+3}\right]$$

$$v_0 = 2v_{max}\left[\frac{1}{2} - \frac{1}{n+3}\right] = v_{max}\left[1 - \frac{2}{n+3}\right] \qquad \text{(A-14)}$$

Combining eq. (A-12) with eq. (A-14) gives

$$v_F = \frac{v_0}{\left[1 - \frac{2}{n+3}\right]} \sqrt[3]{1 - \frac{6}{n+3} + \frac{6}{2n+4} - \frac{2}{3n+5}} \qquad \text{(A-15)}$$

For

$$n \rightarrow 1, \text{ (the Newtonian case)}, v_F = 2\sqrt[3]{\frac{1}{4}} \cdot v_0 = \sqrt[3]{2} \cdot v_0$$

$$n \rightarrow \infty, v_F = v_0$$

The discharge coefficient is

$$C_v = \frac{v_0}{v_F} = \frac{\left[1 - \frac{2}{n+3}\right]}{\sqrt[3]{1 - \frac{6}{n+3} + \frac{6}{2n+4} - \frac{2}{3n+5}}} \qquad \text{(A-16)}$$

where

$$n = \left[\frac{\partial \log D}{\partial \log \tau}\right]$$

APPENDIX III

Evaluation of Elastic Energy in Viscoelastic Fluid Jets

The energy balance existing for viscoelastic flow through a capillary tube was stated in ref. (8), eq. (11), as:

$$P_T Q = P_c Q + m\rho v^2 Q + P_e Q \qquad \text{(A-17)}$$

where P_T is the total pressure applied, in dynes/cm.^{2}; P_c is the pressure taken up by viscous flow, in dynes/cm.^{2}; P_e is the pressure transported

out of the capillary as elastic energy ($P_e \cdot Q$), in dynes/cm.^{2}; Q is the efflux volume, in cm.^{3}/sec.; and $m\rho v^2 Q$ is the kinetic energy, in dyne-cm. (per sec.), (m is substituted for by C_v as in the Hagenbach treatment).

At the exit of the capillary (nozzle), the viscous energy ($P_v Q$) is zero. Then the equation, reduced and restated in terms of velocity, is:

$$C_v \rho v_0^2 Q = C_v \rho v_F^2 Q + P_e Q \tag{A-18}$$

Equation (A-18) states that the elastic energy is the difference between the kinetic energy imparted to the fluid and that utilized to propel the fluid jet through space.

The mean value for elastic energy over the capillary cross section is

$$P_e \cdot \pi R^2 = \int_0^R 2\pi r dr \int_0^s \tau ds \tag{A-19}$$

or

$$P_e = 2 \int_0^1 \left(\frac{r}{R}\right) d\left(\frac{r}{R}\right) \int_0^s \tau ds \tag{A-20}$$

We approximate the general nonlinearity between τ and s by a Power law:

$$\tau = As^{n'}$$

where

$$n' = \left[\frac{\partial \log \tau}{\partial \log s}\right]$$

Then, from eq. (A-20):

$$\int_0^s \tau ds = \int_0^s As^{n'} ds = \frac{A}{n'+1} s^{n'+1} \tag{A-21}$$

The following two relationships established in our previous publications:[8,11]

$$P_{11} = \tau \cdot s \quad \text{yields} \quad P_{11} = As^{n'+1}$$

and

$$P_{11} = (P_{11})_R \left(\frac{r}{R}\right)$$

are incorporated into eq. (A-21) to give:

$$\frac{P_{11}}{n'+1} = \frac{(P_{11})_R}{n'+1}\left(\frac{r}{R}\right)^{n'+1}$$

Therefore:

$$P_e = 2\int_0^1 \frac{(P_{11})_R}{n'+1}\left(\frac{r}{R}\right)^{n'+2} d\left(\frac{r}{R}\right) = (P_{11})_R\left[\frac{2}{(n'+1)\,(n'+3)}\right] \tag{A-22}$$

Introducing eq. (A-22) into eq. (A-18) results in:

$$(P_{11})_R\left[\frac{2}{(n'+1)\,n'+3)}\right] = C_e\rho(v_0^2 - v_F^2)$$

or

$$(P_{11})_R = C_eC_v(v_0^2 - v_F^2)\,\rho \tag{A-23}$$

where

$$C_e = \frac{(n'+1)\,(n'+3)}{2} \tag{A-24}$$

is the "elastic" discharge coefficient.

In order to complete the evaluation of normal stress (i.e., elastic energy) we have to refer to the impressed velocity. This means that the contraction of the jet which would occur for viscoelastic fluids even in the absence of elastic phenomena, has to be taken into account as:

$$v_T = v_0/C_v$$

where v_T is the theoretical flight velocity.

The final equation for the normal stress is:

$$(P_{11})_R = C_eC_v(v_T^2 - v_F^2)\rho \tag{A-25}$$

References

1. Lord Rayleigh, *The Theory of Sound*, Vol. II, Dover, New York, 1945.
2. Weber, C., *Z. Angew. Math. Mech.*, **11**, 136 (1931).
3. Haenlein, A., NACA TM 659 (1932).
4. Hanson, A. R., and F. G. Domisch, Univ. of Minn., Rosemount Aero. Labs. Research Report No. 130 (June, 1956).

5. Russum, L. W., "External Ballistics of Liquid Jet Trajectories," ScD. Thesis. MIT (1947).

6. Hagenbach, E., *Ann. phys.*, **109,** 385 (1860).

7. Gill, S. J., and J. Gavis, *J. Polymer Sci.*, **20,** 287 (1956).

8. Philippoff, W., and F. H. Gaskins, "The Capillary Experiment in Rheology," *Trans. Soc. Rheol.*, **2,** 263 (1958).

9. Boussinesq, J., *Compt. rend.*, **110,** 1160 (1890); **113,** 9 (1891).

10. Birkhoff, G., and E. H. Zarantonello, *Jets, Wakes, and Cavities*, Academic Press, New York, 1957.

11. Philippoff, W., F. H. Gaskins, and J. G. Brodnyan, *J. Appl. Phys.*, **28,** 1128 (1957).

Synopsis

The stability of liquid jets is well known to be described by the theory of Rayleigh which uses the density and surface tension of the liquid as important parameters. Further investigations have taken into account the viscosity, the combination of these three parameters being known as the Weber number. However, polymer solutions are now known to have an elasticity in flow; the mechanism of breakup of solutions of polymers has not heretofore been investigated. We have used a constant volume-driven extrusion device by means of which the velocity of the emerging jet could be calculated exactly, which gave us an additional parameter as compared with the standard pressure-driven device. A number of pure liquids and polymer solutions were investigated. The general result was that the "vena contracta" causes an increase of the velocity of the free flying jet by about 20% for pure liquids, as compared to the predetermined "continuity velocity." This can be explained by the old theory of Hagenbach. Viscoelastic polymer solutions, however, showed a decrease of velocity as compared either to the normal liquids or to the "continuity velocity." Very probably that difference is caused by the elastic energy accumulated in the jet which absorbs some of the kinetic energy of the emerging liquid. The quantitative evaluation showed that we can determine the elastic stress of the liquid and therefore also the normal stress by measuring the difference between the jet velocity and the velocity of the solvent.

TRANSACTIONS OF THE SOCIETY OF RHEOLOGY III, 205–206 (1959)

Communication Problems in Industrial Rheology

Committee Recommendations for Describing Flow Phenomena

Increased study of the flow characteristics of polymers and dispersions has revealed a lack of authoritative definitions and standardized terminology for stress-dependent flow phenomena. Confusion resulting from these deficiencies has become so acute that a Committee on Communication Problems in Rheology has been organized to establish areas of agreement in describing the flow characteristics of materials.

The Committee is sponsored by several American Chemical Society divisions (Agricultural and Food, Colloid, Industrial and Engineering, Paint, Petroleum, and Polymer), the Society of Rheology, and the American Society for Testing Materials.

Before delving into more controversial details, including the definition of viscosity, the Committee considered that it must first establish and define those broad aspects of flow concerning which no serious disagreement exists among practicing rheologists. It was decided that the following realities must be recognized as the framework upon which definitions and terms can be built:

1. The basic measured quantities are shear stress (S), shear rate (D), and time.

2. Shear-dependent properties are necessarily time-dependent, and confusion results from attempts to measure both phenomena simultaneously.

3. The terms used to describe flow behavior are the main source of confusion; the concepts are fairly well established.

The recommendation is made that flow phenomena be described using a broad classification of behavior based on the dependence of applied stress on shear rate. Three broad areas of flow behavior are recognized. They are based on the ratio, S/D. A constant S/D ratio is characteristic of a Newtonian system; a decreasing ratio with increased D is shear thinning, and the material it characterizes is a shear-thinning system; an increasing ratio with increased D is shear

thickening, and the material it characterizes is a shear-thickening system.

The Committee recommends further that flow phenomena be expressed in terms of the directly measured variables S and D, and that reference to terms such as viscosity and fluidity either be avoided or qualified whenever the possibility exists for their misinterpretation in a quantitative sense. It is essential that the dependence of S on D be determined under steady-state conditions.

The usage of new words was considered by the Committee which sampled the opinions of academic and industrial personnel engaged in making and describing measurements of flow behavior. Sentiment was strongly in favor of reducing the number of terms used to describe the three main types of flow behavior, rather than adding two additional terms.

The scientific community is strongly urged to adopt the terms shear thinning and shear thickening in future communications regarding shear-sensitive flow behavior.

Raymond R. Myers, *Chairman*
Donald R. Brookfield
Frederick R. Eirich
John D. Ferry
Leonard Stoloff
Ralph N. Traxler

TRANSACTIONS OF THE SOCIETY OF RHEOLOGY III, 207–216 (1959)

Abstracts of Additional Papers Presented at the Society of Rheology Meeting, November 5–7, 1958

Ultrasonics and Its Use in Rheology

T. A. LITOVITZ
Catholic University of America, Washington, D.C., and
Naval Ordnance Laboratory, White Oak, Maryland

Ultrasonic spectroscopy has demonstrated the existence of volume viscosity in most liquids and has shown that there are many different molecular mechanisms responsible. In all cases in liquids, the absorption of sonic waves has been related to relaxation processes and not to resonance effects. In this paper, resonance and relaxation are discussed in relation to the molecular basis of the ultrasonic loss (or volume viscosity) of liquids.

[To be published in *J. Acoust. Soc. Am.*]

Viscosity of *n*-Hexadecane

A. B. BESTUL and R. C. HARDY
National Bureau of Standards,
Washington, D.C.

Attempts to prepare high-purity *n*-hexadecane from commercial cetane by simple laboratory procedures were unsuccessful. Fractional distillation at reduced pressure of material previously treated with silica gel produced a few small fractions of about 99.5 mole-%

purity. The kinematic viscosities of the original material and of the fraction of highest purity, 99.63 mole-%, were found to be the same, 4.4635 cs. at 20°. All other fractions had lower viscosities. The viscosity of NBS standard sample of *n*-hexadecane, 99.94 mole-%, was found to be 4.4642 cs. or 3.4540 cp. at 20°C. *n*-Hexadecane is not likely to be suitable for use as a second calibration standard for viscometry until a simple, easily defined routine of purification is developed.

Mechanical Resonance Dispersion in Crystalline Solids

EDWIN R. FITZGERALD
The Pennsylvania State University, University Park, Pennsylvania

Measurements of the complex shear compliance at closely spaced intervals in the range of 100 to 5000 cps. have resulted in the discovery of sharp resonance dispersions in polycrystalline metals, crystalline polymers, and single crystals of various materials such as sodium chloride, copper sulfate, and quartz. The results indicate that the phenomena of low frequency resonance dispersion in mechanical compliance are of general occurrence. The data can be analyzed and fitted closely by means of a generalized stress-strain relation involving a linear combination of the strain and its first and second time derivatives. Inclusion of the third derivative leads to an anti-dissipative term which can be used to account qualitatively for a negative absorption or induced emission observed over a narrow frequency region in some materials. The negative absorption seems to be connected with static clamping stresses applied to the sample, decreases slowly with time, and can be reactivated by restressing.

An explanation of the resonances is suggested by calculations of Fermi, Pasta, and Ulam for nonlinear systems in which no tendency toward equipartition of energy among modes was found. Accordingly it is proposed that: (*1*) in crystalline solids, because of the nonlinear nature of the binding forces, equipartition of energy among the various modes of vibration does not take place; instead energy actually is passed back and forth among relatively few of the available modes,

(*2*) the frequency of the energy exchange, in contrast to the lattice frequencies themselves, may be very low, e.g., in the audio-frequency range, and (*3*) the observed resonance dispersions occur at frequencies corresponding to these various acoustic exchange frequencies. This lack of energy equipartition will not necessarily be noticed in specific heat measurements of solids, but may have some consequences in other areas.

Viscous Motion of Dislocations in Crystals

J. J. GILMAN and W. G. JOHNSTON
General Electric Research Laboratory, Schenectady, New York

Direct observations of dislocations in LiF crystals show that there is a quasi-viscous resistance to dislocation motion. This resistance does not involve dislocation interactions, but occurs for dislocations moving in dislocation-free regions of the crystals. The viscosity increases with impurity content, with neutron bombardment, and with decreasing temperature. Measurements have been made over a wide range of dislocation velocities extending from a few atom distances per second up to 10^{12} atom distances per second.

Our microscopic measurements of dislocation behavior have been applied to the calculation of macroscopic stress-strain curves with good results.

[To be published in *J. Appl. Phys.*]

Radiofrequency Spectroscopy Applications

WILLIAM L. ROLLWITZ
Southwest Research Institute, San Antonio, Texas

Radiofrequency spectroscopy covers the heretofore unused portion of the electromagnetic spectrum used for absorption spectroscopy.

The measurements involved are based upon the absorption of radiofrequency energy by nuclei and/or free electrons when they are simultaneously subjected to both a steady magnetic field and a radiofrequency field. The amount of energy absorbed will give a quantitative analysis. The width and shape of the absorption line will give a measure of the chemical and physical environment of the nuclei or electrons. The saturation energy will give added information on internal environment. These measurements can be made under many dynamic conditions so that the chemical and/or physical changes can be measured as a result of varying external environment.

It is therefore possible to apply these radiofrequency spectroscopy techniques to quality control and measurement, as well as to research, in such fields as high polymers, plastics, metals, petroleum products, rubber, paint, and starch.

Dynamic Mechanical Properties of Concentrated Solutions of Poly-*n*-Butyl Methacrylate

P. R. SAUNDERS, DONALD M. STERN, SHELDON F. KURATH, CHAROEN SAKOONKIM, and JOHN D. FERRY
Department of Chemistry, University of Wisconsin, Madison, Wisconsin

Measurements of the real and imaginary parts of the complex compliance (J^*) have been made on solutions of poly-*n*-butyl methacrylate (molecular weight 3.05×10^6) in diethyl phthalate at concentrations of 30, 40, 50, and 60% by weight, using the Fitzgerald transducer apparatus over wide ranges of frequency and temperature. Except for certain anomalies mentioned below, the method of reduced variables provided single composite curves with temperature shift factors which followed the WLF equation; the parameter α_f varied from 2.2 to 2.8×10^{-4}, and for the 50 and 60% solutions, whose glass transition temperatures were determined refractometrically as $-67°$ and $-46°$C., the parameter f_g was 0.024. At the lowest temperatures and highest frequencies, the reduced data for the 60% solution showed an anomaly which was tentatively identified as a β-mechanism but could not be separately resolved. At temperatures and frequencies corresponding to the neighborhood of the maximum in J'', the reduced

data for all four solutions showed an anomaly like that in the undiluted polymer, where the maximum shifts upward and to lower reduced frequencies with increasing temperature. This behavior can be interpreted in terms of a temperature dependence of the number of entanglement coupling points, with an apparent heat of dissociation of 2.1 kcal. in all solutions. Retardation and relaxation spectra have been calculated for each solution, and from these the concentration dependences of the monomeric friction coefficient and other parameters have been obtained.

(This work was supported in part by the Ordnance Corps, Department of the Army.)

[To be published in *J. Colloid Sci.*]

Some Generalizations of Linear Viscoelastic Stress-Deformation Relationships

HERSHEL MARKOVITZ
Mellon Institute, Pittsburgh, Pennsylvania

Oldroyd has developed a method for generalizing rheological equations of state of limited applicability so that they have correct invariance properties and are of a universally valid form. In this paper a general Maxwell body is taken as a basis for various generalizations of the Oldroyd type. These results are then examined for their implications with respect to the rate of shear dependence of the shearing and normal stresses in steady state flow.

Dynamic Mechanical and Creep Properties of a Concentrated Cellulose Nitrate Solution

DONALD J. PLAZEK*
Department of Chemistry, University of Wisconsin, Madison, Wisconsin

Low frequency torsion pendulum and creep measurements have been made on a solution of cellulose nitrate in diethyl phthalate

* Dr. Plazek's present address is Mellon Institute, Pittsburgh, Pa.

(23.0% by weight of polymer) to supplement previously reported work with a Fitzgerald-Ferry double transducer. The torsion pendulum measurements were made at temperatures from −25 to +35°C. within a frequency range extending from 0.07 to 9.0 cycles/sec. Creep runs, also made in torsional shear, were made at temperatures from −33 to +65°C. At the temperatures where crystallinity was present (5°C. and below), the deformation, γ, at long times can be described by the expression $\gamma = \gamma_0 + \beta t^{1/3}$, where t is the time and γ_0 and β are constants.

In spite of the presence of crystallinity, all of the results were independent of thermal history and the dynamic results at −10°C. and above could be and were reduced to a reference temperature (T_0 = 25°C.). The necessary shift factors, a_T, are given by log $a_T = -8.48\,(T - T_0)/(166 + T - T_0)$. At lower temperatures the dispersion is appreciably broadened by the crystallinity.

[To be published in *J. Colloid Sci.*]

On the Thermostatics of Continuous Media

BERNARD D. COLEMAN and WALTER NOLL
Mellon Institute, Pittsburgh, Pennsylvania

This paper discusses materials in states of rest; that is, in states which are achieved in the limit of very slow measurements. When in such a state, every material possesses a strain energy function, and behaves as either a perfect fluid or a perfectly elastic solid. A strain energy function cannot be completely arbitrary. Its possible forms are limited by symmetry considerations (i.e., objectivity and isotropy) and by the second law of thermodynamics. The restrictions caused by symmetry have been understood for some time; in this paper we investigate the thermodynamic requirements. In the course of a derivation of the laws of hydrostatics and elastostatics from thermodynamics, certain inequalities are obtained. These inequalities, which express the thermodynamic restrictions on a strain energy

function, have important implications when applied to the theory of finite elastic strain.

[To be published in *Arch. Rational Mech.*]

Four Separate "Regimes of Flow" or Systems of Blood Rheology

WILLIAM H. DUNHAM, FANN HARDING DUNHAM, and MELVIN H. KNISELY
Department of Anatomy, Medical College of South Carolina, Charleston, South Carolina

Blood flow patterns resulting from different properties of cells, combinations of cells, and plasma, during health and disease have not been thoroughly analyzed. At least four regimes of flow are known:

1. Newtonian flow, which consists of a parabolic velocity distribution of a homogenous fluid around the axis of flow. This occurs when plasma alone flows through a cylindrical vessel.

2. Poiseuillian flow, the commonly described flow pattern, which consists of alternate concentric cylinders of cells suspended in plasma, and plasma, radially symmetrical around the axis of the vessel.

The above two regimes of flow occur during health when blood cells are not agglutinated; during disease, blood cells often agglutinate into masses having different sizes and different degrees of internal rigidity. The following two types of flow sometimes occur during disease:

3. Plug flow, a plastic flow during which the "yield value" of the masses has been exceeded at their boundaries.

4. Gravitationally layered flow, as seen with the observer looking horizontally, which consists of several layers of settled, stationary, and/or sliding cellular constituents, often agglutinated, of different sizes, shapes, densities, and elastic properties. And above these there is often a layer of moving plasma containing suspended small particles such as small masses, free erythrocytes, and leukocytes. This flow is not radially symmetrical around the axis of the vessel.

Between branchings, segments of arteries and of veins are truncated cones, not cylinders (Jeffords and Knisely, 1956). Saunders and

Knisely (1954) found that the maximal internal diameters to which the terminal mesenteric arterioles can distend as they are impacted with masses of sludge are: for hamsters and mice, 9 micra; for rats and rabbits, 8 micra; for cats, 11 micra; and for dogs, 10 micra. These are the narrowest vessels of the vascular system.

The above four separate regimes of flow are considered in terms of the forces of the plasma, influenced by the vessel walls, acting on the surfaces of the suspended particles. The paper was illustrated by lantern slides and motion pictures taken through a horizontally aimed microscope. As far as is known, rheologists have not ordinarily used horizontally aimed microscopes to study the flow of suspensions. The walls of small living blood vessels are nearly transparent, which permits direct observation of the behavior of particles in "flowing" suspensions.

(This research was supported by U.S.P.H.S. Grant H-1683.)

[Published in *Angiology*, **9**, 317 (1958).]

Effects of Drawing on the Mechanical Behavior of Nylon 6 Filaments

J. H. DUSENBURY, C. WU, C. J. DANSIZER, and A. HAUSER
Textile Research Institute, Princeton, New Jersey

The extensional properties, bending moduli, and torsional moduli have been determined for a series of nylon 6 filaments ranging in draw ratio from 1.00 to 5.48. The extensional properties were measured with an Instron tester; the bending and torsional moduli were measured with an electrostatic vibroscope. Both the extensional and bending moduli increase smoothly with increasing draw ratio, whereas the torsional modulus is essentially independent of the draw ratio. These findings are in good agreement with those reported previously for two other melt-spun filaments: nylon 66 and Dacron. The actual values observed for the nylon 6 moduli, however, are about $^2/_3$ the corresponding values observed in the case of nylon 66. During load-extension experiments the filaments of lower draw ratio were observed to go through relatively long periods of extension without appreciable changes in load; they were, in effect, being cold-drawn

under the test conditions. The values observed for the ratio of the bending modulus to three times the torsional modulus suggest that there is no preferential orientation in the undrawn filaments and that these filaments exhibit increasing molecular orientation with respect to the filament axis as the extent of drawing increases. These views are in general agreement with the results of x-ray diffraction studies carried out on the same materials.

The "Effective" Solid Volume–Viscosity Relationship of Rigid Spheres Versus the Dimensions of the Measuring Instrument

STEWART R. OGILBY
Research Division, Goodyear Tire & Rubber Co., Akron, Ohio

A viscosity–solids relationship that is based upon the effect of the solid phase in altering the "effective" dimensions of the measuring instrument is proposed.

The "effective" solid volume fraction has been found to vary with the ratio between the shearing area of the instrument and the diameter of the solid particles relative to the volume of sample under shear. The absorption or interaction forces at the solid-liquid interface affect the "effective" solid-volume fraction V_E in direct relation to the specific surface of the solid phase and the amount of shear.

Two simple equations are used to relate the solid-volume fraction (V) to the "effective" solid–volume fraction over a range of shear that shows both pseudo-plastic and dilatant flow.

A Method of Generalizing the Effect of Temperature and Rate on the Stress-Strain Curves of Nylon

JOHN B. MILES
Chemstrand Corporation, Decatur, Alabama

It has been found possible to considerably simplify the description of the stress-strain curve of nylon as a function of temperature and

of the rate of elongation. The stress-strain curves obtained at a constant rate of elongation in the range of temperature from 21 to 150°C. can be accurately represented by one master curve with the units along the stress axis multiplied by a constant which depends on the te . perature. Thus the stress P is given by

$$P = f(e) \times g(T)$$

where e and T are the strain and temperature, respectively, and $f(e)$ is a function of e only, and $g(T)$ of T only. The temperature function, $g(T)$, has been determined over this temperature range.

A similar type of relationship has been found for different rates of elongation at constant temperature in the range from 0.2 to 200% elongation per minute.

The characteristics of the master curve, $f(e)$, are discussed, with possible interpretation in terms of the mechanism of deformation.

[To be published in *Textile Research J.*]

6 15